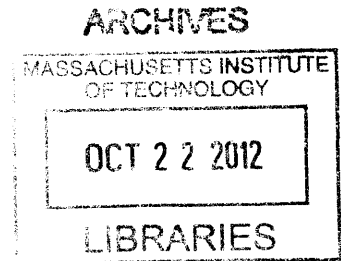# DNA Ruler: Enhancing Nanopore Sizing Resolution by Multiple Measurements on the Same DNA Molecule

By

Yi-Heng Sen

B.S. Electrical Engineering
National Taiwan University, 2004

M.S. Mechanical Engineering
Massachusetts Institute of Technology, 2008

Submitted to the Department of Mechanical Engineering
in Partial Fulfillment of the Requirement for the Degree of

Doctor of Science

at the

Massachusetts Institute of Technology

September 2012

Signature of Author: _____
Department of Mechanical Engineering
July 10th, 2012

Certified by: _____
Rohit N. Karnik
Associate Professor of Mechanical Engineering
Thesis Advisor and Committee Chair

Accepted by: _____
David E. Hardt
Professor of Mechanical Engineering
Chair, Departmental Committee on Graduate Students

DNA Ruler: Enhancing nanopore sizing resolution by multiple measurements on the same DNA molecule

By

Yi-Heng Sen

Abstract

Nanopores are versatile sensors for label-free detection of single molecules and particles that have attracted attention for applications such as DNA sequencing and nanoparticle analysis. Detection of single molecules or particles in nanopores is enabled by monitoring the ionic current through the pore: translocation (passage) of a molecule through the pore results in a measurable transient modulation of the ionic current. However, compared to methods such as electrophoresis, nanopores have a limited capacity to discriminate between DNA molecules of different lengths, which have important applications including genomic analysis, DNA sequencing, fingerprinting, and pathogen detection. This thesis focuses on the development of nanofluidic nanopore devices for enhanced discrimination between DNA molecules of different lengths through statistical averaging over multiple detection events on the same molecule.

Microfluidics-integrated devices incorporating nanopores of dimensions 200 nm × 500 nm × 4 μm and 200 nm × 500 nm × 7 μm were fabricated using soft lithography in polydimethylsiloxane (PDMS). When current through the nanopores was monitored using a Axopatch 200B patch-clamp amplifier, translocation events of single molecules of λ-DNA (48.5 kbp), T7 DNA (39.93 kbp), and a HindIII enzyme digest fragment of λ-DNA (23.13 kbp) were detected as transient increases in the baseline current due to the excess counterions introduced into the nanopore due to the charge on the DNA molecules. To perform multiple measurements on the same DNA molecule, feedback control using LabVIEW was implemented to identify DNA translocation events in real time and reverse the applied voltage bias driving the DNA translocations. DNA molecules were recaptured into the pore with an estimated probability exceeding 99%, enabling the measurement of multiple translocation events on the same molecule. Numerical simulations using a drift-diffusion model were performed to examine the DNA recapture physics and understand the origins of the high recapture rates in the nanopore devices; the measured DNA recapture time distribution was correctly predicted by the numerical simulations. Statistical averaging on multiple measurements resulted in enhancement of the ability of the nanopore to discriminate between DNA molecules of different lengths from a resolution of ~8.5 kbp for single measurements to ~4.5 kbp for multiple measurements, which enabled length-based discrimination of molecules in a mixture of λ-DNA and HindIII-digest λ-DNA, and in a mixture of λ-DNA and T7 DNA.

To isolate the DNA molecule being measured from the DNA sample being analyzed and to improve device stability, next generation nanopore devices were designed with the aims of better device surface control, capability of trapping and detecting DNA molecules, and performing multiple measurements with neither side of the nanopore exposed to the DNA bulk solution. The SU-8 mold for microchannels and trapping chamber was fabricated with UV photolithography, and nanochannels in silica substrate were fabricated with electron-beam lithography, followed by wet etch and reactive-ion-etching (RIE) technique.

Finally, contrary to DNA translocation signals observed in smaller nanopores, a bidirectional modulation of ionic current was observed during the translocation of DNA molecules through the nanopore wherein the ionic current showed a slight decrease followed by a larger increase. Through experiment and simulation, this bidirectional current modulation was shown to be similar in origin to ionic current rectification in a nanofluidic diode, attributed to the spatially asymmetric charge distribution introduced by the DNA molecule as it moves through the nanopore.

This work has shown that multiple measurements on the same molecule in a nanopore device can enhance the ability of the nanopore to discriminate between long DNA molecules of different lengths. Further development of this approach may enable rapid, label-free, high-resolution electrical sizing of DNA molecules by nanofluidic devices, which has hitherto been largely confined to electrophoresis.

Thesis Supervisor and Committee Chair: Rohit N. Karnik, Ph.D.
Associate Professor of Mechanical Engineering
Massachusetts Institute of Technology

Committee Member: Alan J. Grodzinsky, Ph.D.
Professor of Biological Engineering, Electrical Engineering and Computer Science, and Mechanical Engineering
Massachusetts Institute of Technology

Committee Member: Jongyoon Han, Ph.D.
Associate Professor of Electrical Engineering and Computer Science and Biological Engineering
Massachusetts Institute of Technology

Acknowledgements

First of all, I owe numerous thanks to my thesis advisor, Professor Rohit Karnik, for his guidance, encouragement, intellectual wisdom, and professional support. He is one of the nicest people to have as an advisor, and I deeply appreciate his guidance. Without this opportunity, I would not have finished my masters and doctoral degree at MIT.

I would like to thank all of my group members for their help. I am grateful to work together with them. I would like to thank my friends, who have helped me and made my life colorful. I would like to thank Mechanical Engineering department, Microsystems Technology of Laboratories, and Research Laboratories of Electronics.

Finally, I would like to express my deepest appreciation to my family for their support. No words are sufficient to thank them here!

Table of Contents

7

List of Figures

9

the DNA molecule. (b) A single DNA molecule passes through the nanopore in the forward direction (c) After passing through the pore, the molecule moves away from the pore under the influence of the electric field for a fixed delay time. (d) The field is reversed, and the molecule moves towards the pore. (e) The molecule passes through the pore in the reverse direction. (f) A representative current trace for an experiment with a 2 ms delay before voltage reversal. A gap of 6.6 nA is omitted from the middle of the trace. The letters mark the correspondence between the current trace and the schematic illustrations of molecular motion (b–e).

Figure 4.4   (a) Translocation signal obtained for a 1 μg/mL λ-DNA sample with a voltage bias of -1 V. Current increases by about 15 pA during the translocation due to charge effect. (b) No translocation signals were observed when bias polarity was reversed.

Figure 4.5   (a) PDMS nanopore device consists of two microchannels connected by one nanopore. Negative voltage bias is applied across the nanopore to drive the negatively charged DNA molecule (red) from left to right microchannel through nanopore. (b) After the completion of translocation, voltage bias is reversed to recapture the DNA molecule back to the pore for subsequent translocation. This process continues until the DNA molecule has escaped out of the nanopore, or translocation current signal is not large enough to trigger another voltage reversal. (c) Current trace of multiple measurements on the same DNA molecule of 48.5 kbp λ-DNA in 10 mM KCl. For clarity, only 13 out of hundreds of recapture events are shown.

Figure 4.6   Determination of the time DNA enters and exits the nanopore. Black, green, and red dots indicate the time DNA molecule enters, translocates through, and exits the nanopore. Two regression lines were constructed in a time span of 20 ms before and after the translocation event.

Figure 4.7   Scatter plot of translocation time and signal amplitude of multiple measurements (N = 432) on the same DNA molecule. Red dots indicate translocation events, while blue dots indicate the average of 6 consecutive events. The fitted Gaussian curves narrowed down significantly after averaging over multiple measurements, hence increasing the resolution of nanopore system.

Figure 4.8   (a) History of current change of a mixture of DNA (1 μg/mL λ-DNA and 1 μg/mL HindIII digest fragments) Inset: History of current change with only 1 μg/mL λ-DNA in solution does not show abrupt changes in the current. (b) Scrambling the order of the original data followed by statistical averaging.

Figure 4.9   Comparison between scatter plots and histograms with and without averaging of current change and duration obtained for a solution with only 48.5 kbp λ-DNA and a mixture of 48.5 kbp λ-DNA and HindIII digest fragments. (a) Scatter plot of 48.5 kbp λ-DNA before statistical averaging. (b) Scatter plot of a mixture of DNA molecules before statistical averaging. (c) Scatter plots converge into one group after statistical averaging for 48.5 kbp λ-DNA molecule. (d) Scatter plot converges into

several groups after statistical averaging for a mixture of DNA molecules. (e) and (f) are histograms of current change upon statistical averaging over every 6 consecutive events for only λ-DNA and mixture of DNA, respectively. Histogram converges to one Gaussian peak for single DNA, but splits into multiple Gaussian peaks for a mixture of DNA. However, both analytes yield a distribution of one Gaussian peak without averaging (Inset of figure (e) and (f)). The dominance of larger signals is due to sticky ends, and the fact that the algorithm does not enable feedback of fragments smaller than 10 kbp.

chamber and microchannel shows clean gap without unintended connections.

Figure 6.1   Rectifying properties of a single conical nanopore in a PET membrane with the voltage applied on the base side and the tip side grounded. (A) I-V characteristics obtained under symmetric ion concentration at pH 8 and 3 M KCl (solid circles), 1 M KCl (empty squares) and 0.1 M KCl (empty triangles). (B) I-V curves recorded under symmetric 0.1 M KCl at pH 8 (solid squares) and pH 3 (empty triangles).

Figure 6.2   Rectifying effect due to the disparate ion distribution along the nanochannel having negative surface charge and under different polarities of applied potential. The gray scale plots show the relative ionic concentration in different regions of the channel. (a) High concentration C_H side is positively biased relative to the low concentration side C_L. (b) Zero bias. (c) C_H is negatively biased. The gray region within the nanochannel that is bound by the dashed lines represents the electric double layers (EDL).

Figure 6.3   (a) Schematic diagram of a nanofluidic diode consisting of a positively charged surface and a neutral surface in different halves of the channel. The positive charge is produced by avidin, while the neutral charge is produced by biotin moieties. (b) Epifluorescence image shows fluorescently labeled avidin in the left half the nanofluidic diode. (c) Theoretical predictions of the ionic concentration and electric potential profiles along nanofluidic diode calculated using the one-dimensional model. The avidin half of the channel has a positive charge of 3 mC/m^2, and the biotin half is neutral. (Top) Under forward bias of 5 V, there is concentration enhancement in the channel. (Bottom) Under a reverse bias of -5 V, there is concentration depletion in the channel, and the electric potential drops sharply at the junction of positive and neutral surface charge. Channel height is 30 nm, and KCl concentration is 10 mM. (d) Nanofluidic diode I-V characteristics at different KCl concentrations. Solid circles represent experimental data, while the dashed line has slope equal to the conductance measured using a voltage bias range of -50 to 50 mV. Solid lines are theoretical predictions. Biotin side is at a higher potential under forward bias.

Figure 6.4   (a) Schematic of DNA (in red) with a surrounding EDL (in blue) in a nanochannel, and the location of the CP-induced ion-depletion (between planes 1 and 2) and ion-enrichment (between planes 3 and 4). The arrows (in blue) depicting the cationic current are located inside the nanochannel and are directed from left to right, whereas the arrows (in red) depicting the anionic current are located inside the nanochannel and are directed from right to left. (b) The different dimensions corresponding to the DNA transport in a nanochannel. (c) (left) Schematic of the event of a DNA entering a nanopore (radius R), and the locations of the planes 1 and 2 in between which ion depletion will occur. (c) (right) Schematic of the event of a DNA (shown in red) exiting a nanopore, and the locations of the planes 3 and 4 in between which ion enrichment will occur. (d) The

List of Tables

Chapter 1 Introduction to nanopore technology

1.1 Background: nanopore analytics

Rapid and accurate sensing of single molecules is an important research topic in many fields such as biology, chemistry, medicine, and forensics[1]. The capability of detecting and measuring single molecules and other micro/nano scale analytes can lead to the development of rapid diagnostic or analytical/bioanalytical technology. While detection techniques that require labeling analytes with fluorescent molecules are very useful in characterization using microscopy, the requirements of incorporating optics instrumentation and extensive sample preparation steps make it unsuitable for applications that require rapid analysis in a compact system.

Nanopores can detect and characterize analytes by purely electrical signal (Figure 1.1). The working concept of such technology is similar to that of Coulter counter[2]; a driving force, either a voltage bias or pressure difference, is applied across the pore while measuring the corresponding ionic current. When analytes pass through the pore, the resulting current change can be used to detect and characterize the analyte.

Research in the nanopore field has been conducted primarily for DNA sequencing application, and several research groups and startups have been developing such technology to achieve rapid and economical DNA sequencing that could meet the $1,000 genome challenge proposed by the National Institutes of Health[3]. Nanopores for DNA sequencing typically require diameters below 5 nm for molecular-level interactions yielding different electrical signals for different nucleotides[4-6]. Devices with larger pore geometry are needed to characterize larger analytes such as viruses, large proteins and protein complexes that fall within the size range of 10-500 nm.
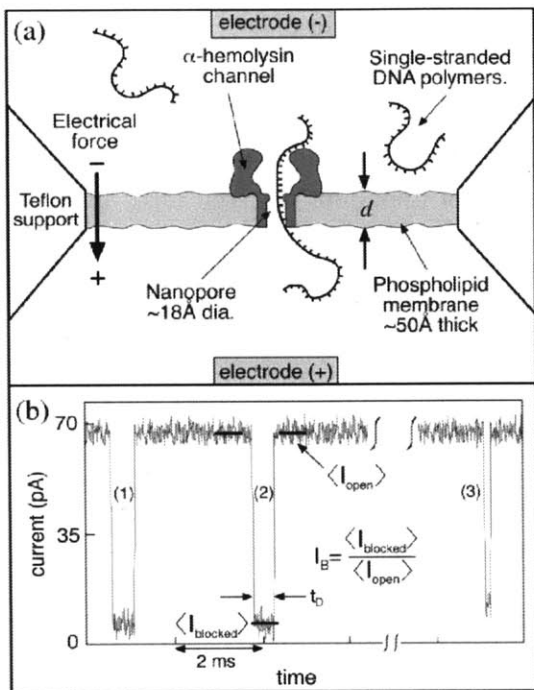
Figure 1.1 Scheme illustrating the principle of nanopore analytics. (a) Single-stranded DNA molecules (negatively charged) and salt ions are electrically driven through a single α-hemolysin protein pore embedded in a phospholipid membrane. Most of the ionic current through the pore is blocked during DNA passage. (b) Three representative translocation current blockades are shown. For each event the translocation time, t_D, and the average event blockade, $<I_B>$, were measured[7].

1.2 Nanopore sensor devices

1.2.1: Protein nanopores

The field of nanopore research was initiated with the advent of the protein nanopore formed by α-haemolysin (αHL) from Staphylococcus aureus. In 1996, Kasianowicz et al. demonstrated that the translocation of single DNA molecules through the naturally occurring hemolysin pore could be detected by monitoring the ionic current through the

pore[8]. The protein pore is embedded in a lipid bilayer, and the inner channel diameter of ~1.5 nm suggests that only single-stranded DNA is allowed to translocate through α-hemolysin, and only up to a 10 bp fragment can reside in the vestibule at one time. Under electrolyte pH of 7-9, α-hemolysin nanopore forms a stable and reproducible channel with <2% variation in channel dimension[9]. As the ssDNA molecule passes through the pore, it sterically blocks the pore, resulting in a transient decrease in the ionic current through the pore. With the stability and a size that is just larger than a single stranded DNA molecule, it enables close molecular interactions between the DNA molecule and the nanopore during translocation. Howorka and Bayley [10] engineered this pore and attached a short DNA strand inside the pore. They were able to infer the electrical potential distribution along the length of the pore by measuring the translocation time and current blockages of DNA strands of different lengths with a sequence complementary to the covalently attached segment. Hemolysin pores could discriminate between current blockages due to purine and pyrimidine segments in a DNA molecule, showing promise for rapid DNA sequencing[11]. Meller et al.[5] demonstrated the potential of hemolysin pores to characterize molecules by discriminating between polynucleotide with similar length and composition, but differing only in sequence. Bates et al.[12] studied DNA polymer biophysics by driving DNA molecules into the hemolysin pore and switching off the driving voltage using feedback control and subsequently looking at escape times of DNA molecules from an entropically unfavorable configuration. Wang et al.[13] further characterized DNA samples and demonstrated that modifications such as phosphorylation result in different statistical signatures of DNA molecules translocating through hemolysin pores. Clarke et al. used

an exonuclease enzyme to cleave individual nucleotide molecules from the DNA, and showed that a protein nanopore with a covalently attached adapter molecule can continuously identify unlabelled nucleoside 5'-monophosphate molecules with accuracies averaging 99.8%[14]. Base selectivity was achieved by modifying the mutant α-hemolysin pore with a cyclodextrin adapter. Raw bases were read with over 99% confidence under optimal operating conditions. By integrating this base identification platform with a highly processive exonuclease, a single molecule sequencing of dGMP, dTMP, dAMP and dCMP by digestion approach were shown by Oxford nanopore technology (figure 1.2).
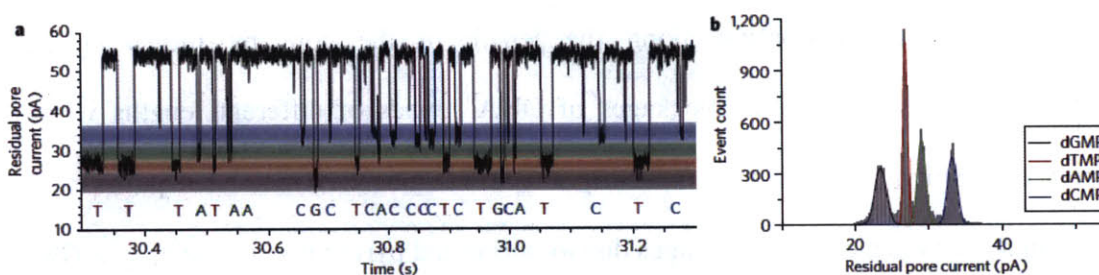
Figure 1.2 Nucleotide event distributions with a permanent cyclodextrin adapter. (a) Single-channel recording from the protein nanopore showing dGMP, dTMP, dAMP and dCMP discrimination, with colored bands added to represent the residual current distribution for each nucleotide. (b) Corresponding residual current histogram of nucleotide binding events, including Gaussian fits[14].

1.2.2 Solid-state nanopores

While protein channels offer a well-defined geometry and are amenable to chemical modification, they are not amenable to integration with upstream or downstream

processing, and it is difficult to adjust the pore size. These drawbacks resulted in the search for methods to fabricate artificial nanopores that are more robust and give control over nanopore geometry. Li et al.[15] introduced the method of ion-beam sculpting, in which a 1.8 nm diameter nanopore could be fashioned in a silicon nitride membrane using the bombardment of argon ions to slowly close a larger pore by redistribution of material around the pore. Storm et al.[16] demonstrated controlled size reduction of a pore in silicon dioxide using a high energy TEM to fluidize the glass and shrink it due to surface tension. The TEM allowed monitoring of the process and the pore diameter could be controlled down to one nanometer precision. Chang et al.[6] fabricated a 50-60 nm long, 4-5 nm diameter pore using e-beam and standard lithography techniques for 200 bp DNA sensing. Smeets et al.[17] studied the dependence of current fluctuations on electrolyte concentration during λ-DNA translocation in KCl buffer for 50 mM to 1 M salt concentrations in a solid-state nanopore (length x diameter = 35 nm x 20 nm), which was fabricated with a combination of wet etch, reactive etching, LPCVD, and TEM. Siwy et al.[18] fabricated a conical nanopore using ion track etching technique. This method entails bombarding a solid material with a collimated beam of high-energy nuclear fission fragments to create parallel damage tracks in the film. The damage tracks are then solution etched into monodisperse cylindrical pores. The diameter of the pores is determined by the etch time, and its density (pores per cm^2) is determined by the exposure time to the fission-fragment beam[19]. It exhibited a voltage-dependent switching characteristic, similar to biological voltage-gated channels, and was also functionalized with molecular binding agents such as biotin and antibodies and was shown to be capable of highly specific molecule detection. Harrell et al[19] deposited gold in conical nanotubes

embedded inside a polymeric membrane for functionalization with thiolated DNA molecules, and showed that the extent of ionic current rectification could be controlled by either a simple chemical method (varying the DNA chain length) or a simple physical method (varying the nanotube mouth diameter).

1.2.3 Sensing in sub-micrometer pores

Nanopores designed for the sequencing of single DNA molecules need to have small diameters (<5 nm) to detect and linearize DNA molecule conformation during translocation. During single DNA translocation, DNA molecule could exhibit different conformation, and thereby yielding different ionic current behavior for the same type of molecule[20]. To ensure adequate current signal, the diameter of the pore needs to be made small enough to decrease the transit time of DNA and yield a detectable signal. However, there is a trade-off in terms of fabrication cost, dynamic range, and it is difficult to analyze larger molecules, proteins, or particles of varying sizes using tailor-made nanopores. A few research groups have utilized miniaturized Coulter counter type systems for targeting analysis of particles and colloids in the submicron size range[21-24]. In 1977, Deblois et al. demonstrated that viruses above about 60 nm in diameter may be rapidly sized to a few nanometers using 400 nm Coulter counter pore[25]. Saleh et al. used rapid prototyping in PDMS and glass etching to make 200-400 nm nanopores for DNA detection and sizing purpose[26]. They demonstrated the detection of λ-DNA[26], 87 nm latex colloids[23], and later used this system for detection of protein binding to colloidal nanoparticles for binding assays[22]. The nanopore was used for the detection of human granulocyte colony stimulating factor and granulocyte and macrophage colony stimulating factor[27]. Other researchers have detected single DNA molecules and

nanoparticles using nanopipettes[24]. Ito et al. used a resistive-pulse Coulter counter based on a membrane containing a single multiwall carbon nanotube channel to simultaneously determine the size and surface charge of 60 nm carboxy-terminated polystyrene nanoparticles, and the resolution was claimed to be comparable to that of transmission electron microscope (TEM)[28]. Uram et al used 500-600 nm diameter laser machined pores to detect a specific virus or a virus-specific antibody in solution, determine the number of antibodies bound to individual virus particles[29], and monitor the assembly of nanoparticles onto templates in situ, all without using fluorescent labeling techniques[30].

1.2.4 Current change during DNA translocation

Nanopore researchers use conductance modulation during DNA translocation to characterize its chemical or biophysical property. Studies on conductance of nanopore filled with conductive electrolyte have shown its dependence on channel geometry, electrolyte concentration, nanochannel surface charge[31], and the analyte (DNA molecules, proteins, nanoparticles) that temporarily resides in the nanochannel[5,17,26]. To explain the aforementioned dependence, consider the model where DNA molecule fully stretches inside a nanopore that is filled with KCl electrolyte. The corresponding conductance change ΔG of such nanopore can be written as[17]:

$$\Delta G = \frac{1}{L_{pore}}(-\frac{\pi}{4}d^2_{DNA}(\mu_K + \mu_{Cl})n_{KCl}e + \mu^*_K q^*_{l,DNA}) \quad \text{.. (1.1)}$$

where d_{DNA} (2.2 nm) represents the diameter of the molecule, $\mu_K = 7.616 \times 10^{-8}$ m^2/Vs and $\mu_{Cl} = 7.9 \times 10^{-8}$ m^2/Vs[32] are the electrophoretic mobilities of potassium and chloride ions, μ^*_K is the effective electrophoretic mobility of potassium ions moving along the DNA, and $q^*_{l,DNA}$ is the effective charge on the DNA per unit length, which is assumed to be constant.

Smeet et al. [17] have performed the study of nanopore conductance during DNA translocation through SiO_2 nanochannel at various KCl electrolyte concentrations. They found that depending on KCl concentration, nanochannel conductance could either decrease or increase during DNA translocation. Conductance decrease is attributed to the first term in equation 1.1 due to ion exclusion by the DNA molecule, while conductance increase is attributed to the increase of the concentration of the potassium ions due to the negatively charged DNA molecule. These two effects are competing against each other during DNA translocation. Because the first term, expressing the change in bulk conductance, depends on n_{KCl}, we can expect a linear relationship for delta $\Delta G(n_{KCl})$ and, hence, a crossover point at which $\Delta G = 0$. Besides, the crossover was also experimentally verified to occur at KCl = 0.37 M^{17}.

1.2.5 Steps involved in DNA translocation

Figure 1.3 explains the event of DNA molecule transportation to and translocation through nanopore, which consists of three major steps: DNA arrival (X), DNA entrance (Y), and DNA passage (Z). DNA arrival step (X) is the process in which DNA molecule arrives at the entrance of the pore from bulk solution. DNA entrance is the step in which DNA overcomes the entropy barrier, and is about to pass through nanopore. DNA passage step (Z) is the process in which it starts from the completion of DNA capture to the end of DNA passage. Step (X) involves transport via diffusion and electrophoresis from reservoir to the entry of the pore, and the second step (Y) involves DNA molecule threading into the nanopore. When DNA molecule is far away from the pore, the electric field is negligible and the transport of molecule approaching the entrance of the pore is dominated by diffusion[33]. As DNA molecule approaches closer to the pore, the electric

field becomes the dominant factor and attracts DNA molecule further to the entrance of the pore. Subsequently, the DNA molecule overcomes the entropic barrier due to its conformation and threads into the pore. The combination of these two steps determines the rate of DNA capture. Chen et al have shown a linear relationship between magnitude of applied voltage bias and λ-DNA (48.5kbp) capture rate in 15 nm solid-state pore[34], while Sen et al. also showed a linear relationship on λ–DNA capture rate in 320 nm PDMS pore[35]. Such linear relationship between DNA capture rate and voltage bias indicates that the DNA arrival step determines the frequency of translocations.

While certain nanopore devices showed the process from reservoir to the pore entrance being the dominant step with linear relationship between voltage and DNA capture rate, other works have shown the exponential relationship between voltage and DNA capture as a result of entropy barrier to DNA entry into the nanopore as being the dominant factor of the entire process. Henrickson et al. have shown the exponential relationship between voltage and capture rate of polyneucleotide in 1.5 nm α-hemolysin pore[36].

The third process (Z) includes the process from the completion of DNA being threaded into the pore to the completion of the entire translocation through the pore. The velocity of the DNA molecule during translocation depends on the size of the pore, the interaction between the nanopore wall and DNA molecule, nanopore surface charge, buffer concentration, and the length of DNA molecule. These three steps comprise the entire process of DNA transportation and translocation event, and the overall analysis throughput of DNA molecule is determined by the slowest of the three.
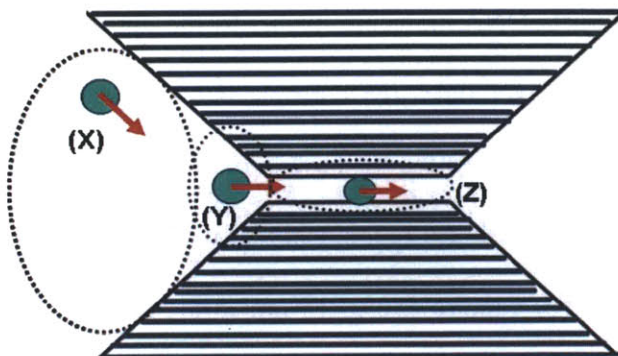
Figure 1.3 DNA transportation and translocation event consist of (X) arrival of DNA molecule from bulk solution, (Y) threading into nanopore, and (Z) passage from entry to end of the pore. Schematic green ball indicates the DNA molecules.

Higher translocation rate implies higher analysis throughput, which is a significant factor affecting the applicability of nanopore technology. For example, the translocation rate could be increased by increasing the voltage bias. However, such increase in voltage magnitude decreases the translocation duration, and therefore decreasing the characterization resolution. To circumvent the problem without affecting signal resolution, Wanunu et al. have found that an ion gradient across the pore can be used to significantly enhance the magnitude of voltage in the cis chamber, greatly enhancing the DNA capture rate without reducing the translocation times[37].

1.3 Thesis background and motivation

1.3.1 DNA sizing

The ability to accurately measure the nucleic acid length and differentiate nucleic acid fragments with different lengths has important implications for diverse applications such

as profiling of short tandem repeat (STR) markers[38], biomedical diagnostics[39], and bio-defense[40]. Currently the most common approach for DNA sizing is electrophoresis[41], which provides high resolution (<1bp) and is the one of the center piece of traditional DNA sequencing technology and other important applications in biochemistry and molecular biology. The electrophoresis method is implemented with a machine that comprises a large matrix or capillary filled with gel material made of agar or polyacrylamide. DNA molecules are injected at one side of the gel, and a voltage bias is applied across the matrix such that these charged DNA molecules will travel through gel medium because of inherent negative charges of DNA molecules as a result of phosphate group (isoelectric point is pH ~1). Although DNA molecules of different lengths are known to have uniform electric mobility in free solution, different length of molecules exhibit different mobility inside gel medium due to strong interactions between DNA and the gel network, and shorter DNA molecules with higher electric mobility travel further distance under voltage bias of a set period of time, and molecules of different lengths can be separated and sized with the optical readout for the positions of the fluorescent-tagged DNA molecules[42].

Several disadvantages of this technology have limited its applications; it requires a large matrix for containing gel material, optical instrument experimental steps required for analysis, billions of DNA molecules to have sufficient optical signal from fluorescent-tagged DNA molecules. These disadvantages result in higher cost, longer analysis time, and limit the mobility of the application such as on-site diagnosis.

With the advent of nanopore technology[8] and microfabrication technology[43], researchers have found promising potentials of sizing DNA molecules on a single chip that contains

nanochannels or nanopores. Nanopore technology has nano-meter scale features and requires only electrical signal for yielding molecular-level physical or biochemical information of the analytes. It presents a great alternative to circumvent the disadvantages in electrophoresis method due to its simplicity in analysis and instrumentation, label-free, portability, and the potential of lower cost if devices are being massively produced.

1.3.2 DNA sizing with nanochannels and nanopores

For DNA molecules separation and sizing application, research groups have used either label-free detections or systems that include optics instrument using nanochannel in SiO_2 or Si material. Han et al. used UV photolithography and RIE for fabricating silica channels with its height being 75 nm in thin region and 1.5 μm in thick region, and samples of long DNA molecules (5000 to ~160,000 base pairs) were efficiently separated into bands in these 15-millimeter-long channels[44]. Fu et al. fabricated anisotropic nanofilter array of 1 μm x 55 nm using photolithography and reactive ion etching techniques[45]. Continuous-flow size-based separation of DNA (50-766 bp) and proteins, as well as electrostatic separation of proteins, was achieved, demonstrating the potential use of this device as a generic molecular sieving structure for an integrated biomolecule sample preparation and analysis system. Chan et al. used e-beam lithography and RIE to fabricate fused silica microfluidic chip, and developed a rapid molecular mapping technology—Direct Linear Analysis (DLA)—on the basis of the analysis of individual DNA molecules bound with sequence-specific fluorescent tags[46]. They validated this technology using the 48.5 kbp λ phage genome with different 8-base and 7-base sequence motif tags. The distance between the sequence motifs was determined with an accuracy

30

of ± 0.8 kbp, and these tags could be localized on the DNA with an accuracy of ± 2 kbp. Foquet et al. manufactured 270 x 1 μm (height x width) silica channel with the fabrication process being derived from the sacrificial layer method[47]. It allows fabrication of 1 μm micro/nanostructured fluidics systems that are both extremely complex and have tight dimensional tolerance. The device consists of a closed rectangular channel, with several constrictions having submicrometer dimensions, and the behavior of DNA molecules inside these channels under an applied electrical field was first studied by fluorescence correlation spectroscopy using M13 double-stranded DNA. Campbell used focused ion beam to fabricate 150 x 180 nm capillary channels to study the electrophoretic behavior of single, fluorescently-labeled, molecules of DNA as a function of capillary size, and DNA mobility was found to increase with decreasing cross-section[48].

1.3.3 Thesis motivation

Potentially, nanopores also offer a platform that is easily integrated with microfluidic devices, and capable of performing label-free quick and accurate real-time analysis on analytes such as single DNA without the need for optical interrogation[3,49-51]. However, the resolution of nanopores to size or map DNA molecules is currently limited by variability in DNA translocation time and conformations, as well as the limited signal-to-noise ratio arising from insufficient measurement time during translocation[52,53]. The electron-charge-deficit (ecd) molecule[52,54], which is the measured time integral of obstructed ionic current or the integrated event area, has been shown to account for different folded conformations of the translocating DNA molecule, and serves as a powerful measure of the DNA length or molecular weight. With such method, however,

till date it has not been possible for nanopore sensors to differentiate DNA molecules with lengths differing by less than 30%[52] , which is calculated by the length difference of DNA molecules that could be distinguished in figure 1.4.
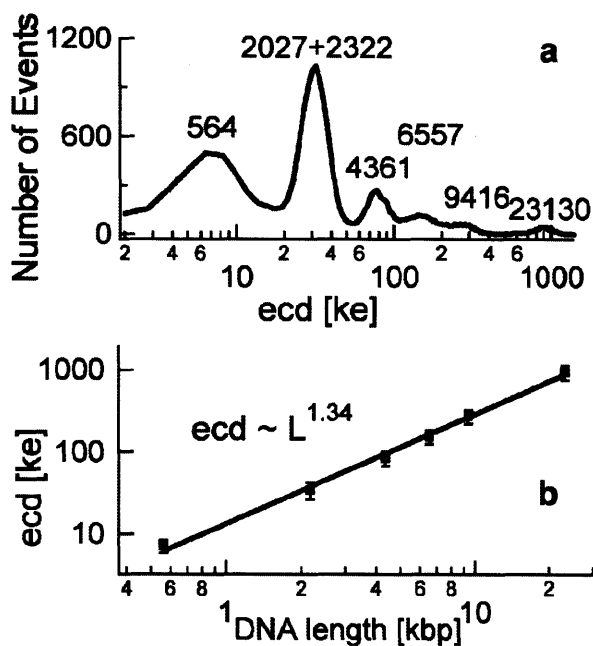
Figure 1.4 (a) Histogram of the ecd observed when the DNA ladder, a mixture of 500, 2027, 2322, 4361, 6557, 9416, and 23 130 bp linear dsDNA was translocated through a nanopore. The experiment was performed in a 12 nm diameter pore. (b) ecd as a function of DNA length L molecule (kbp)[52].

A promising approach to overcome this issue is to repeatedly measure the transient current signal of the same molecule, which can result in improved resolution through statistical averaging[51]. Gershow et al.[55] first showed recapture of 4–10 kbp DNA molecules in solid-state nanopore by reversing the applied voltage bias after detection of

a translocation event, but the DNA molecule recapture rate in their nanopore system was too low to enable statistical averaging and therefore measurement resolution.

In this thesis, the focus is on the improvement in sizing resolution by statistical averaging over the same DNA molecule, and differentiation of DNA molecules of different length with such methodology. The typical approach in nanopore measurement system is to let the analyte escape into reservoir after single measurement. However, if multiple (N) measurements were implemented on the same analyte for the translocation duration and its magnitude of current change, the spread in the distributions would decrease as $1/N^{0.5}$, permitting the use of such nanopores as sensitive probes for label-free analysis of nanoscale particles and molecules[33,51,55] (Figure 1.5 and 1.6).
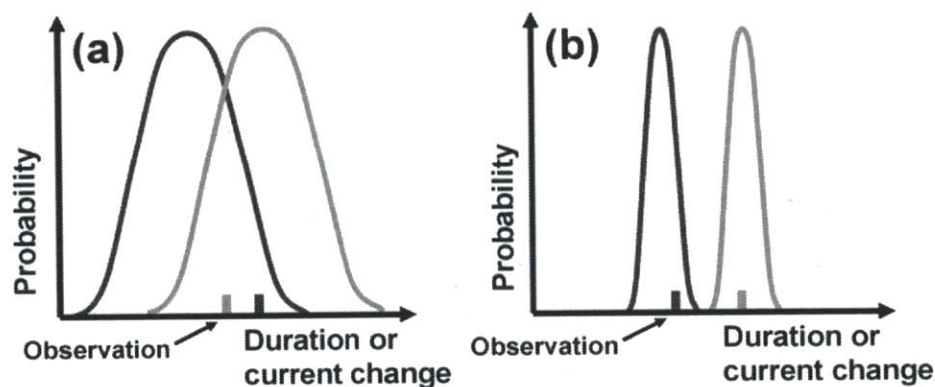
Figure 1.5 Scheme to illustrate the efficacy of multiple measurements. (a) Single translocation event distributions for two different types of molecules (light and dark lines) may exhibit significant overlap. Observation of a single event is insufficient to distinguish between the two molecules. (b) Distributions of events consisting of multiple translocations will be narrower. Since overlap of translocation event distributions for two different types of molecules significantly decrease, observation of a single event

(consisting of multiple translocations of a single molecule) is now sufficient to distinguish between the two molecules.
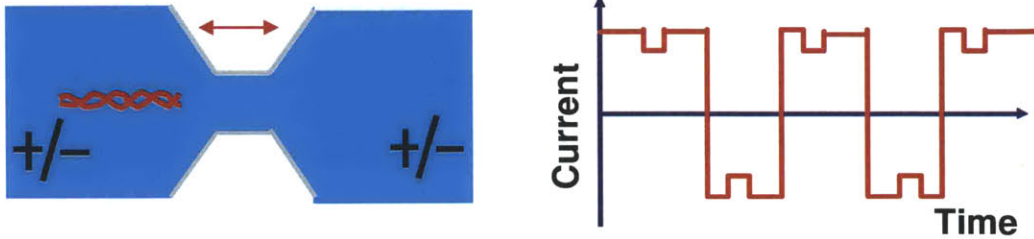
Figure 1.6 Concept of a device in which multiple translocation events may be recorded for each particle using a nanofluidic system with feedback control, greatly enhancing the resolution of the measurement.

1.4 Thesis overview

In this thesis, we focus on characterization and controlling the translocation of single λ-DNA molecules through an artificial PDMS nanopore with the objective of enabling multiple measurements on the same molecule. The rest of the thesis is organized as follows. Chapter 2 describes the fabrication of the 4 μm long PDMS nanopore devices. Chapter 3 describes the experimental setup and software algorithm and interface for the measurement and feedback control implementation. Chapter 4 demonstrates that multiple measurements followed by statistical averaging over the same DNA molecule enables sizing and differentiation in the DNA mixture of λ-DNA and T7 DNA, and λ-DNA and HindIII-digest λ-DNA. Chapter 5 describes the fabrication of SiO_2 nanochannel array and the mold for PDMS microchannels. Chapter 6 describes the experimental result of current rectification phenomenon through nanopore device during DNA translocation, and its analytic model as well as numerical simulation. The final

concluding chapter covers the ongoing work, and suggestions for future directions and

work to enhance the performance and capabilities of our DNA ruler system.

Chapter 2 Design and fabrication of nanopore sensor device

2.1 Introduction

Biological nanopores (e.g. α-hemolysin) and artificial solid state nanopores are the two main categories of nanopores[50]. As stated earlier, solid state nanopores have advantages over α-hemolysin nanopores due to adjustability of the solid state nanopore geometry. Besides, they have the potential to be integrated with different functionalities on the same chip, and can withstand a wider range of environmental and chemical conditions.

Below we will first describe the design considerations for both fabrication process as well as the dimensions of our solid-state nanopore device. Afterwards, we will give an overview of the designed fabrication process, the equipment used for fabrication, and details of the fabrication. Last, we will discuss issues encountered during fabrication.

2.2 Fabrication of nanopore device

2.2.1 Design consideration of the device

We aimed at a nanopore device that serves proof-of-concept demonstration of multiple measurements stated in thesis motivation of in Chapter 1. Specifically, the device should posses capabilities listed below:

1. Ability to detect long (>20 kbp) DNA molecules.

2. Simplicity, reproducibility, and ease of fabrication.

3. Ability to fabricate microfluidic reservoirs of large height (>1 μm) on either side of nanopore.

4. Ability to chemically modify the surface.

5. Ability to accurately control ionic concentration without problems such as evaporation.

6. Dimensions commensurate with diffusion timescales of chemical and biological species to facilitate rinsing and reactions.

There are several fabrication techniques for making nanopores with diameters ranging from ~0.25 nm to 10 nm. These processes include the use of focused-ion-beam[15,56,57], atomic-layer-deposition[58], drilling with transmission-electron-microscope (TEM)[16,57,59], and ion-track etching[60]. However, these methods (1) require fabrication of one nanopore at a time with high fabrication cost, (2) can not be mass produced if needed, (3) are not suitable for large anisotropic (90 degree) 2-D microchannel and therefore not suitable for incorporating nanofluidic reservoirs for trapping analyte at either side of the nanopore, and (5) are not necessary for fabricating devices for detection of long DNA molecules.

Instead, fabrication process of using (1) soft-lithography for PDMS nanopore, and (2) anodic boding or sacrificial layer etching techniques for fabricating silica nanopore could both incorporate nanofluidic reservoirs. Process of fabricating silica nanopore has been conducted, and the result will be discussed in Chapter 5. Since this technique is expensive, and fabrication process is more complicated and time consuming than that using soft lithography, we therefore first adopted soft-lithography for fabricating nanopore devices.

Briefly, soft lithography is a molding-cast process in that it requires no photolithography process once the mold is available[61]. Such fabrication technique possesses several advantages such as short fabrication time, low cost, and convenient for manufacturing micro/nano scale features, and has the potential to integrate with microfluidic networks easily. While fabrication of extremely small nanopores may not be feasible with PDMS (poly-dimethysiloxane, Sylgard 184 elastomer, K.R. Anderson), it has been reported[35]

that nanopores in the 200 nm range are adequate for analyzing long 48.5 kbp λ-DNA, which is sufficient for proof-of-concept.

2.2.2 Nanopore device dimensions

The major consideration for nanopore geometry depends on (1) fabrication feasibility, (2) signal-to-noise amplitude, (3) capability of nanopore to capture and translocate DNA molecules, (4) reliability of nanopore device, and (5) ease of rinsing.

For the measurements of current change during DNA translocation, we utilized current increase mechanism (reasons will be described in Chapter 4) in our system to detect DNA molecules. In this case, the amplitude of the signal during DNA translocation is given by[33]:

$$\Delta I_1 = \mu b \Delta n e \frac{V}{L_{pore}^2} \quad\text{.. (2.1)}$$

Where Δn is the number of charges introduced uniformly into a nanopore of length L_{pore} with a voltage bias V applied across it, e is charge of an electron, μ is ionic mobility, and b is the fraction of mobile counterions[6]. For the magnitude of noise, the equation of dominant (white) noise ΔI is given by[62]:

$$\Delta I = \sqrt{(\frac{4 k_B T \Delta f}{R})} \quad\text{... .... (2.2)}$$

Where k_B = Boltzman's constant, T = absolute temperature, Δf = signal bandwidth, and R = equivalent electrical resistance across the pore.

Equation (2.1) and (2.2) indicates that the amplitude of the DNA translocation signal depends only on the length of the pore, while the magnitude of noise depends on the equivalent electrical resistance across the pore.

With the factors stated above, we chose 500 nm for nanopore width since it has been demonstrated to detect λ-DNA molecule[35], can be fabricated easily with electron-beam lithography, and decreases the chance of having multiple molecules entering it simultaneously. For the height of the nanopore, the design consideration of its size is the similar to that of the width such detectable translocation signal and minimum chance of multiple molecules passing through simultaneously. However, the fabrication limit with soft-lithography sets the lower bound of its dimension, and here we chose 200 nm since it has been reported that for ~150 nm is the minimum achievable pore diameter of PDMS (Sylgard 184) with simple replica molding technique of soft-lithography[61]. For the length of the pore, electrokinetics theory in equation (2.1) indicates that when the whole molecule resides within the nanopore during translocation at low buffer concentration, the signal amplitude is inversely proportional to the square of nanopore length, while the noise is inversely proportional to the square root of the nanopore length (since R in

equation (2.2) = equivalent electrical resistance = $\dfrac{\rho L_{pore}}{A}$).

Previous experiments showed a current increase of ~15 pA for ~7 μm long PDMS nanopore[35]. From the reasoning above, we can increase the current signal-to-noise ratio by further decreasing the length of nanopore to 4 μm, which is close to the feature limit using UV contact photolithography aligner on SU-8 thick photoresist.

2.2.3 Overview of the fabrication process

The fabrication was similar to that of previous fabricated PDMS nanopore devices[35]. Briefly, nanopore devices were fabricated by micromolding in polydimethylsiloxane (PDMS). 200 nm thick, 500 nm wide titanium (Ti) metal lines were patterned using an e-beam lithography liftoff technique to define the nanopore. A thick layer of photoresist

(10 μm, SU-8) was patterned on top of the Ti features to define the connecting microchannels. The length of the nanopores was 4 μm. PDMS was cast on the mold, cured and peeled off, punched for input/output ports, cleaned with ethanol and isopropanol (IPA), followed by bonding to a glass slide using oxygen plasma. The device comprised two microfluidic channels with a single nanopore serving as the only electrical and fluidic connection between the two microchannels. The microchannel and nanopore dimensions were 0.8 cm x 1 mm x 10 mm and 4 μm x 500 nm x 200 nm (length x width x height), respectively. Figure 2.1 shows a schematic of the fabrication process of PDMS nanopore device used in the following chapters.
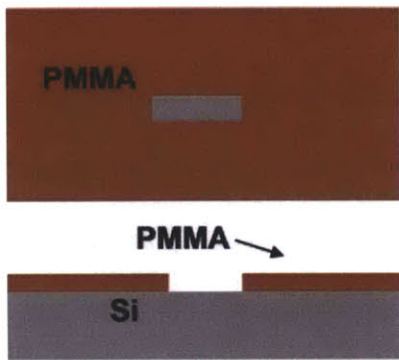
(a) Spin and pattern a nanotrench with electron beam lithography

(b) PVD 200 nm titanium thin film
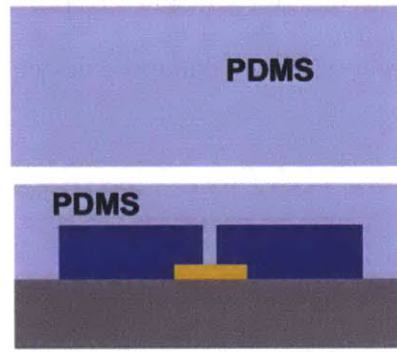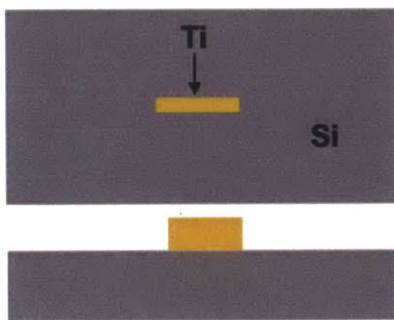
(c) Lift-off to have Ti nanowire as mold of nanopore

(d) Spin and pattern (UV lithography) photoresist for reservoirs' mold

(e) Pour PDMS on the mold
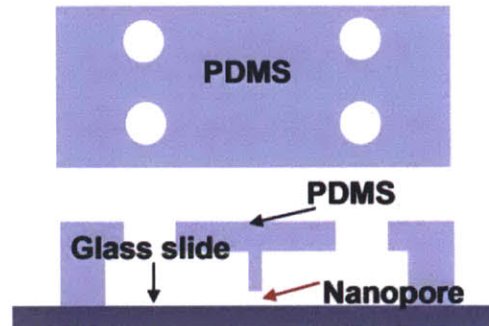
(f) Release from mold, punch PDMS, and bond it to glass slide

Figure 2.1 Schematic of the process for fabrication of the PDMS nanopore device.

2.2.4 Equipment used in the fabrication process

The master mold was fabricated in Massachusetts Institute of Technology (MIT)'s Microsystem Technology Laboratory (MTL) and the Scanning-Electron-Beam Lithography (SEBL) at the Research Laboratory of Electronics (RLE). Soft-lithography was done in our laboratory. Table 1 below lists various equipments used in the process, with a "machine coral name" by which they are known in the MTL and RLE at MIT, and a brief description.

Table 2.1 List of MTL and RLE equipment used in the fabrication process for the master mold.

Machine name	Description
Raith 150	Scanning electron beam lithography
Photo-wet	Photo-wet station for develop, lift-off, and rinsing process
PMMA spinner	Manual photoresist spinner specifically for PMMA
EbeamFP	E-beam evaporator
EV1	4" and 6" UV lithography system
SU8spinner	Manual photoresist spinner specifically for SU-8
Asher	Plasma system with Air, O_2

2.2.5 Fabrication of the master mold

A 4" silicon wafer was used as substrate for the master. A positive photoresist PMMA 950 A4 (polymethyl methacrylate, Microchem corporation) with 4% solid content in anisole was spun at 500 rpm for 5 s, and at 1500 rpm for 45 s to yield a film of 300 nm

thickness. Following this step, the wafer was soft-baked at 180 °C for 8 min to harden the photoresist. Following this step, PMMA was patterned using e-beam lithography to define the configuration of the nanopore. Since the length of the nanopore is defined by the spacing between the two SU-8 micro channels, the patterned length was chosen to be 100 μm to ensure the connection between two SU-8 microchannels. The width of nanopore was chosen to be 200 nm and 500 nm for the reasons stated in previous section. The dose factor for e-beam lithography was 70 $\mu A/cm^2$ to 90 $\mu A/cm^2$, and the electron-beam energy was 10 keV. PMMA was developed in MIBK/IPA 1:2 ratio (volume) at 21 °C. Since the mixing between MIBK and IPA is an endothermic process, it took ~ 3 hours to develop the PMMA after MIBK and IPA were mixed. Subsequently, the wafer was deposited with 200 nm of titanium (Ti) using e-beam evaporation. The thickness of Ti defined the height of the PDMS nanopore. Ti was chosen for its good adhesion to the silicon wafer. Subsequently, the wafer was submerged in acetone for 2.5 hours for lift-off, followed by rinsing with IPA and drying by nitrogen. Following this step, the substrate was cleaned with air plasma for 1 min, followed by 5 min of baking at 300 °C for dehydration. Without these two steps, the SU-8 would peel off from the substrate once developed. Negative photoresist SU-8 2007 was spun for 7 s at 500 rpm, and 1500 rpm for 40 s more to have a thickness of 10 μm. Following this step, the wafer was soft baked at 65 ° C for 1 min and 95 ° C for 2 more min. Gradual heating was necessary in both soft bake and hard bake to prevent the SU-8 from peeling off the substrate. Subsequently, the wafer was aligned and exposed with UV light at 10 mW/cm^2 for 13 s. Following this step, the wafer was hard baked to 95 °C for 5 min, and cooled down to 25 °C. Following this step, the pattern was developed with Propylene Glycol Monomethyl

Ether Acetate (PM Acetate) for 4 min, followed by rinsing with IPA, and drying with nitrogen. Subsequently, the wafer was hard baked to 150 °C gradually for 5 min to eliminate cracks in SU-8. Following this step, the master was ready for soft-lithography.

2.2.6 Soft-lithography for the PDMS nanopore device

Nanopore devices were fabricated using soft lithography in poly(dimethysiloxane) (PDMS) in our laboratory. Soft lithography enables rapid fabrication of devices once a master mold is fabricated. To aid removal of PDMS from the mold, the wafer was placed in a dessiccator with a few drops of tridecafluoro-1,1,2,2-tetrahydrooctyl-1-trichlorosilane (United Chemical Technologies) for 15 minutes. PDMS monomer and curing agent were mixed with the manufacturers-recommended 10:1 ratio and poured on the mold. The curing time and temperature are two critical factors that determine whether the PDMS nanopore would collapse. Here PDMS was cured at 80 °C for 2 days and removed from the mold. We punched two ports with 2 mm holes with micropunch (Ted Pella Inc.) for injecting DNA, and two 0.5 mm ports for rinsing. To ensure the surface cleanness, the PDMS device was cleaned with ethanol and IPA, and bonded to a clean glass slide using oxygen plasma for 40 s at low power in 0.65 torr at 7.16 W to result in a nanopore device (Figure 2.2). KCl or phosphate buffered saline (PBS) and DNA solution was injected right after the treatment of oxygen plasma bonding on the surface of nanopore PDMS devices. Once fabricated, the device was robust, allowing days of measurement. In order to measure the actual device geometry, we performed a current-voltage (I-V) measurement through nanopore in high buffer concentration. Since the length of nanopore is 4 um, and the conductivity of 1 M KCl is 11.38 S/m, the cross sectional area of the nanopore can be determined area to be 1.07×10^{-13} nm^2 with

the measured I-V curve of the fabricated nanopore in 1 M KCl (figure 2.3), which is ~7%

larger than projected nanopore cross-sectional area (200 nm x 500 nm).
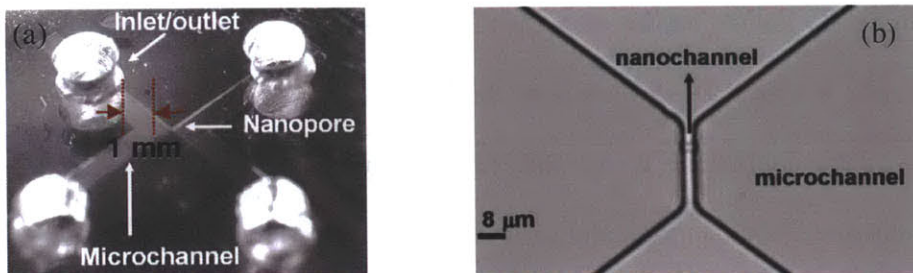
Figure 2.2 (a) Overview of PDMS nanopore device. (b) Two microchannels connected by

a nanopore of 200×500 nm $\times 4$ µm.
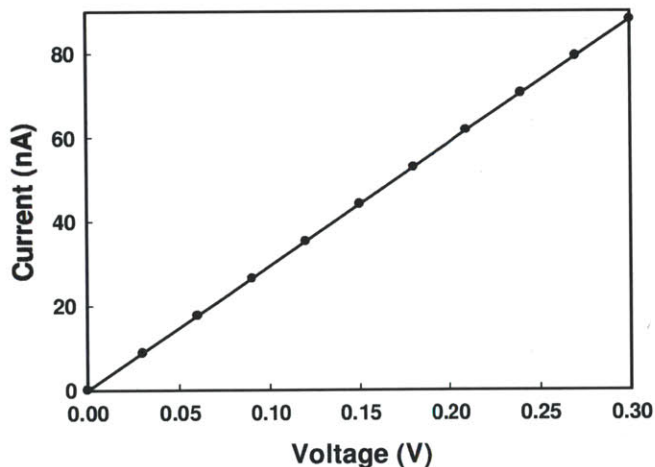
Figure 2.3 I-V curve of the PDMS nanopore device in 1M KCl.

2.3 Discussion

During the fabrication process of the 4 µm nanopore device, the major issue we

encountered was the unwanted connection between two adjacent SU-8 microchannel

molds. Since the length of nanopore was defined by the gap between two SU-8

46

microchannels that should only be connected by titanium wire, any unwanted connections between SU-8 in this gap will result in failure of the device.

In order to have the highest yield of the nanopore mold, i.e., nanopore device mold without any unwanted connection between microchannels, we performed the mold fabrication with different recipes such as the soft-baking time, post-baking time, precise control of temperature, UV lithography exposure mode using either continuous or pulse exposure, UV exposure time, thinner SU-8 layer, longer time in development solution after UV lithography and post-bake. Besides, special attention was paid to ensure hot plate flatness for heating and cooling of SU-8, and the cleanness and dryness of the wafer substrate before spinning on SU-8. No significant improvements were found through these sets of parameter tuning. The most probable reason for causing the low device yield was attributed to the non-uniform and inconsistent performance from the holder of photo mask in contact alignment lithography machine, since the successful device molds were distributed in a concentrated region, and we once had a yield of 100% when the photo mask stuck slightly to the substrate after UV exposure step.

Besides, the control of time duration between the detachment of PDMS from the mold and the irreversible bonding step is critical for maintaining the consistent performance of the device. It was found that under the recipe stated in previous sections, three days after the removal of PDMS from the mold is the optimal time to have uniform adhesion between PDMS surface and glass slide without leakage, but without having collapsed nanopore during irreversible bonding.

2.4 Conclusion

Here we have successfully fabricated a PDMS nanopore sensor device of 200 nm $\times$ 500 nm $\times$ 4 μm. The cleanness and dryness of the wafer, the uniformity of the hot plate for SU-8 soft-baking and hard-baking, the uniformity of lithography mask holder, the temperature and length of time for baking PDMS, the time between PDMS removal from the mold and irreversible bonding step, the cleanness of the PDMS surface before bonding to glass slide, are all important factors for having a successful nanopore device. In the next chapters we will use these devices for experiments multiple measurements with statistical averaging on analytes of 48.5 kbp λ-DNA, 40 kbp T7 DNA, and HindIII-digest λ-DNA.

Chapter 3 Implementation of feedback control for multiple measurements on the same DNA molecule

3.1 Introduction

As stated in Chapter 1, multiple measurements on the same DNA molecule has the potential to improve sizing resolution of the system. Figure 3.1 depicts the expected DNA motion and corresponding current behavior as a result of the implementation of feedback control; (a) a voltage bias is applied across the pore to drive DNA molecule through it. (b) When molecule translocates through the pore, it results in a current change. (c) After the DNA molecule completes translocation and exits the pore, ionic current returns back to baseline current. Subsequently, the voltage bias is reversed to bring the same DNA molecule back to the pore. (d) When molecule re-translocates through the pore, it results in another current change. (e) After it finishes translocation process and exits the pore, ionic current returns back to baseline current, and the voltage polarity is again reversed to recapture the same DNA molecule for another translocation. (f) Another cycle of the process starts.
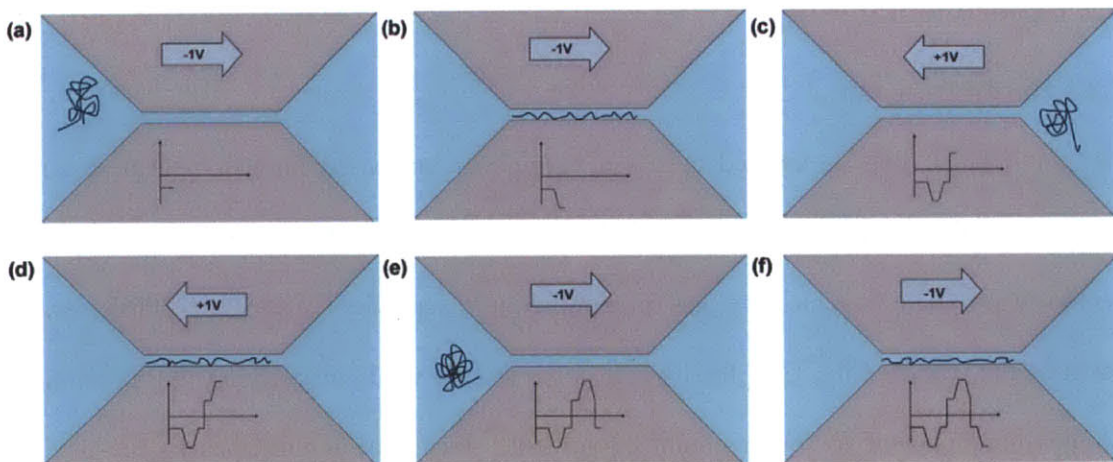
Figure 3.1 Manipulation of DNA molecule in a PDMS microfluidic-nanopore system for multiple measurements with feedback control on a single molecule. (a) DNA in the left reservoir, ionic current value equals to open-pore value. (b) When DNA translocates through the pore, the ionic current increases. (c) DNA in right reservoir, ionic current goes back to open-pore value (d) When DNA traverses through the pore, the ionic current increases. (e) DNA in left reservoir, ionic current goes back to open-pore value. (f) When DNA translocates through the pore, the ionic current increases.

In my Masters thesis, I have demonstrated two measurements on the same molecule using home-made LabVIEW algorithm along with Axopatch 200B current amplifier. However, such number of measurements is not sufficient to enable meaningful statistical averaging to improve measurement resolution. To address such drawback from the previous system, I will show the improvement in hardware setup and the optimization of the software LabVIEW algorithm, which enable hundreds of measurements on the very same single DNA molecule in this chapter.

3.2 Experimental setup

3.2.1 Hardware setup

Here, a voltage bias is applied across a nanopore, and based on the measured ionic current signals, a feedback control action is implemented. Since the ionic current falls within nano-ampere scale, we use a patch-clamp amplifier (Axopatch 200B, Axon Instruments, Union City, CA) for its low noise feature while magnifying the magnitude of measured current for downstream equipment. Electrical connections to the device

were made with Ag/AgCl electrodes (In Vivo Metric) and current measurements were taken inside a Faraday cage to shield from any electromagnetic interference (Figure 3.2). To record the DNA translocation signals, the current signal I_{pore} was transferred to the Axopatch amplifier, and filtered by embedded low-pass Bessel filter (80 dB/decade) at 1 kHz cutoff frequency to have maximum signal-to-noise ratio. Filtered current signal was first converted to voltage signal V_I, and then digitized at 20 kHz/16 bits using Digidata 1440A, and saved into hard disk in the computer with associated Digidata 1440A software.

For the implementation of feedback control for multiple measurements, current data was digitized at 20 kHz/16 bits using a Data Acquisition Card (DAQ) (PCI-6251M, National Instruments, Austin, TX) controlled by LabVIEW program (National Instruments). Based on the measured current signal, a magnitude of voltage V_{pore} across nanopore was applied by the Axopatch current amplifier, which was controlled by LabVIEW program's output voltage V_v (Figure 3.2).
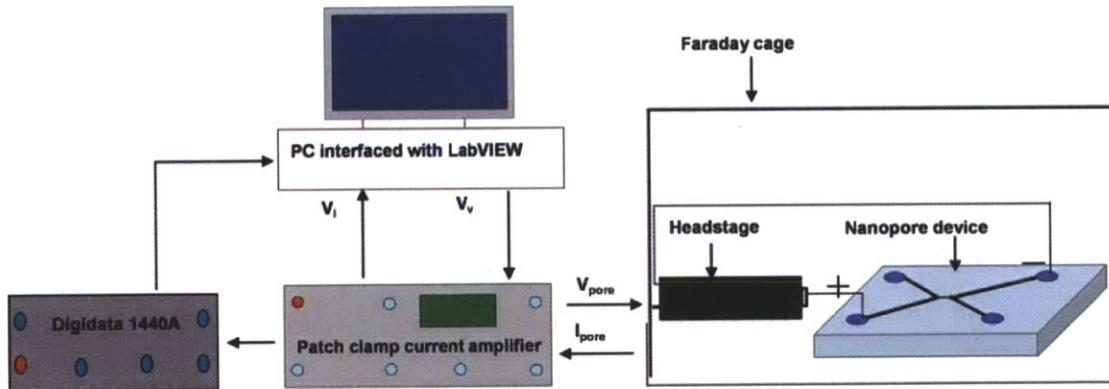
Figure 3.2 Experimental setup for measuring the translocation of DNA through a PDMS nanopore device.

3.2.2 LabVIEW algorithm

The objective of feedback control algorithm in LabVIEW is to toss the very same DNA molecule back and forth through the nanopore multiple times. The concept of the algorithm (Figure 3.3) is to (1) first detect the entry of a single DNA molecule into the nanopore, which results in an increase in the ionic current. Then, (2) the algorithm waits for 20 ms for DNA to complete its translocation and travel further into the other reservoir. (3) The voltage bias is reversed to translocate this DNA molecule back into the nanopore for the next measurement.
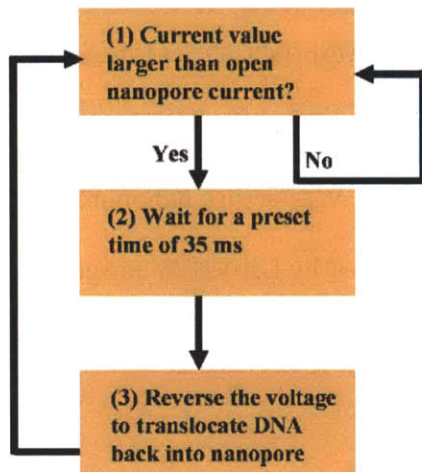
Figure 3.3 Flow chart of feedback control for multiple measurements on the same molecule.

Below we will first describe this algorithm in detail (figure 3.4), and show how it is implemented with LabVIEW later (figure 3.5-3.12).

(a) Algorithm

(A) The ionic current value was measured in real time t_o, and was compared with the baseline current I_b (ionic current value without DNA passing through the nanopore).

Since there was a continuous drift in the baseline current, its value was obtained by averaging ionic current from $(t_o - 5)$ ms to (t_o) ms. This current value was compared with real time ionic current value I_r, which was obtained by averaging ionic current from $(t_o - 2)$ ms to t_o ms.

(B) When $I_r - 8pA > I_b$, the algorithm waits for a set period of time (~20 ms) before reversing the voltage bias to bring the same DNA molecule back. As mentioned earlier, the increase of real-time ionic current is due to the entry of DNA into the nanopore. Since the magnitude of peak of current increase is about 13 pA, we set the criterion of 8 pA to ensure the entry of DNA event could be detected. The preset period of waiting time was to ensure the completion of DNA translocation, as well as to drive DNA molecule further away from the pore in the other reservoir, and therefore ensuring the translocation of recaptured DNA molecule taking place far from the ionic current overshoot due to sudden voltage reversal.

(C) After the voltage bias reversal, the algorithm waits for 5 ms before resuming the code for DNA translocation event identification. Such delay avoids false triggering due to current overshoot right after the sudden voltage change, and could correctly identify actual DNA translocation event even in the region of transient current region. After that, the algorithm will start from step (A) for another DNA translocation cycle.
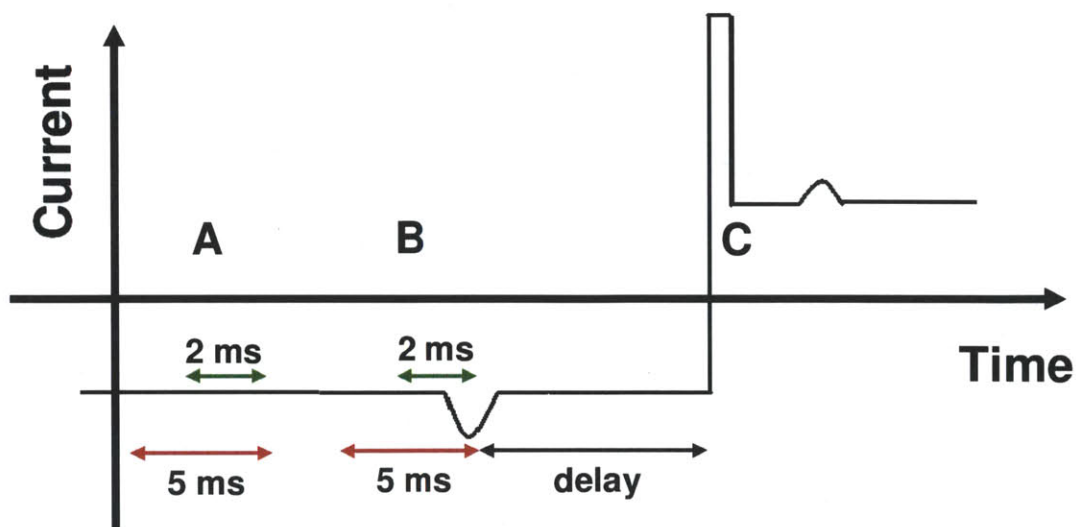
Figure 3.4 Schematic illustration of feedback control. Orange arrow corresponds to open pore nanopore current, black arrow represents real-time ionic current. (A) The algorithm compares real-time ionic current value with open nanopore current to see whether it is larger than open nanopore current. (B) When real time current is larger than baseline current by pre-specified amount, voltage reversal is triggered with a preset delay. (C) After voltage reversal, DNA identification code is paused for a short period of time to avoid transient current region and resultant false trigger.

(b)Implementation

Here we used LabVIEW to implement feedback control algorithm (figure 3.5-3.12). LabVIEW was chosen for its friendly graphical user interface (GUI) and powerful data acquisition card (DAQ). Our LabVIEW code comprises of three main blocks: (I) Time delay for DNA translocation identification, (II) DNA translocation identification, and (III) voltage output and reversal. The code executes by the order of II (detect DNA translocation) → III (reverse the voltage polarity) → I (delay for 5 ms to avoid false

triggering in large current gradient region) in a cyclic fashion. Figure 3.5 gives an overview of the whole program, while figure 3.6 to 3.12 gives detail explanations of each subpart. Below we will explain each subpart in the order of II→III→I in more detail.
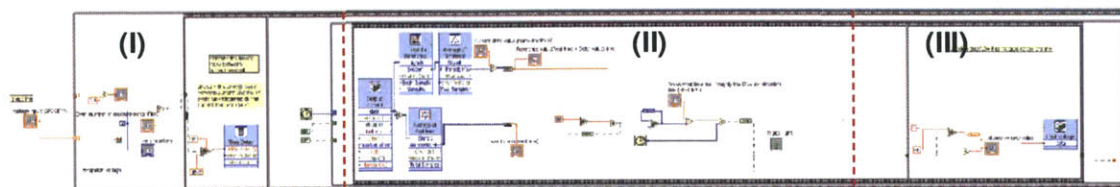
Figure 3.5 Overview of the program consists of (I) Time delay for DNA translocation identification, (II) DNA translocation identification, and (III) voltage output and reversal. Red-dashed lines were super-imposed to separate the adjacent blocks.

Block (II)

In section II (figure 3.6 -3.8), measured analog ionic current through nanopore was read, digitized, and then acquired by "DAQ input" (A) in figure 3.6. The sampling clock (or sampling rate) was 20 kHz, and acquisition mode was "continuous mode" to continuously read the converted signal without losing any information due to speed of the program or the computer (figure 3.7). "Continuous mode" sampling indicates that the DAQ hardware is continuously reading the voltage (which was converted from current) at the input and converting it into bits on the buffer (a place to temporarily store acquired but unprocessed digital data), at a rate dictated by the sample clock. Therefore, "continuous mode" sampling is the ideal choice when missing samples due to the speed of the program or the computer is of concern. The speed at which the DAQ hardware acquires samples is always given by the sample clock settings, and this part of the acquisition is entirely done by the hardware. Also, the size of samples to read was

chosen to be 100, which correspond to 5 ms length of the signal with 20 kHz sampling rate setting (figure 3.7). This choice determines the number of samples that were collected by "DAQ input" and stored in a buffer for every single loop execution. This number was optimized by trial-and-error in the range from 50-250 to ensure adequate processing speed by (1) minimizing the time spent on transferring data between DAQ hardware and LabVIEW software while (2) having the appropriate length of data segment for current spike identification. Also, we chose "differential" as our terminal configuration since the electrode of negative voltage side was connected to Faraday cage, and therefore does not share the same common ground with the rest of our nanopore measurement system. Besides, the differential configuration measures the difference between the positive and negative (grounded) voltage inputs and provides good rejection of common-mode voltage and noise (figure 3.8).
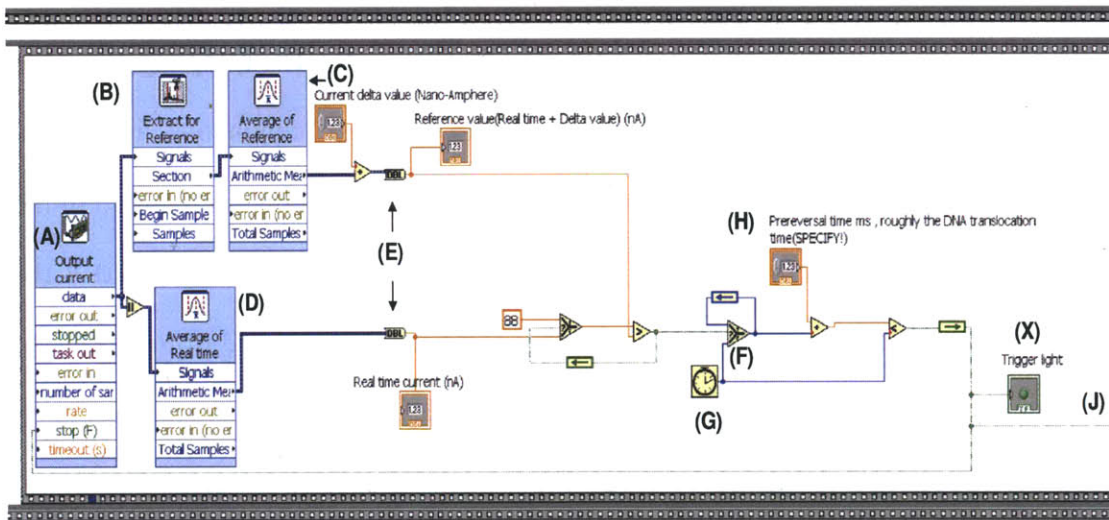
Figure 3.6 Block diagram (II), DNA identification part, of LabVIEW code for feedback control.
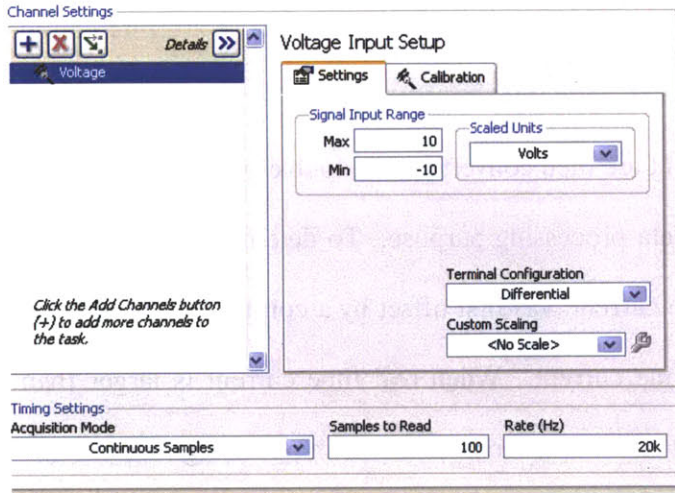
Figure 3.7 Details for "DAQ input" (A) in figure 3.6.
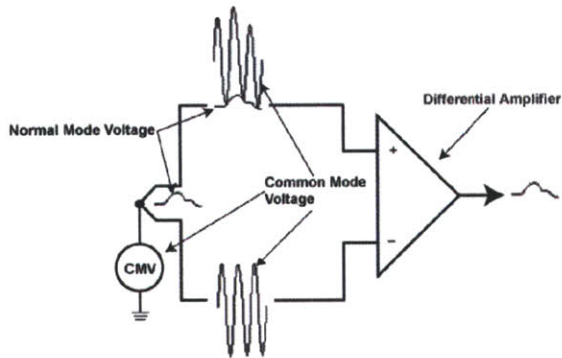
Figure 3.8 Differential terminal configuration rejects common-mode voltage (CMV) noise, thereby increasing measured signal quality.

Acquired signal from DAQ is shared by two streams. The first stream collects and extracts only 2-ms portion of the 5 ms samples by (B), and performs averaging by (C) to have real-time current value. The second stream collects the whole 5 ms acquired sample, and performs averaging by (D) function block to have baseline current, which may shift gradually during current measurement. Baseline current is compared with real-

time current continuously to monitor sudden current spikes that correspond to DNA translocation events. Also, small fluctuations due to high frequency noise are filtered out with aforementioned averaging blocks (C) and (D).

Both the baseline and real time current are then converted to a double-precision, floating-point number by (E) for following data processing purpose. To determine the existence of DNA translocation event, baseline current was first offset by a constant value of 8 pA and then was compared with real time current. When real time current is larger than baseline current by this pre-specified amount, it turns the Boolean number going into (F) from zero to one, and thereby starts the clock (G) before voltage reversal action. This delay for voltage reversal was designed to ensure the completion of DNA translocation through nanopore, and to drive DNA molecule further into the reservoir on the other side of nanopore. This delay reaches its end when the elapsed time (from the start of the clock) is larger than the amount set by (H). After that, voltage is reversed and the light (X) is switched on to indicate such reversal.

Block (III)

At this point LabVIEW has finished running codes in block II that identify DNA translocation, and starts running code in block III for reversing the voltage. The magnitude of voltage applied across the pore is either +1 or -1 volt, we will use (K) along with a Boolean number (J) from previous frame to implement voltage switching between these two values. Here voltage output is executed by "DAQ output" (L). The generation mode is set to be "1 sample (on demand)" since the voltage value applied will be changed only when another voltage reversal is needed (figure 3.9 and 3.10).
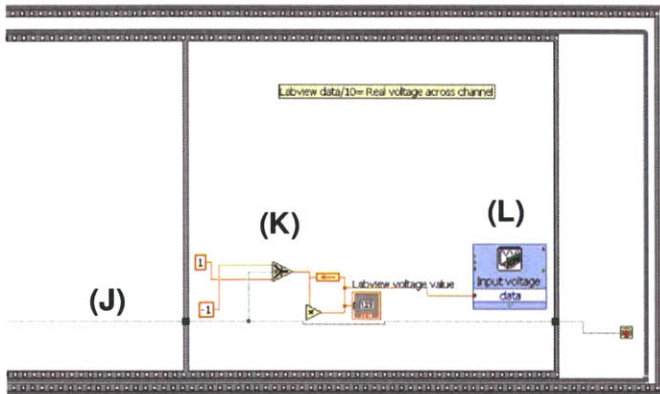
Figure 3.9 Block diagram (III), voltage output and reversal part, of LabVIEW code for feedback control.
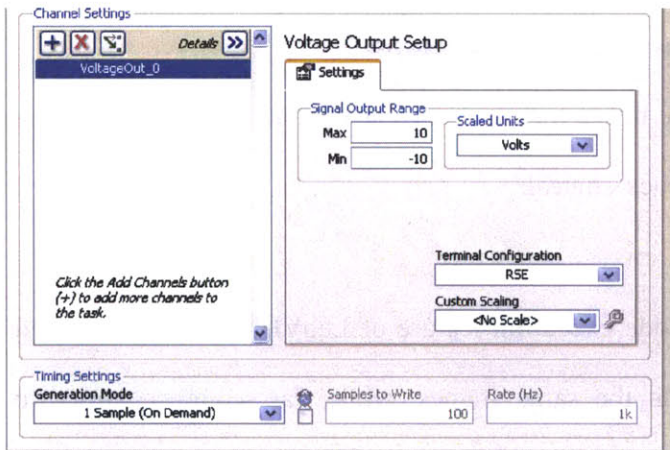
Figure 3.10 Details for "DAQ output" (L) in figure 3.9.

Block (I)

Now LabVIEW has finished running codes in block III that reverse voltage polarity applied across the nanopore, and starts running code in block I for delaying the ionic current measurement in the region of large current gradient. In block I (figure 3.11), a time delay (M) is initiated before the restart of current measurement and DNA

identification. This delay is enabled to avoid false triggering of another voltage reversal during transient current change of large gradient. After that, the code loop resumes back to frame where "DAQ input" receives and digitizes measured ionic current, and another cycle of the program repeats.
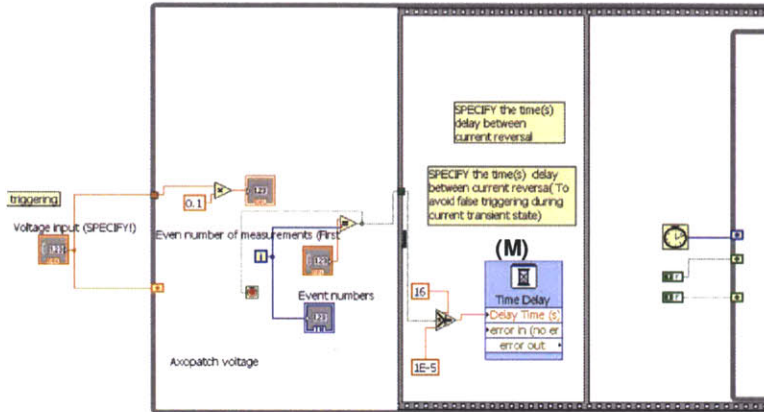
Figure 3.11 Block diagram (I), time delay for ionic current measurement after voltage reversal, of LabVIEW code for feedback control.

It is worth noting that the parallel code execution feature of LabVIEW is implemented whenever the code is constructed in the same frames, while flat sequence structure separated by solid line boundary (figure 3.5, and 3.6) ensures that a subdiagram executes before or after another subdiagram. Frames in a flat sequence structure execute from left to right and when all data values wired to a frame are available. The data leaves each frame as the frame finishes executing. This means the input of one frame can depend on the output of another frame. We utilize this feature to ensure voltage reversal takes place only after DNA translocation has been identified, while perform statistical averaging for and make comparison between real time and baseline current simultaneously.

Figure 3.12 shows the interface for the algorithm. It is worth noting that we only retain the necessary part of the code for feedback control to maximize our program execution speed, and remove feature such as real-time current plot or fast Fourier transform (FFT) for real time current trace.
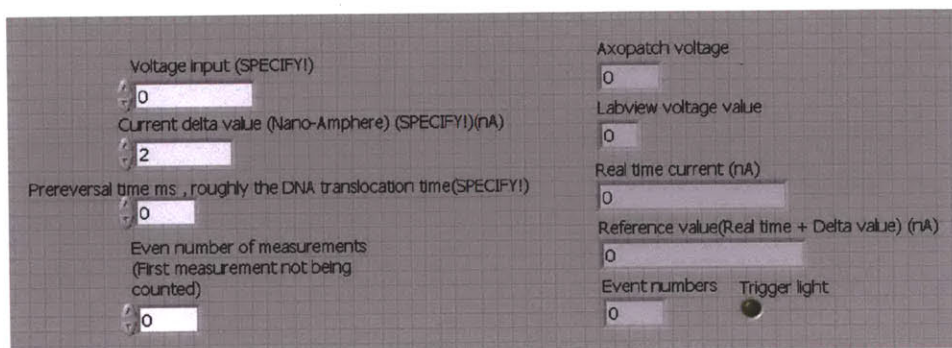
Figure 3.12 Interface of the LabVIEW code for feedback control.

3.3 Conclusion

In this chapter, we have shown the hardware setup and software implementation for ionic current measurements and implementation of feedback control algorithm in LabVIEW code. The setup are arranged to measure ionic current of nano-ampere scale while recapturing the same DNA molecule after its last translocation, and repeat such process cyclically. In the next chapter, I will show experimentally the success of multiple measurements with this setup, and the improvements of DNA sizing resolution.

Chapter 4 DNA sizing by multiple measurements with feedback control

4.1 Introduction

In conventional measurements, the analyte molecule escapes into the solution after a single measurement. As discussed in Chapter 1, nanopore sensing techniques measuring only one translocation of a given molecule may be insufficient to distinguish differences between different molecules in a given sample. Multiple measurements followed by statistical averaging have the potential to increase signal-to-noise ratio by narrowing down the initially scattered data distribution, and can therefore enable discrimination between different molecules of similar length.

4.1.1 Past work on multiple measurements

Researchers have used optical[63], magnetic[64], and pure electrical[55] approaches to implement multiple measurements, as described below.

(a) Optical tweezers: Keyser et al. used optical tweezers both as a tool to controllably insert a single DNA molecule into a nanopore and as a probe of electrical force on the DNA in the nanopore[63]. A polystyrene bead coated with λ-DNA molecule was trapped using an infrared laser, allowing control of its position in close proximity to the nanopore. An applied voltage bias across the nanopore drives a DNA molecule into the nanopore. As in a simple translocation experiment, insertion of a DNA molecule into the nanopore is detected by a change in the ionic current and a change in the bead position in the optical trap. In this way, the same DNA molecule could be flossed back and forth slowly (~100 bases/s) with the control of voltage polarity and restoring force from optical trap. Figure 4.1 explains the experimental setup and its working principle.
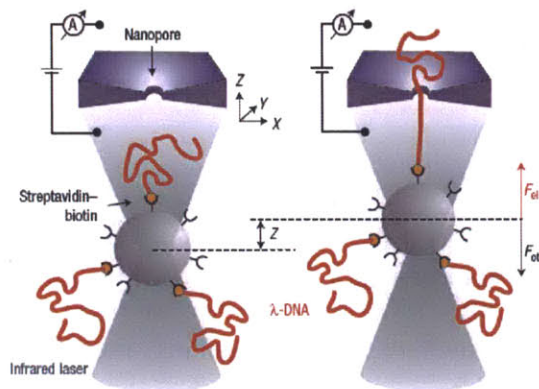
Figure 4.1 Experimental configuration DNA multiple translocation by optical tweezer. A tightly focused laser beam is used to trap a DNA-coated bead near a solid-state nanopore immersed in a saline solution (left). Application of a voltage bias drives an ionic current through the nanopore and the negatively charged DNA into the nanopore. When a DNA molecule enters the nanopore (right), an electrical force is exerted on the bead which is displaced to a position where the optical force and the electrical force are balanced[63].

(b) Magnetic bead: Although optical tweezer approach can be used to measure the force on the DNA molecule and control it to translocate at a very slow speed, this approach suffers from a number of fundamental drawbacks and difficulties. First of all, it is difficult to operate in a large number of nanopores in parallel. Secondly, due to the absorption of laser light by the buffer, the ionic current is coupled with the motion of the optical bead, and the absorption of laser light by the buffer causes the ionic current to fluctuate dramatically. Thus it is difficult to simultaneously measure ionic current while the DNA is being dragged in a dynamic fashion. Peng et al. adopted a magnetic tweezers approach that is effective in slowly flossing the same DNA molecule (~10^4 bases/s) back and forth through nanopore. The basic concept of the experiment is shown in figure 4.2.

DNA molecules are attached to magnetic beads via the streptavidin–biotin bonds. The free end of the DNA can be captured into the nanopore by the applied electric field. Subsequently, a precisely controlled magnetic force can be applied to the magnetic bead to balance the electrical force on the trapped DNA. Since one can construct a magnetic-field gradient over a large space, this technique is inherently applicable to a large number of addressable nanopores.
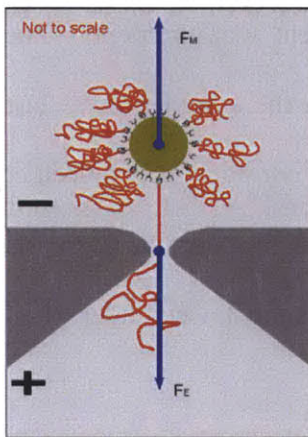
Figure 4.2 Schematic of the reverse DNA translocation using magnetic tweezers. Two reservoirs, filled with ionic buffer, are separated by a nanopore chip (shown in gray). A voltage bias is applied across the nanopore chip. DNA molecules (shown in red) are attached to the magnetic bead via streptavidin–biotin bonds. Electrical force F_E on the DNA and magnetic force F_M on the magnetic bead are depicted in blue[64].

(c) Electrical method: Although magnetic and optical tweezers can control and translocate the very same DNA molecule back and forth through nanopore for multiple measurements, the implementation requires complicated optical or magnetic setup, and the overall throughput is inherently low due to the nature of the implementation, and part of the molecule cannot be analyzed due to the its binding to a much larger bead.

Gershow et al. implemented multiple measurements on the very same DNA molecule (4 and 6 kbp) in SiN_x nanopore without the need of using biochemical binding procedures or optical/magnetic setup. A single DNA molecule is translocated through a nanopore under influence of a voltage bias. The DNA molecule is allowed to complete the translocation and escape the pore while monitoring the ionic current flowing through it, and the voltage bias is reversed to reverse the translocation direction and recapture the very same DNA molecule back to the pore for another current measurement. The recapture probability (~70%) depends on the duration between the completion of last translocation and following voltage reversal, the diffusion constant of molecule, geometry of the device, and the magnitude of voltage. A total of 27 measurements on the same molecule have been reported in the work. Figure 4.3 shows the device under TEM and its operation principle[55].
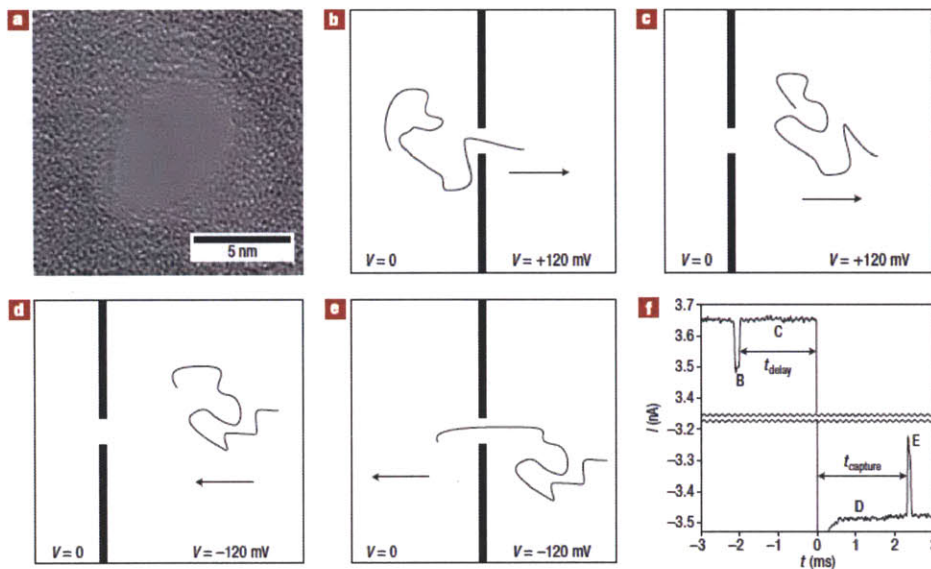
Figure 4.3 Overview of the recapture experiment. (a) Transmission electron micrograph of the SiN_x nanopore used. (b–e) Schematic representation of the experiment. The arrow represents the direction of the electric force on the DNA molecule. (b) A single DNA

molecule passes through the nanopore in the forward direction. (c) After passing through the pore, the molecule moves away from the pore under the influence of the electric field for a fixed delay time. (d) The field is reversed, and the molecule moves towards the pore. (e) The molecule passes through the pore in the reverse direction. (f) A representative current trace for an experiment with a 2 ms delay before voltage reversal. A gap of 6.6 nA is omitted from the middle of the trace. The letters mark the correspondence between the current trace and the schematic illustrations of molecular motion (b–e)[55].

4.1.2 Structure of Chapter 4

It is evident that multiple measurements by electrical method posses several advantages over the others such as high throughput, label and optics free, requiring no special biochemical processing steps, and simple electrical instrumentation setup. Multiple measurements on the same molecule with such method were demonstrated by other research groups[55]. However, the recapture probability and number of measurements on the same molecule is insufficient to enable meaningful statistical averaging.

To address this issue, we designed, fabricated, and set up a nanopore system that enables a large number of measurements on the same DNA molecule, and demonstrated that statistical averaging following multiple measurements can enhance DNA sizing resolution.

In the remaining of this chapter, we will first explain the theory of current change during DNA translocation, and explain our experimental setup for measurement and feedback control. Next, we will exhibit the functionality of our device by showing the detection of

λ-DNA molecule in our nanopore measurement system. Subsequently, we will demonstrate our implementation of hundreds of measurements and statistical averaging over three kinds of analytes: (1) Analyte solution with only λ-DNA (2) Analyte solution with λ-DNA and HindIII digest λ-DNA mixture, and (3) Analyte solution with λ-DNA and T7 DNA. For (1), we will show the improvement of the DNA signal distribution as a result of the methodology. For DNA mixture analytes in (2) and (3), we will show differentiation between different molecules. Finally, we will discuss the analytical model for physics of DNA recapture, perform numerical simulation of the DNA recapture process, and compare the result with experiments. The simulation and analytical model give us more insight into the reasons behind the success of DNA recapture, and help us design next generation nanopore measurement systems.

4.2 Theory for current change due to translocation of λ-DNA through a nanopore

Here the calculation of current change is based on the molecules of 48.5 kbp λ-DNA in KCl buffer solution, and the size of the nanopore is 200 nm × 500 nm × 4 μm. As stated in Chapter 1, the transport of DNA can affect the current in two ways[6,65]: (i) change of ionic concentration, and (ii) blockage of nanopore with DNA molecule. While mechanism (i) tends to dominate at low buffer concentration, mechanism (ii) tends to dominate at high buffer concentration.

For mechanism (i) that dominates in low buffer concentration, the current increases due to the negative charges on DNA molecules. The translocation of DNA will induce additional counterions (K^+ ions) to neutralize the net charges of DNA within the pore,

and therefore the ionic current will increase[6,31,65]. The expected current increase can be calculated by equation (2.1). With an ionic mobility of 7.9×10^{-8} m^2/Vs for KCl, $b = 0.5$, $\Delta n = 97004$, $L_{pore} = 4$ μm, and $V = 1$ volt, we expected the magnitude of current increase $\Delta I_1 \approx 37.5$ pA.

For mechanism (ii), bulk ionic current would decrease due to physical blockage by the DNA molecules. For particles of diameter much smaller than that of the nanopore, previous work on colloids[23] has shown that the ratio of peak height ΔI_1 to open pore ionic current I is approximately equal to the volume ratio of particle $V_{particle}$ to pore V_{pore}:

$$\frac{\Delta I_1}{I} = \frac{V_{particle}}{V_{pore}} \quad\quad\quad (4.1)$$

Where the theoretical open nanopore ionic current I under voltage bias V is[66]:

$$I = \frac{V \sigma A}{L_{pore}} \quad\quad\quad (4.2)$$

The radius of DNA strand $R = 1.1$ nm and the corresponding DNA length $L_{DNA} = 48502 \times 0.34$ nm $= 16.5$ μm, the volume $V_{particle}$ of λ-DNA would be $\pi \times R^2 \times L_{DNA} = 62341.8$ nm^3. As we have pointed out in section 3.2, the maximum ionic current that could be measured in our system is ± 10 nA. Therefore, from equation (4.1) maximum current change that can be measured due to blockage with single molecules of DNA in 200 nm $\times$ 500 nm $\times$ 4 μm nanopore is 10 nA $\times$ $(\frac{V_{particle}}{V_{pore}}) \approx 1.5$ pA, which is much smaller than the current change due to mechanism (i).

69

We therefore come to the conclusion that it is desirable in our system to use *low* buffer concentration so that the mechanism of current change when λ-DNA passes through the nanopore would be dominated by current *increase*.

Moreover, we now calculate the net current change $\Delta I = \Delta I_1 - \Delta I_2$ for DNA translocation events in 10 mM KCl solution. Here σ = conductivity of 10 mM KCl = 0.1332 Ω^{-1} m^{-1}, A = cross section area of the nanopore = 200 nm × 500 nm, L_{pore} = 4 μm, and V = 1 V. The theoretical open nanopore ionic current I is 3.325 nA. From equation (4.1), the magnitude of current decrease due to mechanism (ii) is $\Delta I_2 = I \times (\dfrac{V_{particle}}{V_{pore}}) \approx 0.5$ pA.

Since current increase ΔI_1 due to mechanism (i) was calculated to be about 37.5 pA, the net current change is $\Delta I = \Delta I_1 - \Delta I_2 \approx 37$ pA.

4.3 Experiment for DNA detection and translocation in 7 μm nanopore device

We first performed DNA translocation experiment without feedback to verify the functionality of the 7 μm nanopore device (In later sections we will use 4 μm one). The experimental setup used here is described in Chapter 3 in more detail. Briefly, a patch clamp current amplifier (Axopatch 200B) with Ag/AgCl electrodes was used to apply a voltage bias, record the corresponding ionic current through the nanopore, and filter the data (80 dB/dec) at 1 kHz cutoff frequency. The measured current data were digitized and recorded using Digidata 1440A and associated software.

To improve the device stability, bovine serum albumin (BSA, Sigma Aldrich) was introduced to prevent aggregation of DNA molecules inside the nanopore. 1 mg/mL of BSA dissolved in 10 mM KCl buffer was introduced into the device for 10 min, followed by rinsing with deionised water before introduction of DNA analytes. For experiment with single kind of DNA molecule, 48.5 kbp λ-DNA (500 μg/mL in 10 mM Tris-HCl pH 8.0, 1 mM EDTA) was obtained from New England BioLabs, Inc., and was diluted in 10 mM KCl buffer solution.

At low KCl concentrations, the effect of charges on 48.5 kbp double-stranded λ-DNA molecules results in current increase during translocation of the dsDNA molecule through a nanopore. With a voltage of -1V across the nanopore, and Δn (the number of charges introduced uniformly into a nanopore) = $48500 \times 2 = 97000$ we expect a current increase of about ~16 pA in our device, using equation (2.1). Figure 4.4 (a) shows ionic current through our 200 nm × 500 nm × 7 μm PDMS nanopore under a voltage bias of -1 V with 1 μg/mL 48.5 kbp λ-DNA in 10 mM KCl on only one side of the nanopore. The baseline current was ~1.86 nA, and the peak height due to DNA translocation is ~15 pA, which falls in the expected range based on the above calculation. Control studies with voltage polarity switched showed no molecule translocation current signature, which confirmed that events were due to translocation of λ-DNA, and the transport of DNA molecules was driven by electrophoresis (Figure 4.4b).
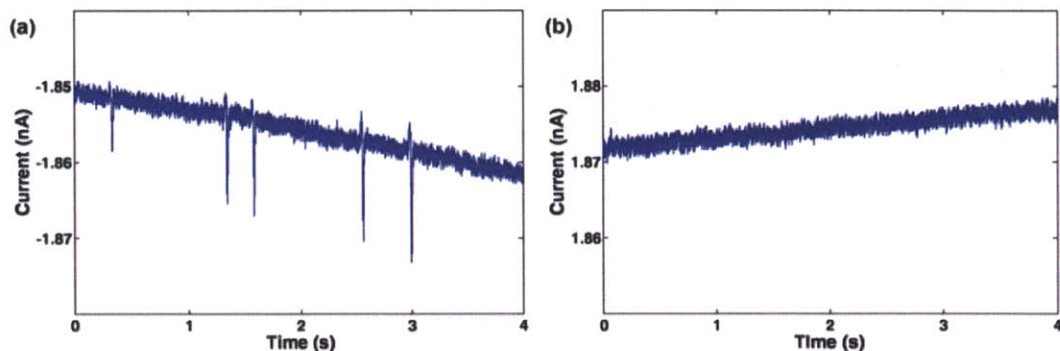
71

Figure 4.4 (a) Translocation signal obtained for a 1 μg/mL λ-DNA sample with a voltage bias of -1 V. Current increases by about 15 pA during the translocation due to charge effect. (b) No translocation signals were observed when bias polarity was reversed.

4.4 Multiple measurements on single λ-DNA molecules

4.4.1 Experimental setup

As described in more detail in Chapter 3, when performing feedback control and multiple measurements on single molecules, current data for identifying DNA translocation event was digitized using a DAQ controlled by LabVIEW (National Instruments). Here LabVIEW was used to send a voltage signal to the Axopatch amplifier to control the polarity of driving voltage (±1V) by identifying DNA molecule translocation event with a home-made algorithm. 1 μg/mL of λ-DNA in 10 mM KCl buffer solution was introduced on only one side of the nanopore, and reversal of the driving voltage was triggered upon detection of a DNA molecule in the nanopore. Entrance of a DNA molecule into the pore was determined, and voltage was subsequently reversed after a delay to recapture the same molecule after it completes the last translocation. The LabVIEW algorithm was designed to repeat this process as long as a translocation signal

was detected (Figure 4.5a and b). Current data was later saved as text file, and analyzed with MATLAB R14 (The MathWorks, Natick, MA) to construct figures such as histograms, scatter plots, and current history.

Figure 4.5 (a) PDMS nanopore device consists of two microchannels connected by one nanopore. Negative voltage bias is applied across the nanopore to drive the negatively charged DNA molecule (red) from left to right microchannel through nanopore. (b) After the completion of translocation, voltage bias is reversed to recapture the DNA molecule back to the pore for subsequent translocation. This process continues until the DNA molecule has escaped out of the nanopore, or translocation current signal is not large enough to trigger another voltage reversal. (c) Current trace of multiple measurements on the same DNA molecule of 48.5 kbp λ-DNA in 10 mM KCl. For clarity, only 13 out of hundreds of recapture events are shown.

4.4.2 Automated data analysis with MATLAB code

Automated data analysis was implemented using MATLAB for characterizing current change and duration for each DNA translocation, and constructing the corresponding histogram, scatter plot, current trace, and current change.

Data was first acquired at 20 kHz and then was subsequently digitally filtered by a moving average method over a window of 1 ms. The entry and escape of DNA translocation were determined by identifying the time at which current trace deviates from and resumes back to open nanopore current trace (Figure 4.6). Open nanopore current trace was determined by performing linear (first-order) interpolation within a time interval of 20 ms immediately before and after each DNA translocation event. Magnitudes of current change were determined as the difference between the average of open nanopore current at the entrance (black dot) and exit (red dot) of molecule, and the maximum current value during translocation (green dot).
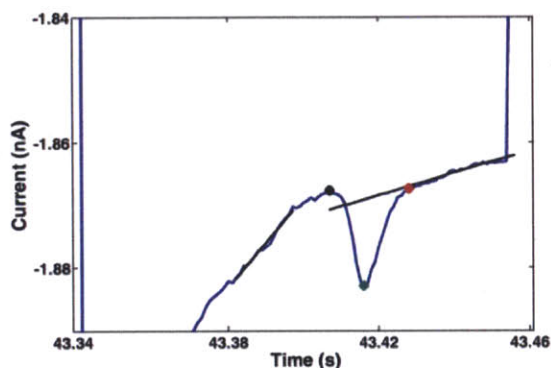
Figure 4.6 Determination of the time DNA enters and exits the nanopore. Black, green, and red dots indicate the time DNA molecule enters, translocates through, and exits the nanopore. Two regression lines were constructed in a time span of 20 ms before and after the translocation event.

4.4.3 Multiple measurements on single λ-DNA molecules

Figure 4.5 (c) shows a typical current-time trace recorded with the nanopore device using feedback control. The current remained near its baseline value till a translocation event was detected. This triggered voltage reversal, which resulted in a transient current response and a second translocation signal corresponding to the same molecule returning back into the nanopore. This process continued and multiple translocation signals were observed as the molecules traversed back and forth through the pore. Since the DNA molecules were not introduced on the other side of the pore, it implies that the DNA molecule was immediately recaptured after translocation.

Typical current trace patterns consisted of a large fraction of translocation events occurring in series, with a large number of uninterrupted sequences with >100 translocation events. The largest number of consecutive translocation events recorded was 561. Interruption of the sequence of multiple measurements occurred due to two reasons, namely failure to trigger feedback control, or due to the entry of a second DNA molecule into the nanopore. Failure to trigger feedback occurred when the algorithm failed to recognize a translocation event due to additional noise in the LabVIEW data stream, but in all such cases visual inspection of the data recorded by Digidata 1440A revealed the presence of a translocation event. Due to the fact that one side of the nanopore was exposed to a solution of DNA molecules, the possibility of a second molecule entering the nanopore was significant. We observed that when a second molecule entered the nanopore, the two molecules were tossed back and forth several times before one of the molecules escaped into the solution. While feedback control remained uninterrupted during this process, these sequences did not represent multiple

measurements on a single molecule, and the sequence was considered to be disrupted when a second molecule entered the nanopore. The fact that two molecules in close proximity of the pore simultaneously translocated through the pore multiple times suggests that interchange of a DNA molecule by another molecule was a rare event. Furthermore, upon examining >30 multiple measurement sequences, we never observed escape of a DNA molecule into the solution. Thus, the recapture rate was limited only by the feedback control and by the presence of other DNA molecules in solution.

4.4.4 Data analysis on multiple measurements on single λ-DNA molecules

As stated in Chapter 1, the measurement resolution can be improved by performing multiple measurements over the same molecule. In this case, due to the availability of having data with >100 multiple measurements over each molecule, we picked one series that consisted of 432 measurements on the same molecule, and performed statistical averaging over every 6 consecutive translocation events (figure 4.7). This number was chosen conservatively to exclude the possibility of interchange of DNA and to preserve the sharpness of the transition from measurement of one molecule to another in later section with DNA mixture, and was used here for data analysis uniformity.

Before statistical averaging, both translocation duration and current change are scattered over a wide region in the histogram and scatter plots (red dots). After statistical averaging, the distribution narrows down in both time duration and current change (blue circles). According to central limit theorem, the standard deviation of the distribution should improve inversely proportional to $6^{0.5}$ for the sample number of six. Such improvement was verified by the resultant averaged histogram superimposed with predicted curve assuming a Gaussian distribution.
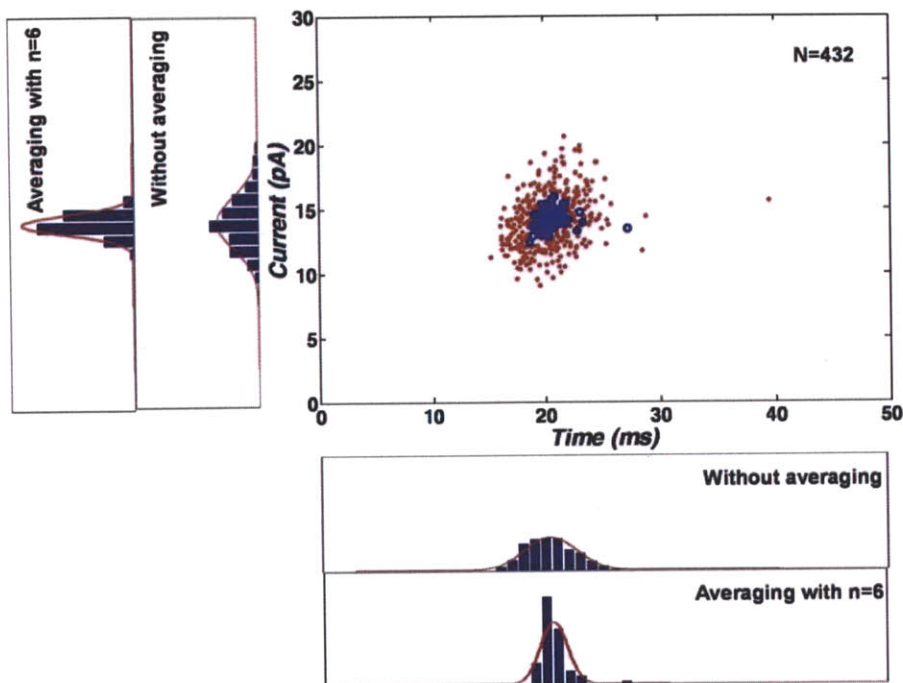
Figure 4.7 Scatter plot of translocation time and signal amplitude of multiple measurements (N = 432) on the same DNA molecule. Red dots indicate translocation events, while blue dots indicate the average of 6 consecutive events. The fitted Gaussian curves narrowed down significantly after averaging over multiple measurements, hence increasing the resolution of nanopore system.

4.5 Measurements on λ-DNA and HindIII-digest λ-DNA mixture

4.5.1 Experimental setup and materials

After showing that statistical averaging over multiple measurements on a single molecule resulted in a decrease in the measurement noise, we investigated whether multiple measurements using feedback control could enable discrimination between molecules that were otherwise difficult to distinguish using the same nanopore without multiple measurements. Here we picked a DNA mixture consisting of λ-DNA and HindIII-digest

λ-DNA since HindIII-digest λ-DNA has several DNA fragments (23.1, 9.4, 6.6, 4.4, 2.3, 2.03, 0.56, and 0.13 kbp) with largest one having 50% of the length of λ-DNA.

Equal concentrations (1 μg/mL) of 48.5 kbp λ-DNA and its HindIII digest fragments (500 μg/mL in 10 mM Tris-HCl pH 8.0, 1 mM EDTA, New England BioLabs, Inc.) were dissolved in 10 mM KCl to a final concentration of 1 μg/mL of λ-DNA and 1 μg/mL of HindIII digest fragments. The DNA mixture in KCl buffer solution was loaded on one side of the nanopore and analyzed using feedback control. While current data was measured and digitized using Axopatch 200B interfaced with Digidata 1440A, feedback control was implemented using Axopatch 200B interfaced with LabVIEW. For the sake of comparison, the experimental procedure for DNA mixture was the same with single DNA experiment in that the feedback control was interrupted periodically and the voltage bias was held at zero to enable a different molecule to enter the nanopore.

4.5.2 Data analysis of multiple measurements on DNA mixture

The amplitude and duration of current change during translocation were extracted as described in section 4.4.2, followed by statistical averaging over every 6 consecutive translocation events. Here we showed the advantages of multiple measurements by presenting the average current change of each 6 translocation events in a chronological order. Chronological ordering of the averaged amplitudes of current change revealed a characteristic pattern consisting of fluctuations around a certain value for several measurements and sudden jumps to other values that occurred when feedback control was interrupted or the molecule escaped (Figure 4.8a). The fact that amplitudes of current change fluctuated around certain values for a while and abruptly jumped to another value indicate that the molecule being measured was replaced by another molecule with

different amplitude of current change corresponding to a different size. In contrast, when only λ-DNA molecules were introduced into the device, these sudden jumps were absent (except for one aberration that was discarded) and the current fluctuated around a value that did not change during the entire measurement of about 1800 events (Figure 4.8a, inset). The advantage of feedback control for consecutively performing multiple measurements on the same molecule can be further appreciated by considering Figure 4.8b which shows the result obtained by scrambling the order of the original data followed by statistical averaging. In this case, statistical averaging does not yield useful information and it is difficult to see that there are different types of molecules translocating through the nanopore.
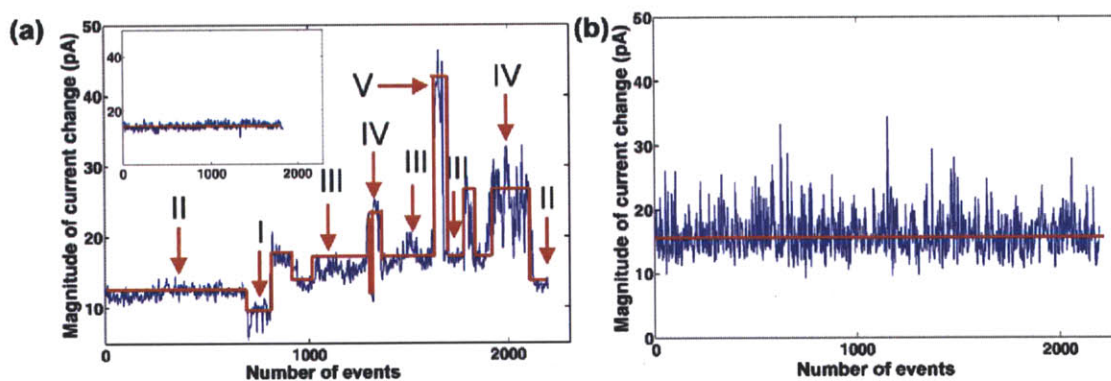
Figure 4.8 (a) History of current change of a mixture of DNA (1 μg/mL λ-DNA and 1 μg/mL HindIII digest fragments) Inset: History of current change with only 1 μg/mL λ-DNA in solution does not show abrupt changes in the current. (b) Scrambling the order of the original data followed by statistical averaging.

Figure 4.9 depicts scatter plots of current change and translocation duration for the case of λ-DNA and a mixture of λ-DNA and its HindIII digest fragments. Only the largest

fragment of 23.1 kbp length was capable of triggering feedback control in the system; some of the smaller fragments (<10 kbp) could be detected, but could not trigger voltage reversal due to their small signal amplitude. Without statistical averaging, the scatter plots in the two cases (Figure 4.9a,b) show some differences, but it is not possible to distinguish between different types of molecules in the scatter plots. Upon statistical averaging over 6 consecutive events, the spread in the scatter plots decreases, and several different groups are evident in the case of λ-DNA and its fragments (Figure 4.9d). Due to the wide distribution of the amplitude of the current change signal for the DNA molecules without averaging, histograms of current change resembled one Gaussian peak regardless of whether the solution contained only λ-DNA (Figure 4.9e, inset) or a mixture of λ-DNA and its HindIII digest fragments (Figure 4.9f, inset). Interestingly, the distribution of the amplitudes of current change corresponding to the case of only λ-DNA converged to one group with a significantly narrower distribution after performing statistical averaging over every 6 consecutive events (Figure 4.9e). However, after statistical averaging, the distribution in the case of λ-DNA and its fragments revealed five distinct groups (Figure 4.9f), with the dominant group corresponding to a current change near 13 pA, which may be attributed to translocation of single 48.5 kbp λ-DNA molecules. Assuming that the current change scales linearly with the length of DNA molecules, the small peak around 7 pA may be attributed to 23.5 kbp HindIII digest fragments. The 18 pA group may correspond to a combination of 48.5 kbp λ-DNA and its 23.5 kbp fragment, since one end of the 23.5 kbp fragment has a sticky end that is complementary to one of the sticky ends on λ-DNA molecules[67]. A combination of two or three molecules of 48.5 kbp λ-DNA either due to sticky ends or entanglement is likely

to explain the groups around 26 and 40 pA. Interestingly, these groups were absent in the case of measurements performed in the solution containing only λ-DNA.

Figure 4.9 Comparison between scatter plots and histograms with and without averaging of current change and duration obtained for a solution with only 48.5 kbp λ-DNA and a mixture of 48.5 kbp λ-DNA and HindIII digest fragments. (a) Scatter plot of 48.5 kbp λ-DNA before statistical averaging. (b) Scatter plot of a mixture of DNA molecules before statistical averaging. (c) Scatter plots converge into one group after statistical averaging for 48.5 kbp λ-DNA molecule. (d) Scatter plot converges into several groups after statistical averaging for a mixture of DNA molecules. (e) and (f) are histograms of current change upon statistical averaging over every 6 consecutive events for only λ-DNA and mixture of DNA, respectively. Histogram converges to one Gaussian peak for single DNA, but splits into multiple Gaussian peaks for a mixture of DNA. However, both analytes yield a distribution of one Gaussian peak without averaging (Inset of figure (e) and (f)). The dominance of larger signals is due to sticky ends, and the fact that the algorithm does not enable feedback of fragments smaller than 10 kbp.

4.5.3 Examination of DNA dynamics with the aid of multiple measurements

The ability to perform consecutive measurements on single molecules also enabled observation of interesting dynamics of DNA molecules translocating through the nanopore. In the case of a mixture of λ-DNA and its fragments, large amplitude signals were seen to decompose into two signals of smaller amplitude, suggesting potential dissociation or disentanglement of two DNA molecules that were initially joined by sticky ends. Figure 4.10 shows a single large signal that decomposed into a larger and a smaller signal. These two signals appeared together for several feedback cycles, presumably due to simultaneous translocations through the pore. At one point, only the smaller molecule translocated through the pore before voltage reversal was triggered, leaving the larger molecule on the other side. The smaller molecule then returned back to the original side, and both molecules were seen to translocate after the following voltage reversal. Several observations of similar dynamics were made during the experiments. These observations lend further support to the hypothesis that the larger amplitude signals observed in the case of a mixture of λ-DNA and its fragments were due to combinations of DNA molecules.
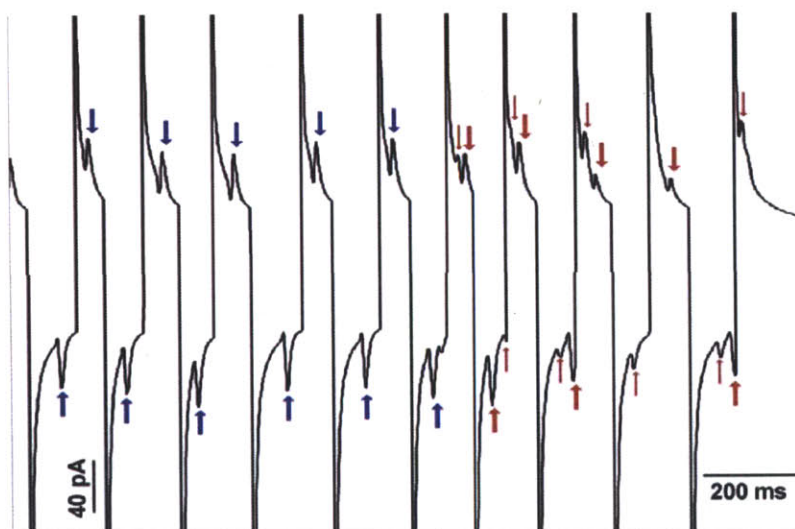
Figure 4.10 Current vs. time traces during feedback control of a mixture of λ-DNA and its fragments. A single large signal (blue arrows) was seen to break up into one small and one larger signal (small and large red arrows) that translocated together for a few cycles. Since feedback was triggered by a single translocation, at a certain point one molecule was left behind (only one red arrow), but reappeared in the following cycle, and again disappeared. Current reversal was not triggered in the final translocation.

4.5.4 Correlation of the amplitude of current change during translocation with the magnitude and rate of change of the baseline current

Several reasons could result in different regions of current changes when analyte consists of a mixture of different DNA molecules. Firstly, change of buffer concentration because of evaporation would result in fluctuation of open nanopore current, and differences in open nanopore current might yield different current changes for translocations of the same molecule. We therefore examined the correlation between open nanopore current and magnitudes of current change of only 48.5 kbp DNA molecules. Figure 4.11 (a)

shows the correlations between current change and open nanopore current in one measurement series. By fitting first order curve onto the data points, we arrive at a negative correlation with coefficient of determination R^2 of only 0.0265, indicating that there is little evidence showing a consistent correlation between the two.

Secondly, the time of the molecules being recaptured back through the nanopore is in the range where ionic current is in the transition region after instantaneous voltage reversal. We therefore inspected the correlation between the rate of change of open nanopore current and magnitude of current change. Figure 4.11 (b) shows correlations between the rate of change of open nanopore current in transition region and current change during DNA translocation in one measurement series. By fitting first order curve onto the data points, we arrive at a negative correlation with coefficient of determination R^2 of only 0.002, indicating that there is little evidence showing a consistent correlation between the two. With this reasoning, we attribute the various groups of current change indeed to different lengths of molecules being trapped and measured multiple times.
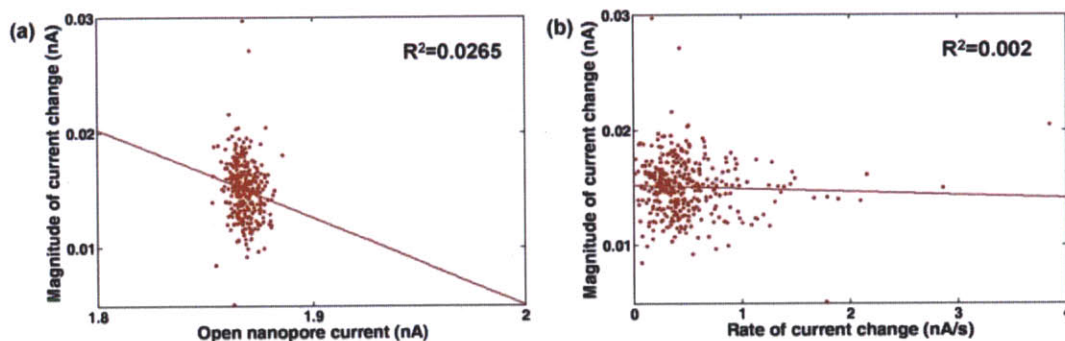
Figure 4.11 (a) First order linear regression line showed no significant correlation between open nanopore current and magnitude of current change during DNA translocation. (b) First order linear regression line showed no significant correlation

between rate of current change and magnitude of current change during DNA translocation.

4.5.5 Discussion

From multiple measurements to post-experiment data processing, there were some imperfections at each stage of the whole process. Below we list the issues by the order of experiment flow.

(a) Recapture of λ-DNA molecules in the device

The recapture rate was determined by the number of continuous DNA molecule recapture events immediately after each voltage reversal in one series without interruption. The feedback control system required a threshold magnitude of current change of about 4 pA, below which voltage reversal could not be triggered. Hence, DNA fragments smaller than about 10 kbp were not able to trigger voltage reversal. However, for 48.5 kbp DNA molecule with an average current change of 13 pA, hundreds of successive recapture events were easily obtained. Typically, >60 measurements were achieved. Failure to achieve a larger number of measurements was limited by two factors: (a) interruption due to a second DNA molecule entering the nanopore, and (b) failure of the algorithm to trigger voltage reversal because the translocation current signal was too small. In the second case, the translocation signals were all observable when the current traces were inspected manually, indicating that the molecules were still recaptured successfully back to the nanopore.

(b) Interchange of DNA molecules during multiple measurements

When the same molecule is being tossed back and forth through the nanopore, there is a possibility that another molecule would come into the pore to displace the one being

measured. Several observations suggest that this phenomenon was not significant in our data. Firstly, the time between each DNA translocation was ~320 ms and 8 s under forward bias and reversal bias, respectively. When a molecule was being tossed back and forth, the time between each voltage reversal and following molecule being recaptured was ~40 ms when molecule was at either side of the pore. In other words, the recapture time was consistently about 8 times and two orders of magnitude shorter than the time between voltage reversal and following molecule translocation back to the pore during forward and backward voltage bias, respectively.

Moreover, if it were not the same molecule being translocated back and forth, current change of a mixture of DNA molecules would have exhibited current change of different molecules like that of Figure 4.8b. In addition, we observed that when the pore captured another molecule from the reservoir before voltage reversal was triggered, multiple translocation events would happen a few times with positive voltage applied at either side. Therefore, molecules being tossed before and after these multiple translocation events were considered as different molecules in our data analysis.

(c) Data processing

For events in current history of single λ-DNA, a few series of measurement events were disregarded due to (1) Current behavior was too difficult to characterize molecule translocation time or magnitude of current change (figure 4.12). (2) Frequency of multiple DNA translocation events through the pore rose occasionally because the local DNA concentration varied around the entry of the nanopore. Corresponding scatter plot and histogram were all constructed from the same events being extracted for current history. In addition, figure 4.12 also demonstrated that the event of DNA molecules

conjugating to each other also take place when analytes consists of only 48.5 kbp λ-DNA, hence results in abnormally large magnitude of current change during translocation.
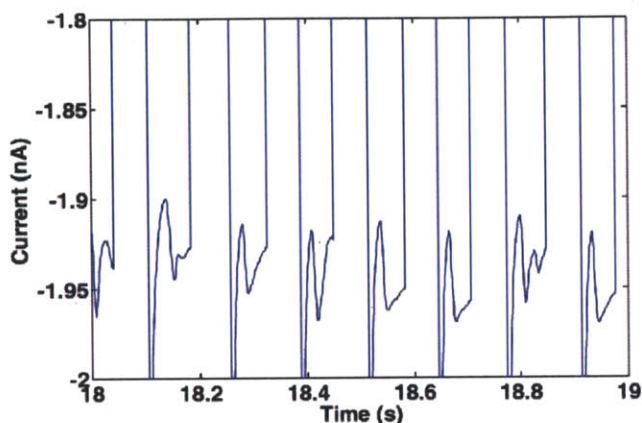
Figure 4.12 48.5 kbp λ-DNA molecules conjugated to each other during translocation.

For the experiment with a mixture of DNA molecules, a few series of measurement events were discarded. To be specific, a portion of multiple measurements series corresponding to 13 pA was discarded due to its repeated large number of translocation events at this value, and therefore including data of all 13 pA change makes the other series of data less obvious in the histograms. In addition, a few series of events with a low number of translocation events were discarded. Such series with a low number of translocation events took place due to either failure to trigger voltage reversal because of too small of the current change, or multiple DNA translocating through the nanopore simultaneously. Corresponding scatter plot and histogram for a mixture of DNA in figure 4.9 were all constructed from the same events being extracted for current history in figure 4.8.

4.6 Multiple measurements on DNA mixture: T7 and λ-DNA

After showing multiple measurements on DNA mixture of λ-DNA and HindIII-digest λ-DNA, we chose to further demonstrate the capabilities of multiple measurements on a different DNA mixture. Due to the limitation of our PDMS nanopore measurement system, we aim to have a recapture experiment with clean translocation signal for all DNA analytes, high recapture rate, and a reliable device that can be used over days. Towards this goal, we made several improvements on device design, DNA mixture analytes, and buffer type.

4.6.1 Experimental setup, nanopore device, and materials

(a) **Device design:** Since the magnitude of current change for DNA translocation is inversely proportional to the square of nanopore length, we fabricated and measured the translocation with a nanopore of 4 μm length so that the majority of the voltage drop would be dissipated across the nanopore (previous device has length of 7 μm), therefore yielding more easily detectable DNA translocation current signals. Details of the fabrication process of the 4 μm pore devices are described in Chapter 2. The dimensions of the microchannel (0.8 cm × 1 mm × 10 μm, length by width by height) led to an electrical resistance roughly 50 times smaller than that of nanopore (4 μm × 200 nm × 500 nm). Besides, a sufficiently strong electric field outside the nanopore is needed to enable a high recapture probability, and the geometry was therefore designed to have an electric field that dominates over diffusion at relevant distances away from the nanopore entry. Since the cross-sectional area of nanopore is an order of magnitude smaller than that of connecting microchannel, the distribution of electric field around the entry was assumed to be spherically symmetric. Under such condition, we calculated the location

where the combined electrokinetic velocity equals to the diffusion velocity as the "recapture radius"[55] (Details of recapture radius are explained in section 4.7). Since our geometry is ¼ of a sphere instead of ½ because the nanopore is at the bottom of the microchannel, the radius of recapture, $R = \mu I/\sigma \pi D = 95$ μm, with $I = 4$ nA, $\mu = 4 \times 10^{-9}$ (m²/V s), $D = 4 \times 10^{-13}$ (m²/s), $\sigma = 0.1441$ S/m (expected baseline current, diffusivity and mobility of λ-DNA, and theoretical conductivity). This radius is much larger than the microchannel height. When the distance away from the nanopore exceeds that of the height of microchannel, the 3-D spherical environment becomes 2D, which further confines the electric field for recapturing the molecule. Therefore, the large recapture radius, and the 2D confinement when the distance away from the channel exceeds the channel height, are indicators of a high recapture probability.

(b) Buffer choice: For the type of buffer used in the experiment, we diluted 1X Phosphate Buffer Saline (10g NaCl, 0.25g KCl, 1.8 g Na_2HPO_4, 0.3 g KH_2PO_4, 1000 mL H_2O) at pH=7.4 by a factor of 15. Using a buffer instead of pure KCl electrolyte reduced fluctuations in pH variation. Since the surface charge on the nanopore is a function of pH, buffering the solution should decrease variations in the conductivity of the pore relative to pure electrolyte.

(c) DNA analytes: For DNA analytes, we picked a DNA mixture containing λ-DNA and T7 DNA. The length of T7 (39.9 kbp) is 20% shorter than that of λ-DNA (48.5 kbp). Under our nanopore measurement system, it was shown that translocation signals at a driving voltage of ±1 V yielded sufficiently large translocation amplitudes and durations (20-50 pA, 4 ms) for automated real-time detection with LabVIEW.

To prepare the device for the experiment, the nanopore surface was passivated with bovine serum albumin (BSA, Sigma Aldrich) to prevent adhesion of the DNA molecules to the surface of the nanopore. 1 mg/mL of BSA was dissolved in $^1/_{15}$X (diluted from 1 X) phosphate buffered saline (PBS, σ = 0.1441 S/m, pH 7.4) and flowed into the device for 10 min before introduction of DNA. The resultant solution had an estimated conductivity of σ = 0.1441 S/m, and it was calculated from first principles using the electrophoretic mobilities of the ions (5.4$\times$ 10^{-8} m^2/V.s for sodium ions and 8.1$\times$10^{-8} m^2/V.s for potassium ions). The concentration of NaCl was roughly 11 mM, which is equivalent to 7.7 mM KCl based on the ratios of their electrophoretic mobilities. By choosing a relatively low ionic concentration, the device yields significant current increase while having negligible current decrease due to the current blockage effect[17]. DNA samples (48.5 kbp λ-DNA, New England Biolabs and 39.9 kbp Bacteriophage T7 DNA, Boca Scientific) were dissolved in 1/15X PBS to a final concentration of 1 μg/mL of λ-DNA, or a mixture of 1 μg/mL of λ-DNA and 1 μg/mL of T7 DNA. The DNA solution was then injected on one side of the nanopore, while the other side was injected with only 1/15X PBS solution. The setup for measurement hardware and software LabVIEW control algorithm was the same with the one used in previous multiple measurement experiment.

4.6.2 DNA detection and translocation

Figures 4.13 a,b depict the nanofluidic device, which comprises a single nanopore connecting two microchannels on either side. At low buffer salt concentrations (1/15X PBS) with an applied bias of 1 V, the devices were capable of detecting single molecules of λ-DNA (48.5 kbp) and T7 DNA (39.9 kbp) from the transient increase in ionic current

through the channel (ΔI). The transient current increase is due to the introduction of mobile counter-ions screening the inherent charge on the DNA molecules into the nanopore[17,65]. Assuming that the entire DNA molecule is enclosed in the nanopore, we expect a current increase of 15.6 pA for λ-DNA and 12.6 pA for T7 DNA using equation (2.1) ($\mu = 5.4 \times 10^{-8}$ m^2/Vs for Na$^+$, $b = 0.3$ for ~10 mM NaCl salt concentration[32,68]), which is consistent with the observed translocation current increase of 20-50 pA (figure 4.14).
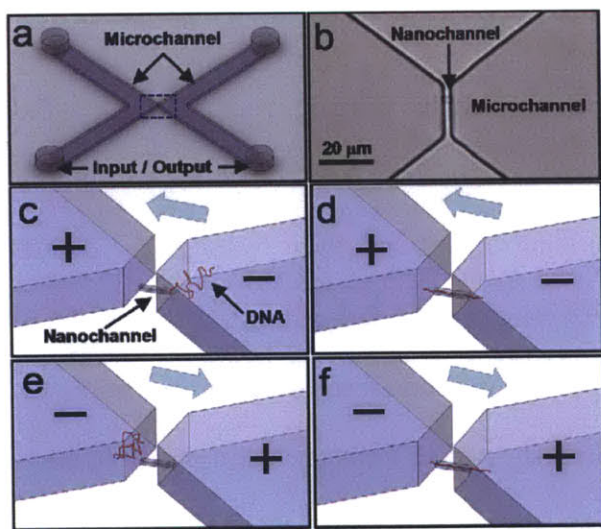
Figure 4.13 Nanofluidic device. (a) Schematic of device showing inlet and outlet reservoirs and microchannels. (b) Micrograph of the device (dotted area in (a)) showing a 200 nm $\times$ 500 nm $\times$ 4 μm nanopore that connects the two microchannels. (c,d) Application of a voltage bias across the nanopore drives the DNA into the nanopore. (e,f) Upon completion of the translocation, the voltage bias is reversed to translocate the same molecule in the reverse direction. This process is repeated to obtain multiple translocations of the same DNA molecule through the nanopore[33].
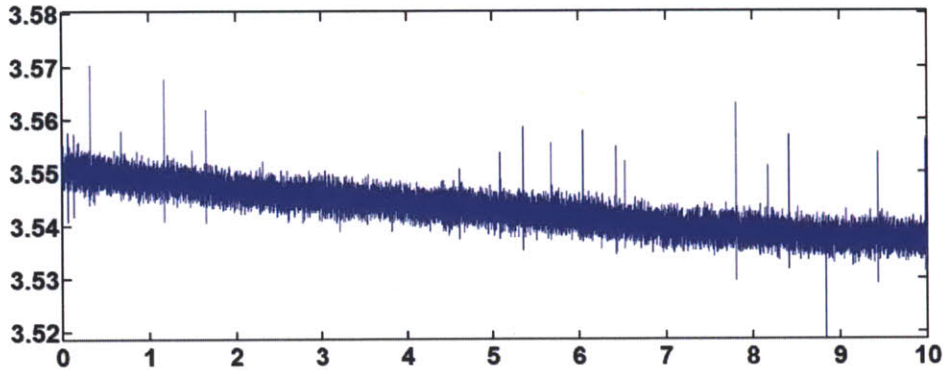
Figure 4.14 λ-DNA translocation signals in 1/15X PBS in 4 μm PDMS nanopore device.

At relevant salt concentrations and surface treatments, the electroosmotic mobility of the BSA-coated surfaces can be estimated $\mu_{EOF} = 2 \times 10^{-8}$ m^2 / V s[69]. The experimentally measured effective DNA translocation duration of ~ 4 ms given by $L/(\mu_{EP} - \mu_{EOF})E$ corresponds to an electrophoretic mobility of roughly $\mu_{EP} = 2.4 \times 10^{-8}$ m^2 / V s, which is consistent with the free-solution mobility of DNA in the presence of Na$^+$ as measured by Ross et. al[70]. Thus, while the DNA molecules moved from the negative to positive electrode, the electroosmotic flow significantly decreased their velocity.

4.6.3 Multiple measurements on λ-DNA and T7 DNA mixture

To implement feedback control on the DNA mixture, the algorithm for feedback control implementation was identical to the one used in previous multiple measurement experiments. A typical current trace pattern for a solution containing a mixture of 1 μg/mL λ-DNA and 1 μg/mL T7 DNA (Figure 4.15) reveals successive events comprising a DNA translocation followed by a voltage reversal. After voltage reversal, the current changes sign and starts decreasing rapidly to its baseline value. Upon detection of a

DNA translocation event, the voltage bias is again reversed after a delay of 30-40 ms (Figure 4.15a). The translocation events occur alternately at forward and reverse voltage bias, as expected when the DNA molecule is recaptured back into the nanopore and translocated alternately in forward and reverse directions (Figure 4.13c-f). Viewed over a longer period of time (Figure 4.15c), the current trace reveals that the translocation events are grouped into distinct sets separated by pauses. The pauses between neighboring sets in Figure 4.15c indicate that a translocation event was not detected either following escape of the molecule being recaptured or failure of the algorithm to detect the translocation. Upon detection of another translocation event, the pause terminates and another set of successive measurements begins. The regular translocation events in each set interrupted by much longer pauses suggest that each set corresponds to a single DNA molecule being actively shuttled back and forth through the nanopore.
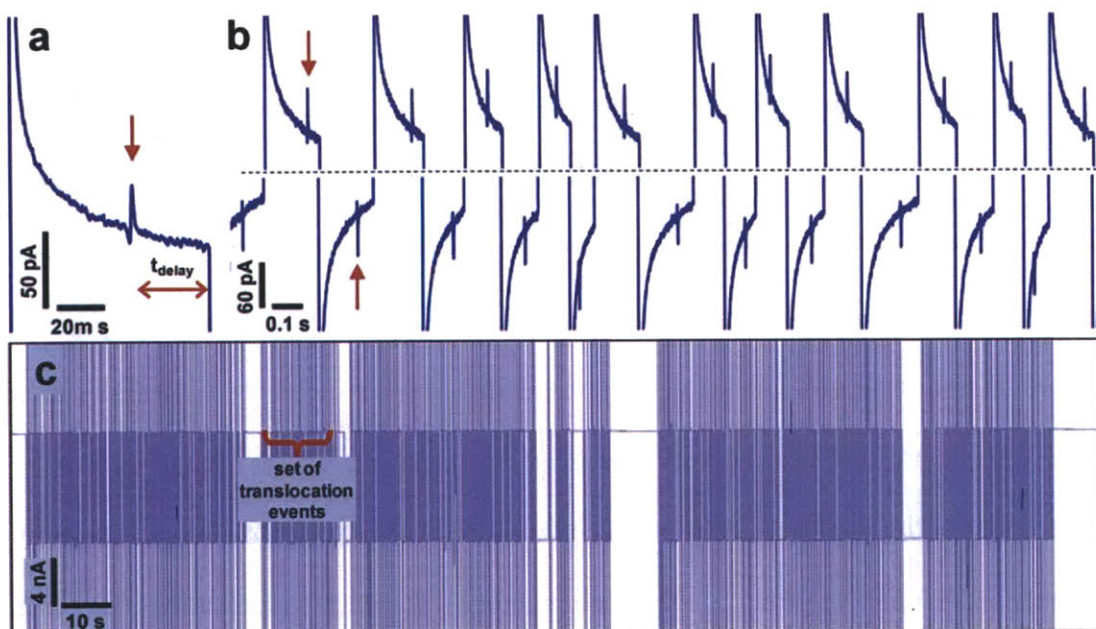
Figure 4.15 Current traces with feedback control for a mixture of 1 μg/mL λ-DNA and 1 μg /mL T7 DNA. (a) Translocation signal of a single DNA molecule (red arrow). Delay time before voltage reversal is also indicated. (b) Current traces showing multiple measurements presumably on the same DNA molecule. When each translocation event (red arrow) is detected, the applied voltage bias is reversed, resulting in successive recapture and translocation of the same molecule. (c) Current traces over a longer period show sets of translocation events separated by pauses that occur whenever the DNA molecule escapes or the translocation is not identified by the real-time algorithm. Vertical lines in the plot correspond to transient current changes that occur when the applied voltage bias is reversed, with each vertical line indicating a voltage reversal following detection of a translocation event[33].

4.6.4 Data analysis of multiple measurements

To enable statistical averaging over multiple measurements on single molecules, it is important to identify sets of translocation events that correspond to back-and-forth translocations of the same molecule. A series of measurements on the same molecule was defined as a set of translocation events with (a) exactly one voltage reversal between successive translocations, and (b) <500 ms delay between neighboring translocation events (compared to a mean arrival time of ~10 s under a constant voltage bias and a mean recapture time of 30 ms after voltage reversal). In an experiment with a mixture of 1 μg/mL λ-DNA and 1 μg/mL T7 DNA comprising N_{trans} = 4200 translocations, 32 series were identified that satisfied the above criteria and comprised at least 64 translocation events. Each series contained an average of 130 measurements. Arrangement of

extracted translocation signal amplitudes in chronological order revealed distinct shifts in the translocation signals (Figure 4.16a), which may be expected if one DNA molecule is switched with another molecule of different length between different series (Equation 2.1). We also investigated reasons for termination of a series of consecutive measurements by violation of the above criteria. The analysis revealed that ~25% of terminations (8 series) occurred due to detection of a second translocation event prior to voltage reversal (double translocation), ~28% (9 series) were caused by failure of the real-time LabVIEW algorithm to detect a DNA translocation (no trigger), ~25% (8 series) were caused when the voltage was reversed by the algorithm prior to DNA translocation (false trigger), while ~22% (n_{escape} = 7 series) occurred due to failure of the DNA molecule to be recaptured (escape), as shown in figure 4.17. For the details of the analysis, please refer to Appendix I.

95
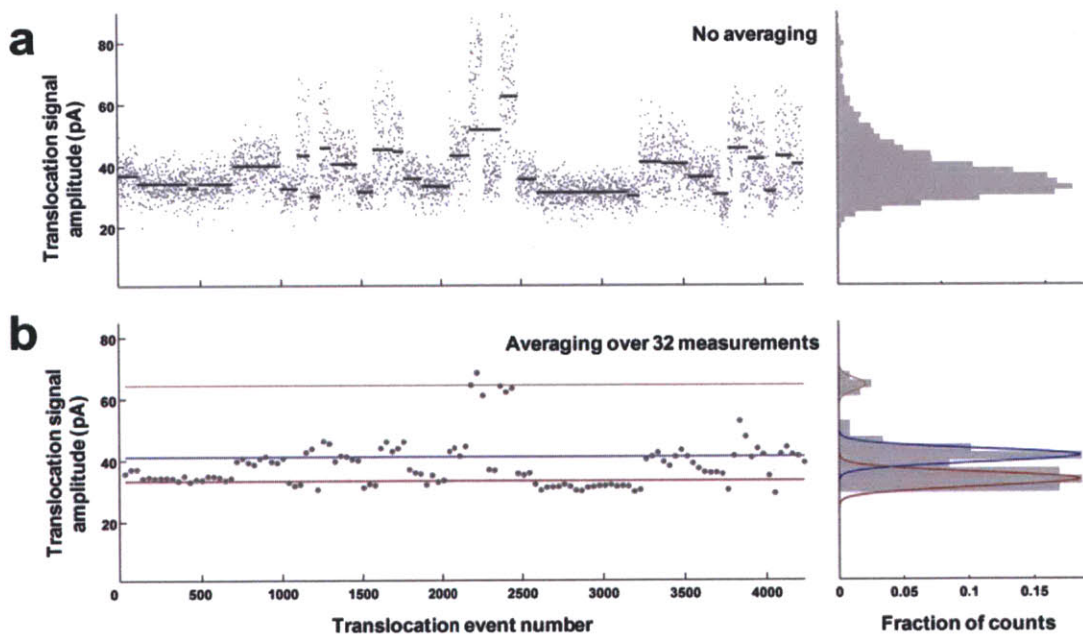
Figure 4.16 (a) Chronological sequence of translocation signal amplitudes exhibits distinct shifts in the mean amplitude between series. Horizontal bars denote mean value of the translocation signal for each series. Histogram of the translocation signal amplitude without any averaging (right). (b) Chronological sequence of translocation current amplitudes after averaging over 32 consecutive measurements within each series accentuates the shifts in the mean amplitude between series. The corresponding histogram of translocation signal amplitudes after averaging over 32 consecutive measurements reveals distinct groups of translocation signals (right). Fit to two Gaussian distributions is depicted; the outlying set is excluded from the fit[33].
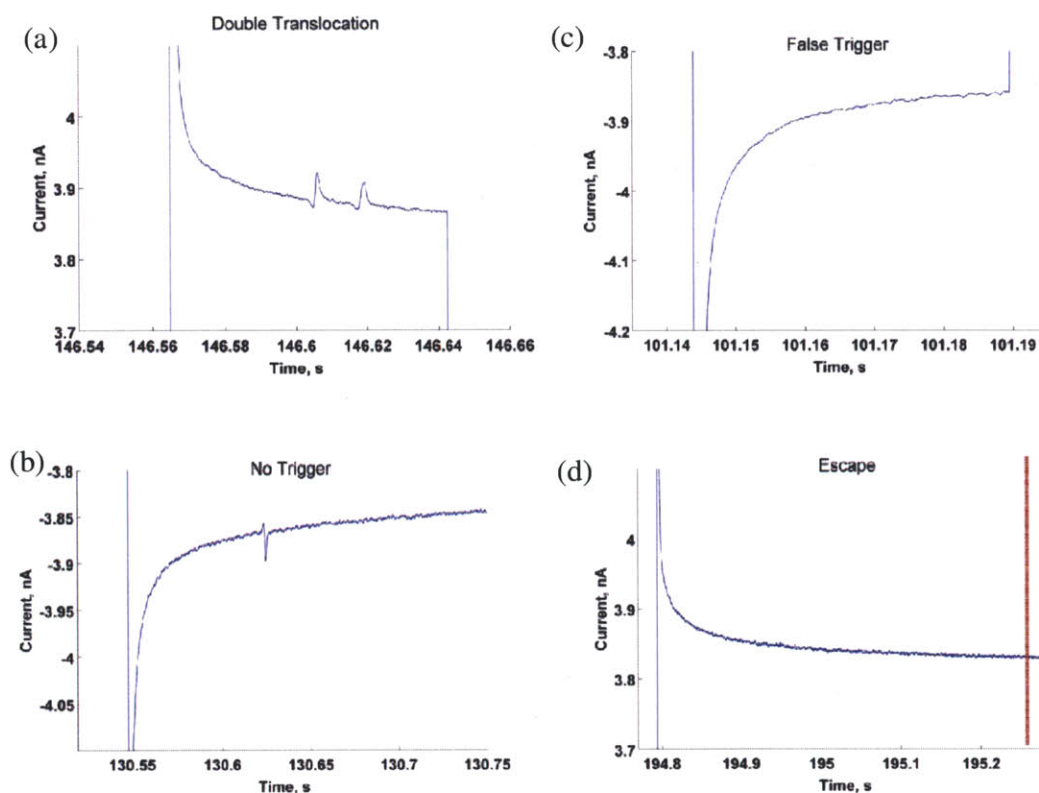
Figure 4.17 Causes of series failure. (a) Double translocation: a second molecule translocating within 50 ms of the first translocation. (b) No Trigger: the real-time

algorithm fails to detect the translocation event or has detected a pre-set number of translocations in the series. Consequently, there is no voltage reversal soon after the translocation. (c) False Trigger: LabVIEW falsely detects a translocation event, and initiates a voltage reversal prior to the translocation of the molecule. (d) Escape: no translocation is detected within 500 ms after the last translocation in the series. The red line indicates the 500 ms cutoff wait time[33].

Assuming that the probability of escape is independent of the previous measurement, the recapture probability can be calculated as:

$$P_{recap} \approx 1 - \frac{n_{escape}}{N_{trans}} \dotfill (4.3)$$

Equation (4.3) yields the recapture probability for 7 escape events out of 4200 translocations as 99.83%.

The distinct shifts in the measured translocation signals become more apparent when successive measurements within each series are averaged (Figure 4.16b). The translocation signal histogram appeared to have a single peak when no averaging was performed (Figure 4.16a), indicating the failure to discriminate between λ-DNA and T7 DNA molecules in the absence of any chronological information. However, the histogram resolved into three distinct peaks after averaging over 32 measurements (Figure 4.16b). In accordance with Equation 2.1, the mean translocation signal amplitude depends on the number of excess charges introduced into the nanopore. If the entire DNA molecule is enclosed within the nanopore during translocation, the number of charges introduced into the channel and hence the translocation signal amplitude is expected to be proportional to the DNA length. Thus, the three peaks (33.4, 41.2, and

64.5 pA, respectively) in the histogram may be assigned to T7 DNA, λ-DNA, and a dimer of λ-DNA that can occur due to cohesive ends of the molecule[19]. Interestingly, the ratio of mean translocation signal amplitudes of T7 and λ-DNA matches the ratio of their lengths within 5%, suggesting that the molecules were enclosed within the nanopores during translocation. Although the length of a translocating DNA molecule is hard to estimate, the equilibrium length L_{eq} of a DNA molecule inside a nanopore is given by the deGennes theory as[71]:

$$L_{eq} = \frac{(\lambda w)^{1/3}}{d^{2/3}} L \quad \text{...} (4.4)$$

Where $d = 316$ nm is the equivalent width of the nanopore, L is the contour length of the DNA, λ is the persistence length of the DNA, and w is the molecule width. The equilibrium lengths of T7 and λ-DNA molecules inside the nanopores were calculated to be 1.7 and 2.1 μm respectively, which is consistent with the above observations. Larger DNA molecules above ~100 kpb have an equilibrium length that exceeds the nanopore length. We observed that the translocation amplitude of the λ-DNA dimer (97 kbp) was only 56% greater than that of λ-DNA, suggesting that it is not completely enclosed in the nanopore during translocation. Sizing of longer DNA molecules could be easily achieved by increasing the length of the nanopore so that the whole DNA molecule fits in. On the other hand, although smaller DNA molecules result in proportionally lower translocation current amplitudes, noise in the feedback loop prevents multiple measurements of DNA molecules smaller than about 25 kbp. Sizing of smaller DNA molecules could be achieved by decreasing the channel length, or modulating the cross-sectional area of the nanopore[72].

4.6.5 Comparison between multiple measurements on a mixture of DNA molecules and single-length DNA molecules

To verify the changes in the translocation signal amplitude (Figure 4.16) were due to measurements on DNA molecules with different lengths, a control experiment was performed with a homogenous solution of λ-DNA molecules without any T7 DNA molecules. 1 μg/mL of λ-DNA in 10 mM KCl buffer solution was loaded on one side of the nanopore and analyzed using feedback control. As mentioned before, the experiment was periodically interrupted (setting the voltage bias to 0 V) to enable a different molecule to enter the nanopore. These experiments were conducted in a 7 μm nanopore device. Figure 4.18a illustrates the translocation signal amplitudes over 2200 translocation events arranged in chronological order, where the mean value remained relatively constant. Figure 4.18b also demonstrates that averaging over 32 consecutive measurements narrows the translocation signal amplitude distribution while maintaining a single peak, which agrees with multiple measurements taken on a single type of DNA molecule.
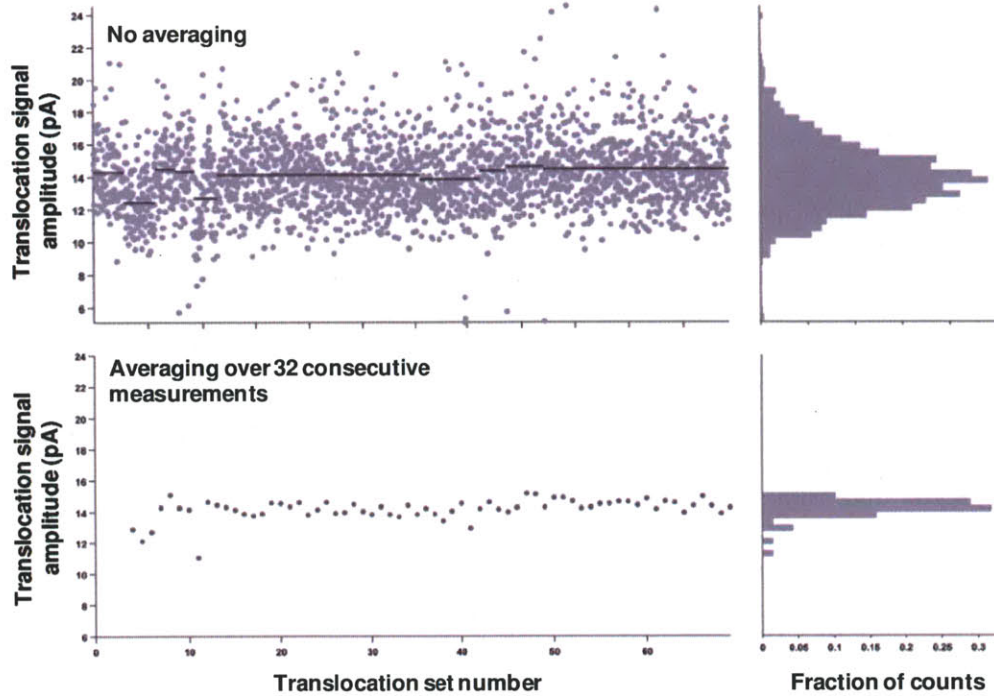
Figure 4.18 (a) Illustration of the translocation signal amplitudes of λ-DNA molecules over 2200 translocation events arranged in chronological order, where the mean value remained relatively constant. (b) Averaging over 32 consecutive measurements narrows the translocation signal amplitude distribution while maintaining a single peak, which agrees with multiple measurements taken on a single type of DNA molecule.

In conclusion, the results of multiple measurements demonstrated above indicate that averaging over multiple measurements enhanced the measurement resolution and enabled discrimination between T7 DNA and λ-DNA molecules, or the components in HindIII-digest λ-DNA and λ-DNA mixture, which was not possible with single measurements.

4.7 Recapture time distribution: simulation and experiment

The success of multiple measurements relies heavily on the success of recapture of the molecule. The recapture of a DNA molecule by a nanopore or nanopore depends on the competition between diffusive and electrokinetic transport. It can be characterized by a recapture radius such that a molecule within this distance from the pore can be recaptured into the pore with a high probability. The dependence of recapture radius could be derived as follows; since nanopore cross sectional area is very small compared to the connecting reservoir, the probability distribution of the DNA molecule transporting out of nanopore into adjacent reservoir can be assumed as hemispheric symmetric with its origin residing at the pore entrance. The electrophoretic velocity of DNA molecule $= \mu E$, where μ stands for DNA electrophoretic mobility, and E stands for electric field. Around the hemispheric symmetric entry of the pore, electric field $E = VA/l\pi r^2$, where V = voltage bias, A = cross-sectional area of the pore, l = length of the pore, r = distance away from the pore, and the average DNA diffusion velocity away from the pore is equal to D/r [33]. The effective radius r below which DNA is unlikely to escape due to electric field is determined by equilibrating the diffusion velocity with electrophoretic velocity so that $r = \mu VA/Dl\pi$.

This recapture radius scales proportionally with the current through the pore, and inversely with the solution conductivity and molecular diffusivity[55]. In the present device, the large cross section area of the nanopore, large applied voltage (1 V), and the low diffusivity of the λ-DNA and T7 DNA molecules, all favor a larger recapture radius compared to the case of a nanopore in a membrane[55]. Assuming spherical symmetry, the calculated recapture radius for λ-DNA in the device is 88 μm, which exceeds the

101

microchannel height of 10 μm. Thus, beyond a distance of ~10 μm, the microchannel further confines the electric field.

Figure 4.19 Environment for DNA transport around nanopore entry is approximated as spherically symmetric.

To investigate the mechanism of DNA recapture and the role of the microchannels, we compared the molecule recapture time distribution with numerical simulations. The recapture time is defined here as the time between voltage reversal and translocation of the molecule. Prior to recapture, transport of DNA molecules around the nanopore is influenced by diffusion, electrophoresis, and electro-osmosis. Since the cross-sectional area of nanopore is more than an order of magnitude smaller than that of the adjacent microchannel, the DNA transport in this region can be approximated as spherically symmetric for length scales smaller than the microchannel height (Figure 4.19). Simulation of DNA transport is obtained by solving the one-dimensional time-dependent drift-diffusion equation in spherical coordinates[55]:

$$\frac{\partial c(r,t)}{\partial t} = \frac{1}{r^2}\frac{\partial}{\partial r}r^2(\mu E c(r,t) + \frac{D\partial c(r,t)}{\partial r})$$ .... (4.5)

Where DNA diffusivity $D = 4 \times 10^{-13}$ (m^2/s), r is the distance away from the nanopore, c is the concentration (in this case the probability density) of the DNA molecule, and $\mu = 4 \times 10^{-9}$ (m^2/V s) is the measured DNA mobility. The electric field in the microchannels was obtained by solving Gauss' equation for the device geometry and applied voltage.

The initial condition for the probability distribution, c, was set as a delta function located close to the nanopore entrance. The probability distribution was allowed to propagate under an electric field for 32.5 ms, which corresponds to the period before the applied voltage is reversed, during which the DNA molecule continues to move away from the nanopore due to electric field, and is also influenced by diffusion. The direction of the electric field was then reversed to drive the probability distribution towards the nanopore. The recapture time distribution was calculated by computing the fraction of the probability distribution outside the nanopore between time steps (Figure 4.20 (a) to (f)).
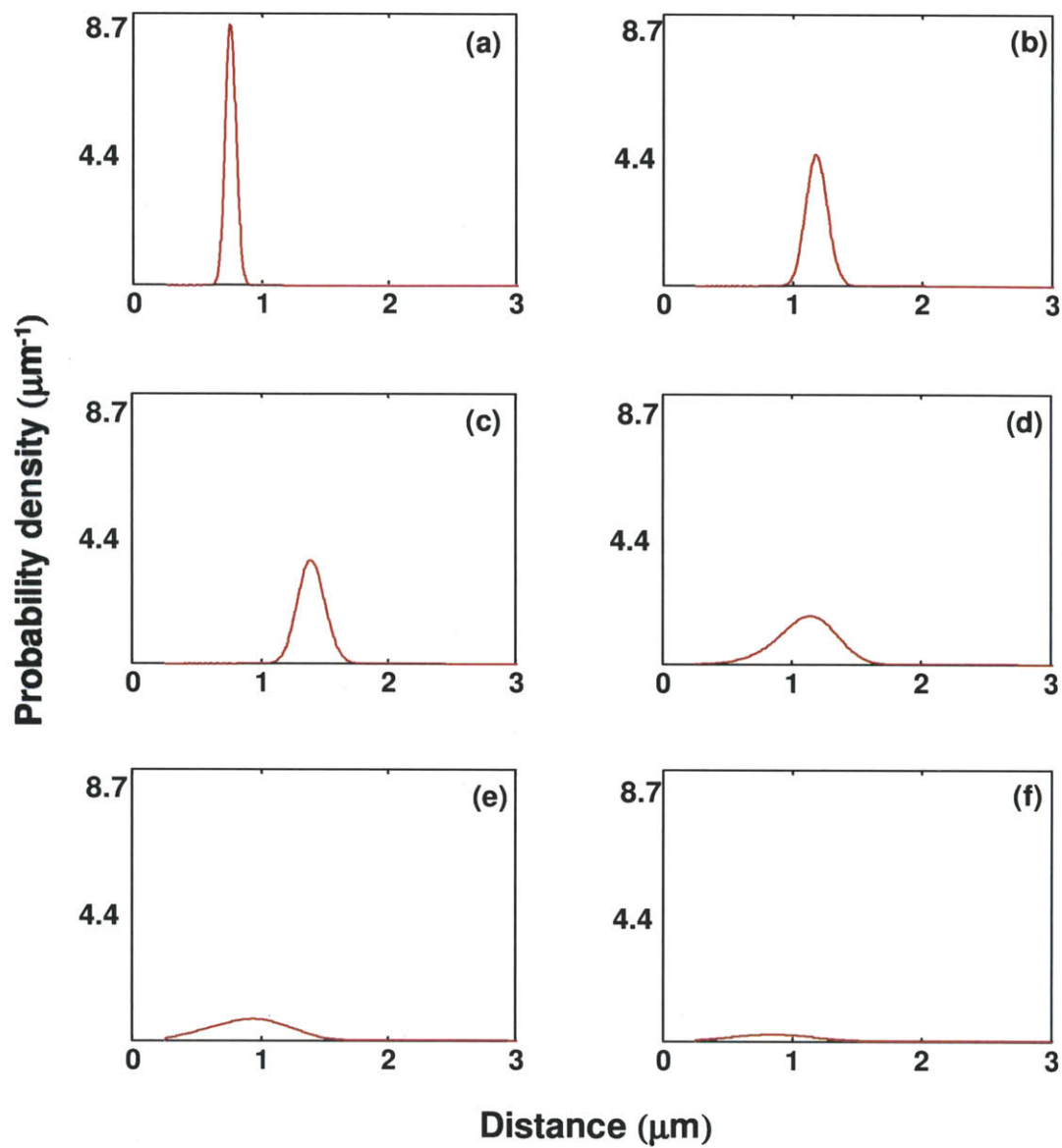
Figure 4.20 Numerical solution of the drift-diffusion equation showing the DNA probability distribution during the DNA recapture process when the applied voltage bias is reversed at time t_0 (ms) after translocation. (a) $t_0 = 5$ ms (b) $t_0 = 20$ ms (c) $t_0 = 32.5$ ms (d) $t_0 = 50$ ms (e) $t_0 = 65$ ms (f) $t_0 = 80$ ms.

Figure 4.21 compares the simulated recapture time distribution for a pre-reversal time of 32.5 ms to the experimentally measured recapture time distribution for pre-reversal times in the range of 30-35 ms. The experimental results agree with the simulation result, where most of the molecules were recaptured within 100 ms, and both experimental and simulation peaks of the recapture time were centered around 40~50 ms. The small discrepancies at the right end of the distribution may be attributed to the effects of surface charge[73], interaction between DNA molecules and channel walls, the effect of electric field strength on DNA conformation, and the finite DNA size, which were not included in the simulation.

The simulated mean DNA travel distance during the pre-reversal time (1.38 μm) and the characteristic diffusion length scale during recapture (0.3 μm) were both significantly smaller than the microchannel height (10 μm) and the recapture radius of 88 μm (using baseline current I=3.7 nA and equation $R= \mu VA/DI\pi$. These results suggest that the primary mechanism for the high recapture probability in the device was the larger recapture radius due to a combination of the larger nanopore size, higher applied voltage, and lower DNA diffusivity, and that the electric field confinement due to the microchannels did not directly aid in DNA recapture.
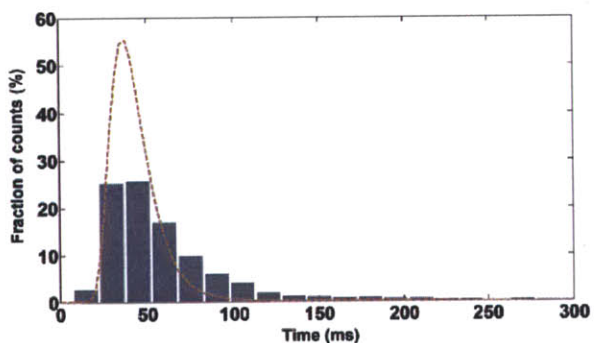
Figure 4.21 Experimental histogram and simulation for DNA recapture time distribution (The time between voltage reversal and molecule arrival)[33].

4.8 Conclusion

In conclusion, we have demonstrated that multiple measurements of the translocation signals of single DNA molecules in nanopores increases the ability of the nanopore to discriminate between different molecules and enables observation of dynamic events in λ-DNA and HindIII-digest λ-DNA mixture. The device can recapture DNA molecules with a probability of greater than 99%, and consistently perform >100 measurements on single DNA molecules. The resulting improvement in DNA sizing also enables discrimination between 48.5 kbp λ-DNA and 39.9 kbp T7 DNA molecules, which was not possible with a single measurement per molecule. Further development of this approach may enable accurate sizing of DNA fragments, which may substitute gel electrophoresis in certain applications where time-to-result is important. In combination with microfluidics, such devices may also enable interesting single molecule assays such as restriction fragment length polymorphism (RFLP). The present results also have implications for accurate sizing of colloids and nanoparticles, where standard benchtop techniques based on light scattering are difficult to implement when the sample is polydisperse, turbid, fluorescent, or when the sample size is limited. The ability to perform sequential measurements in time potentially opens new avenues for observation of single molecule or single particle dynamics and reactions. The combination of microfluidics and nanopores with active control over the transport of single molecules and particles could enable rapid and accurate sizing as well as observation of reactions

106

and dynamic behavior, which could lead to new single-molecule assays with better accuracy or time to result.

Chapter 5 Fabrication of silica nanopore devices

5.1 Motivation

We have showed the fabrication process, and multiple measurements of the same DNA molecule along with its improvements on differentiating and sizing molecules in the PDMS nanopore device. PDMS nanopore devices have the advantages of ease of fabrication after the completion of the mold and are economical. However, the minimum feature size achievable by PDMS material is limited[72], the surface is highly hydrophobic[74], and the surface charge of PDMS is not as controllable as that with silica nanopores[75]. Besides the material and geometrical aspect, our design of newer nanopore device should be capable of measuring the same DNA molecule with high confidence. As discussed in Chapter 4, we have encountered several obstacles that terminate a series of measurements on the same molecule, and therefore limit the quality of our data. The analysis in multiple measurements in DNA mixture of λ-DNA and T7 DNA revealed that ~25% of terminations (8 series) occurred due to detection of a second translocation event prior to voltage reversal, which was due to one side of the nanopore being exposed to DNA solution.

5.2 Design of silica nanopore device

Here we designed and fabricated a nanopore device for multiple measurements, with the aims of (1) being able to detect short to medium-size DNA molecules (~10 kbp), (2) being able to trap the molecule in a buffer chamber, and performed multiple measurement with neither side of the nanopore being exposed to DNA bulk solution, and (3) having a more controllable surface on the nanopore part of the device (charge controllability and hydrophilic surface). It is well known that silica owns the merits of better surface

property, and < 20 nm features can be patterned in this material with appropriate fabrication techniques[76].

Figure 5.1 shows the design for the device. Its working principle is as follows:

(1) DNA molecules are injected into left reservoir (A).

(2) Voltage is applied between left (A) and top (C) reservoirs to translocate and detect DNA molecule from its original reservoir (A) to the trapping chamber (B) through left nanopore.

(3) Voltage is turned off, and the DNA molecule would be trapped inside chamber (B) since the entropic barrier between chamber and nanopore of confined regions cannot be overcome without sufficient voltage bias[7].

(4) AC voltage is applied between top (C) and right (D) reservoirs to perform multiple measurements on the right nanopore.

(5) For rinsing or filling the trapping chamber, a pressure gradient is applied between top (C) and bottom (E) reservoirs. Multiple connecting nanopores facilitate rinsing due to low hydrodynamic resistance.
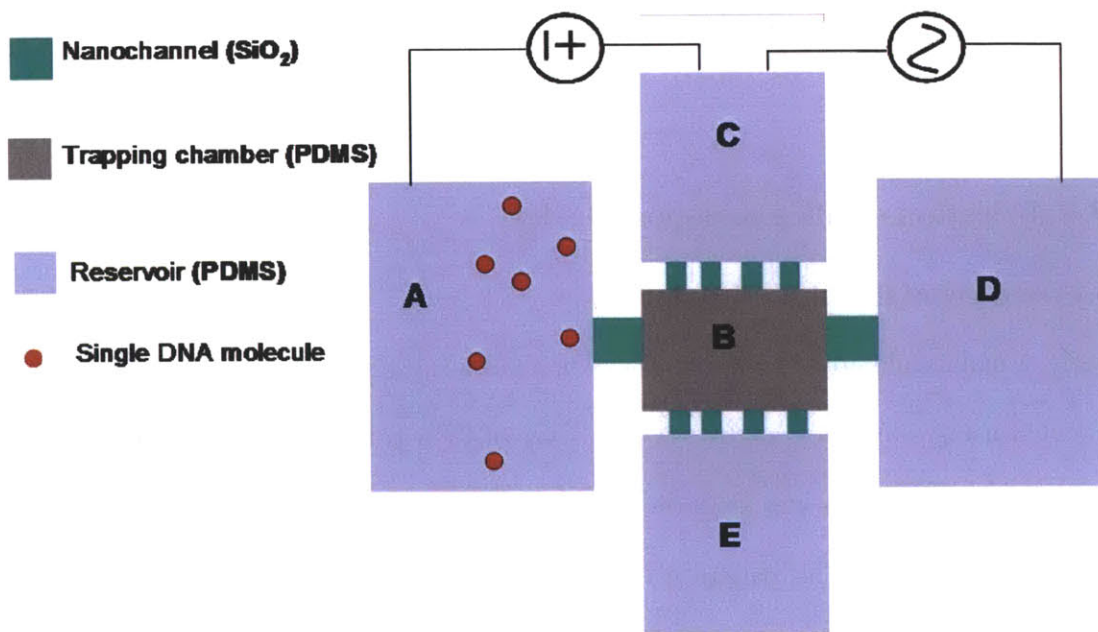
Figure 5.1 Design of the silica nanopore device for trapping and multiple measurement purposes.

The device consists of nano-meter features (100~200 nm) and micro-meter features (1~10 μm) in plane and in the vertical direction. For the nano-meter features, we chose 100 nm x 100 nm x 100 nm (width x height) since such features can be patterned by electron beam lithography and reactive ion etching (RIE) easily. The spacing between adjacent nanopores is chosen to be 1 μm since such gap will have negligible impact from reflection of electron beam from adjacent nanopore. The lengths of nanopores are controlled by the spacing between two microchannels, and therefore are controlled by the resolution of UV lithography with contact mask. Here we chose 4 μm since it is the resolution limit of such machine, and has been demonstrated in our previous PDMS nanopore device. For the part that requires micro-meter scale features in out-of-plane direction, we adopted the cast-molding process of soft lithography since (a) large feature in out of plane direction is not easily patterned with traditional microfabrication method,

and (b) the surface material in the part will not affect the device performance significantly.

5.3 Fabrication of silica nanopore device

5.3.1 Overview of the fabrication process

Briefly, a nano-scale groove was patterned on a silica substrate, and microchannels were fabricated using soft-lithograpghy. A thin layer of Cr was first evaporated on a 4-inch silica wafer, and PMMA was spun on and patterned using electron-beam lithography to define the nanopores. This pattern was first transferred to the underlying Cr using wet-etch, and was transferred from the Cr layer to the silica substrate using dry etch of depth 100 nm.

Microchannels and trapping chamber were fabricated using soft-lithography. A thick layer of photoresist (10 μm, SU-8) was patterned to define the connecting microchannels and trapping chamber. The length of the nanopores was 4 μm. PDMS was cast on the mold, cured and peeled off, punched for input/output ports, cleaned with ethanol and isopropanol (IPA), followed by bonding to the silica substrate. Figure 5.2 shows a schematic of the fabrication process of silica nanopore device.
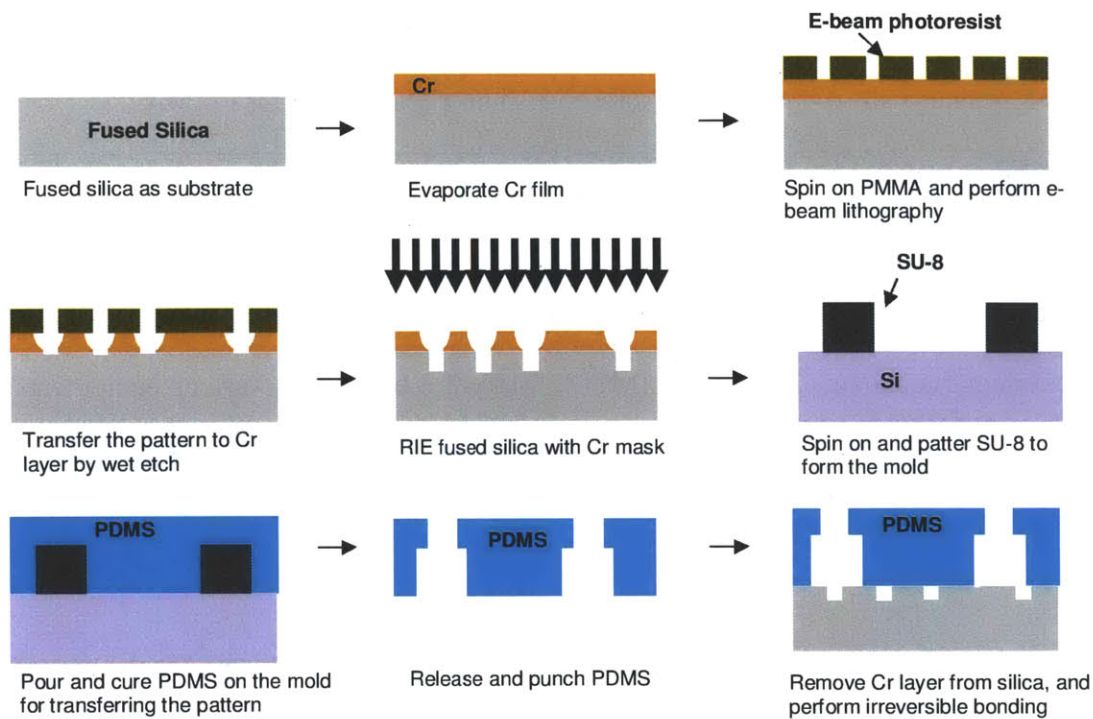
Figure 5.2   Schematic fabrication process of silica nanopore device.

5.3.2 Equipment used in the fabrication process

Silica nanocahnnels were fabricated in MIT's NanoStructure Laboratory (NSL) and Electron-Beam Lithography (SEBL) at Research Laboratory of Electronics (RLE). Table 5.1 below lists various equipment used in the process, with a "machine coral name" by which they are known in the NSL and RLE at MIT, and a brief description.

Table 5.1 List of MTL and RLE equipment used in the fabrication process for the silica substrate

Machine name	Description
Raith 150	Scanning electron beam lithography

113

RIE in NSL	Reactive Ion Etching Machine
PMMA spinner	Manual photoresist spinner specifically for PMMA
EbeamFP	E-beam evaporator

The master mold was fabricated in the Massachusetts Institute of Technology (MIT)'s Microsystem Technology Laboratory (MTL). Table 5.2 below lists various equipments used in the process, with a "machine coral name" by which they are known in the MTL at MIT, and a brief description.

Table 5.2 List of MTL and RLE equipment used in the fabrication process for the master mold

Machine name	Description
Raith 150	Scanning electron beam lithography
Photo-wet	Photo-wet station for develop, lift-off, and rinsing process
PMMA spinner	Manual photoresist spinner specifically for PMMA
EbeamFP	E-beam evaporator
EV1	4" and 6" UV lithography system
SU8spinner	Manual photoresist spinner specifically for SU-8

5.3.3 Fabrication of the silica nanopores

Fabrication process starts with 4 inch quartz silica wafer substrate. We evaporate 80 nm of Cr on top of silica wafer, and spin on 100 nm PMMA on top of Cr thin film. We used

electron beam lithography to pattern nanopores on PMMA. The width and depth of nanopore were both chosen to be 100 nm for the reasons stated in previous sections. The dose factor for e-beam lithography was 450 $\mu A/cm^2$, and the electron-beam energy was 30 keV. PMMA was developed with MIBK/IPA 1:2 ratio (volume) at 21 °C for 3 minutes. After developing the electron beam pattern on PMMA, we then transferred the pattern to the underlying Cr layer using wet etch with PMMA as mask. Cr layer was etched by Cr-7 etchant for 20 seconds, and rinsed with water immediately after the etch process to remove the remaining Cr-7 from the Cr layer and substrate. We removed the remaining PMMA with acetone, and transferred the patterned from the Cr layer to the nanopore to the underlying quartz wafer substrate using RIE. Here the etching gas is 20 (sccm) CHF_3, the self-bias voltage was at 350 Volts, the pressure of the chamber was 10 mTorr, and the etch rate for the quartz material was 10 nm/minute under this condition. The substrate was etched for 10 minutes to yield 100 nm deep grooves, and the remaining Cr layer mask was removed by Cr-7 after RIE (Figure 5.3a).

5.3.4 Fabrication of the microchannel mold

Negative photoresist SU8-2007 was spun for 5 s at 500 rpm, and 1500 rpm for 40 s more to obtain a thickness of 10 μm. Following that step, the wafer was soft baked at 65 ° C for 1 min and 95 ° C for 3 more min. Gradual heating was necessary in both soft bake and hard bake to prevent the SU-8 from peeling off the substrate. Next, the wafer was aligned and exposed with UV light of 10 mW/cm^2 for 13 s. Next, the wafer was hard baked at 95 °C for 4 min, and cooled down to 45 °C. Finally, the pattern was developed with ethyl lactate for 3 min, followed by rinsing with IPA, and drying with nitrogen. Following that step, the wafer was hard baked to 150 °C gradually for 6 min to eliminate

cracks in SU-8. After that, the mold of microchannels was ready for the following soft-lithography step (Figure 5.3b, c).
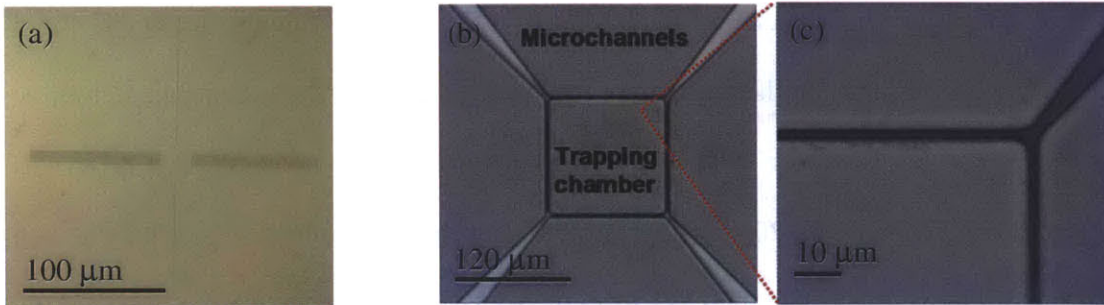
Figure 5.3 (a) Silica nanopores. Thick stripes correspond to an array of 15 nanopores with 1 μm spacing. (b) SU-8 mold for trapping chamber and microchannels. (c) Zoom in on the 4 μm spacing between trapping chamber and microchannel shows clean gap without unintended connections.

5.3.5 Discussion

During the fabrication process, we encountered several issues that initially prevented us from fabricating successful nanopores and SU-8 mold for microchannels and trapping chamber. Below we list the issues by the order of fabrication process.

(1) Spacing between silica nanopores: Spacing between adjacent nanopore in nanopore arrays is determined by electron-beam lithography software mask. When the spacing between adjacent nanopores are small (<500 nm), electron-beam recipe such as dose factor will affect the outcome significantly; when the dose intensity is too high, the reflection of electron beams to the adjacent nanopore pattern could result in unwanted crosstalk and connections, while too low of the dose intensity could not yield nanopore after development. Here we

116

picked a spacing of 1 μm since the crosstalk effect will be negligible under typical dose factors (80-500 μA/cm^2), and the nanopore array with such spacing is dense enough to allow sufficient spacing for alignment error.

(2) Spacing between trapping chamber and microchannels: During fabrication of SU-8 mold, we encountered unintended crosstalk between adjacent SU-8 patterns. Such phenomenon could be mitigated by careful attention to uniformity of hot plate, strict control over heating temperature and time. However, the gap between photomask and substrate remains an uncontrollable but important factor, and a yield of 16% (6 out of 36) was attained in our SU-8 microchannel mold.

5.4 Conclusion

Here we have successfully fabricated an array of nanopores of 100 nm wide in SiO$_2$ substrate, and the SU-8 mold for microchannel and trapping reservoir. Nanopores were fabricated using electron-beam lithography, followed by wet and dry etching processes, while SU-8 mold was fabricated by conventional UV lithography. The device with such design has the potential to trap and perform multiple measurements on the same molecule with high confidence, and future steps of the project involves electrical testing of the device, and DNA molecule trapping and multiple measurements on the same molecule.

Chapter 6 Dynamic bidirectional current modulation during DNA translocation in a nanopore

6.1 Introduction

Electrokinetic effects can result in unique transport phenomena in nanofluidic channels when the effect of surface charge becomes significant[77]. Asymmetry in the geometry or charge in artificial nanofluidic channels can lead to rectification of ionic current, which is a nonlinear electrokinetic effect manifesting as a spatial enhancement or depletion of ionic concentration occurring within or near the ends of the nanopore[78]. Nanofluidic current rectification has been observed using symmetry-breaking geometry of the nanopore[79], asymmetric nanopore surface charge[80,81], or symmetric nanochannel with unequal bulk concentrations at either ends of the channel[82]. In the remaining sections of this chapter, we will first briefly describe ionic current rectification in each case mentioned above, and later on report experimental result and numerical simulation of a consistently observed bidirectional modulation of ionic current when a DNA molecule translocates through a nanopore. This phenomenon consists of a current increase and decrease during each single DNA translocation event, and we explain its mechanism with a model similar to that used for modeling ionic transport through nanopores with surface charge asymmetry.

6.1.1 Past work on ionic current rectification in nanochannels and nanopores

A single conical nanopore is a typical nanofluidic device that utilizes geometric asymmetry for ionic current rectification. The conical pore shape and its negative surface charge result in current rectification and also the ability to pump ions against concentration gradients driven by electric-field oscillation[83]. The rectifying effect also

depends on the ionic strength and on the pH of the electrolyte. Figure 6.1 shows the typical current-voltage (I-V) characteristics of a single conical PET nanopore measured under symmetric KCl concentrations in the baths at the two ends.
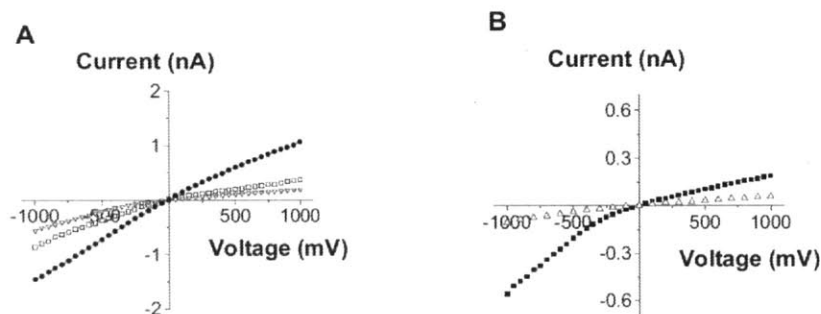
Figure 6.1 Rectifying properties of a single conical nanopore in a PET membrane with the voltage applied on the base side and the tip side grounded. (A) I-V characteristics obtained under symmetric ion concentration at pH 8 and 3 M KCl (solid circles), 1 M KCl (empty squares) and 0.1 M KCl (empty triangles). (B) I-V curves recorded under symmetric 0.1 M KCl at pH 8 (solid squares) and pH 3 (empty triangles)[83].

Asymmetric Bath Concentrations

The rectifying effect can also be produced by an asymmetric ion distribution along a nanochannel. Cheng et al. performed an experiment on planar nanochannels in which one bath with low concentration (termed C_L) is fixed at 0.1 mM KCl, and the other bath with a higher concentration (termed C_H) varies from 0.1 mM to 1 M KCl (Figure 6.2). The rectifying effect was attributed to the disparate ion concentration profiles produced under the applied potentials of different polarities. As illustrated in Figure 6.2, voltage bias of different polarities applied across a nanochannel, along with the concentration

120

gradient in the channel, can extend or shrink the proportion of EDL overlap in the nanochannel and, therefore, cause the asymmetric ionic conductance.
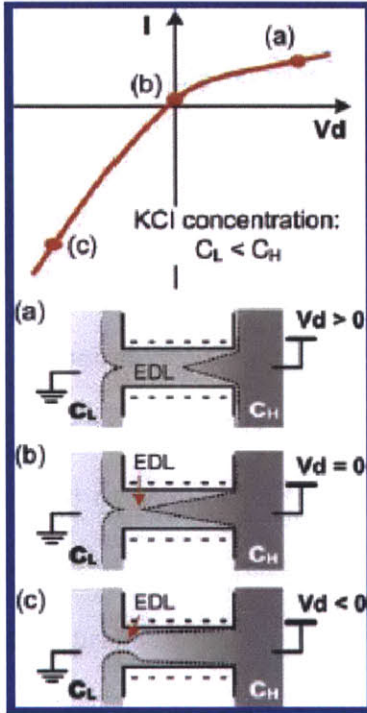
6.2 Rectifying effect due to the disparate ion distribution along the nanochannel having negative surface charge and under different polarities of applied potential. The gray scale plots show the relative ionic concentration in different regions of the channel. (a) High concentration C_H side is positively biased relative to the low concentration side C_L. (b) Zero bias. (c) C_H is negatively biased. The gray region within the nanochannel that is bound by the dashed lines represents the electric double layers (EDL). Reproduced from reference [82].

Asymmetric Surface Charge Distribution

Another way to produce ionic current rectification is by directly creating an asymmetric surface charge that effects an asymmetric ion distribution along the nanochannel. To induce such asymmetry that resembles a diode, Karnik et al. have developed diffusion-limited patterning (DLP) to pattern positively charged avidin inside biotinylated nanochannels[80]. Figure 6.3a and b show a schematic diagram and epifluorescence image of fluorescently labeled avidin in a nanochannel diode.

The mechanism of current rectification was studied by calculating the ionic concentration profiles and corresponding electric potential in 10 mM KCl at bias voltages of +5 and -5 V, respectively (figure 6.3c). The left half of the nanochannel is assumed to have a surface charge of 3 mC/m^2 (avidin-coated), while the right half is assumed to be neutral (biotinylated). When there is no electric field along the channel, negative chloride ions accumulate in excess in the avidin half of the channel to neutralize the positive charge on avidin. When a positive voltage bias is applied to the biotin side, chloride ions from the avidin side travel to the biotin side. It results in concentration enhancement in the channel, and the magnitude of the axial electric field varies accordingly such that a constant current of chloride ions is maintained. The electric potential varies smoothly along the channel, there is high ionic current, and the diode is in forward bias. However, when the biotin side is at a negative voltage bias, chloride counterions in the avidin side are driven away from the biotin side. It results in concentration depletion inside the channel, and the electric potential drops sharply across the avidin-biotin junction. Under this condition, very little ionic current flows through the channel, and the diode is in reverse bias.

122

The ion rectification of the nanofluidic diode is dependent on electrolyte concentration (figure 6.3d). It is seen that current rectification is prominent at intermediate concentrations of 1 mM and 10 mM KCl, but not at higher or lower concentrations, since at higher concentrations of KCl, the effect of surface charge is small due to high bulk ionic concentration.
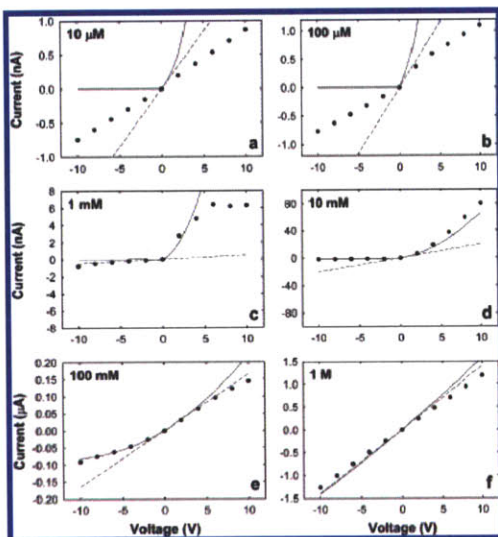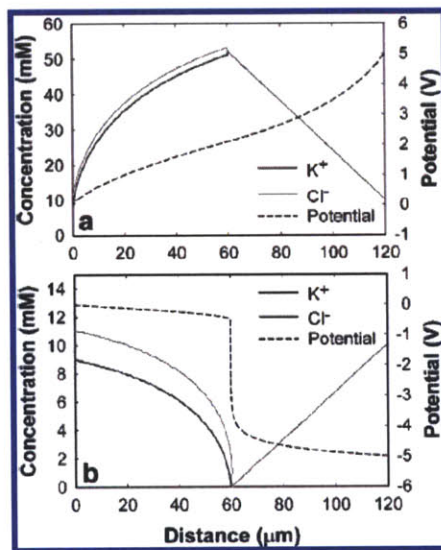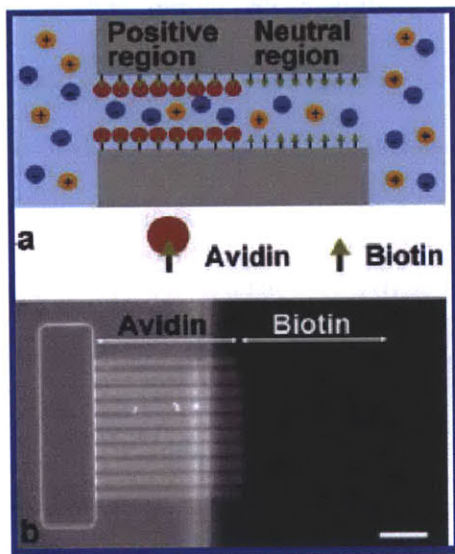
Figure 6.3 (a) Schematic diagram of a nanofluidic diode consisting of a positively charged surface and a neutral surface in different halves of the channel. The positive charge is produced by avidin, while the neutral charge is produced by biotin moieties. (b) Epifluorescence image shows fluorescently labeled avidin in the left half the nanofluidic diode[80]. (c) Theoretical predictions of the ionic concentration and electric potential profiles along nanofluidic diode calculated using the one-dimensional model. The avidin half of the channel has a positive charge of 3 mC/m^2, and the biotin half is neutral. (Top) Under forward bias of 5 V, there is concentration enhancement in the channel. (Bottom) Under a reverse bias of -5 V, there is concentration depletion in the channel, and the electric potential drops sharply at the junction of positive and neutral surface charge. Channel height is 30 nm, and KCl concentration is 10 mM. (d) Nanofluidic diode *I-V* characteristics at different KCl concentrations. Solid circles represent experimental data, while the dashed line has slope equal to the conductance measured using a voltage bias range of -50 to 50 mV. Solid lines are theoretical predictions. Biotin side is at a higher potential under forward bias[80].

Charge asymmetry during translocation of DNA molecules through a nanopore

Recently Eijkel et al. provided a theory to show that high-field electrokinetic translocation of DNA through nanopores or nanochannels can cause ionic current rectification due to large transient variations of the ionic concentrations in front and at the back of the DNA due to concentration polarization (CP)[84], i.e. ionic concentration enhancement or depletion. CP classically occurs at locations of sudden local change of ionic current transport numbers in presence of external electric fields, and the presence of

nanoconfined DNA causes a sudden local change in transport numbers due to the ionic composition of its electrical double layer (EDL). An EDL is formed when an ionic solution comes in contact with a charged surface and is characterized by a charge imbalance (which nullifies the substrate charge). They theoretically showed that CP will occur at the opposite ends of a nanoconfined DNA molecule moving electrophoretically (figure 6.4a,c) because the EDL formed around the DNA induces ionic concentration differences between the planes with and without the DNA molecule (planes 3 and 4 and planes 1 and 2 in figure 6.4a and 6.4c). The resulting transport number differences result in CP-induced ion-depleted and ion-enriched zones in front and at the back of the translocating DNA (figure 6.4a,c). Most importantly, this causes transient changes of the conductance of the nanopore through which the DNA translocates.

Figure 6.4 (a) Schematic of DNA (in red) with a surrounding EDL (in blue) in a nanochannel, and the location of the CP-induced ion-depletion (between planes 1 and 2) and ion-enrichment (between planes 3 and 4). The arrows (in blue) depicting the cationic current are located inside the nanochannel and are directed from left to right, whereas the arrows (in red) depicting the anionic current are located inside the nanochannel and are

125

directed from right to left. (b) The different dimensions corresponding to the DNA transport in a nanochannel. (c) (left) Schematic of the event of a DNA entering a nanopore (radius R), and the locations of the planes 1 and 2 in between which ion depletion will occur. (c) (right) Schematic of the event of a DNA (shown in red) exiting a nanopore, and the locations of the planes 3 and 4 in between which ion enrichment will occur. (d) The different dimensions corresponding to the DNA translocation in a nanopore, having radius R. Reproduced from reference [84].

6.1.2 Bidirectional current modulation during DNA translocation

In this chapter, we report experimental result of a consistently observed bidirectional modulation of ionic current when a DNA molecule translocates through a nanopore. As stated in Chapters 1 and 3, present theory for current change during DNA translocation predicts either a current decrease due to volume exclusion effect or current increase due to charge neutralization effect. In this thesis, we used low buffer concentration to detect DNA translocation, and expected a current change during each DNA translocation event. However, we consistently observed a small current decrease that precedes a large current increase during every DNA translocation event (figure 6.5b), and the theory for current change discussed in Chapter 3 could not explain this bidirectional current modulation.

Since this bidirectional current modulation bears similarity to ionic current rectification, we therefore proposed a potential mechanism that attributed this phenomenon to the asymmetric charge distribution[80] introduced by the molecule as it moves through the nanopore, as suggested by Eijkel et al[84]. As stated in the preceding section, current rectification effect due to asymmetric charge distribution is dependent on electrolyte concentration, and it becomes less prominent in buffers of higher ionic strengths. As a

result, the bidirectional current modulation effect during DNA translocation event should decrease with the increase of buffer concentration. Specifically, the magnitude of current decrease relative to the baseline current should decrease with increasing buffer concentration, as opposed to remaining relatively constant if the current decrease is due to blockage of the nanopore entrance as the DNA first enters the pore. In the following sections, we examine this hypothesis by performing the experiments of DNA translocation in various buffer concentrations. Besides, we investigated the theoretical current change by numerically solving one-dimensional electrokinetic equations in the nanopore, which further verified our assumption of asymmetric charge distribution as the main cause of observed bidirectional ionic current modulation during DNA translocation.

6.2 Experiment and results

6.2.1 Experimental setup and PDMS nanopore device

We used rapid prototyping in PDMS to fabricate nanopores (figure 6.5a) with approximate dimensions of 500 nm x 200 nm x 4 μm (Chapter 2). For the buffer, phosphate buffered saline (PBS, pH 7.4) at different dilutions in deionized water was used. The experimental setup for current measurement is the same as that used in Chapter 3, and the procedures for device bonding and surface passivation were also reported in previous chapters.

In order to characterize surface charge effect, we first need to accurately characterize the nanopore geometry. The PDMS nanopore dimensions were verified by measuring the ionic current at high ionic strength where surface charge effects are expected to be negligible. For 1 M KCl, the nanopore exhibited a conductance of 2.93×10^{-7} (S), which

is consistent with a conductance of 2.83×10^{-7} (S) calculated for the designed nanopore cross-section (500 nm x 200 nm) and length (4 μm) assuming a buffer conductivity of 11.38 (S/m). Assuming PDMS has a uniform negative surface charge, its magnitude could be estimated from the nanopore conductance in 1/15X PBS, based on equation (1.1) in Chapter 1, to be 0.037 (C/m^2) using nanopore dimensions determined by previous high ionic strength experiment.

6.2.2 DNA translocation signal

The PDMS nanopore successfully detected translocation of λ-DNA molecules (48.5 kbp, New England Biolabs) in PBS buffer with strength in the range of 1/15 X to 1/60 X (i.e. 15-fold and 60-fold dilutions, respectively), with applied voltage bias in the range of 0.4-1 V. 1 X Phosphate Buffer Saline (pH=7.4) comprises 10 g NaCl, 0.25g KCl, 1.8 g Na$_2$HPO$_4$, 0.3 g KH$_2$PO$_4$, and 1000 ml H$_2$O. At PBS buffer strengths exceeding 1/15 X, the translocation signal was weak due to the diminishing surface charge effect and larger noise, while at lower buffer strengths (< 1/15X PBS), DNA translocation signal with current increase were measured consistently. Lower buffer concentration was not used since the electrokinetic effects at the entrance will impede the entrance of DNA molecules into the nanopore[73]. While application of higher voltages was not possible using the amplifier, voltages lower than ~0.3 V showed no translocations presumably due to the entropic barrier that the DNA molecule needs to overcome when entering the nanopore[35]. Detection of long DNA molecules under low ionic strength conditions even in relatively large nanopores is enabled by the effect of the high negative charge on the DNA molecule that leads to an increase in ionic current during DNA translocation[33,35]. However, during each DNA translocation event, we observed a slight current decrease

that preceded the expected current increase due to the excess charge introduced by the DNA into the nanopore (Figure 6.5b). At 1/15X PBS, the average amplitude of the current decrease was 3-6 pA compared to a current increase of 10-15 pA (Figure 6.5c)
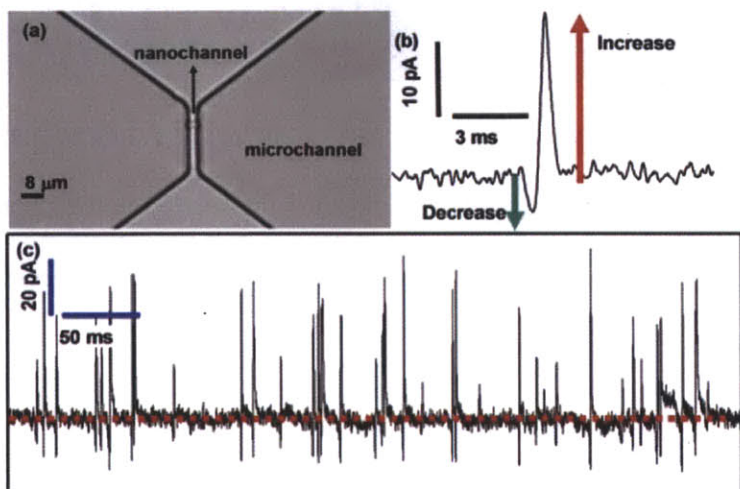
Figure 6.5 (a) PDMS nanopore device. (b) DNA translocation signature indicates both conductance depletion followed by conductance enhancement. (c) Current trace showing consistent bidirectional current modulation. Here λ–DNA of 1 μg/mL was dissolved in 1/15X PBS, and the voltage bias was 0.7 V.

6.2.3 Bidirectional modulation of ionic current during DNA translocation at different buffer strengths

As stated in the preceding section, a recent report suggests that this bidirectional conductance modulation may result from concentration polarization induced by the asymmetric charge distribution in the nanopore during DNA translocation[84]. The DNA molecule presents a moving negative charge in the nanopore that leads to dynamic charge distributions within the nanopore. These charge distributions are similar to those in a nanofluidic diode with asymmetric surface charge[80] (Figure 6.6).
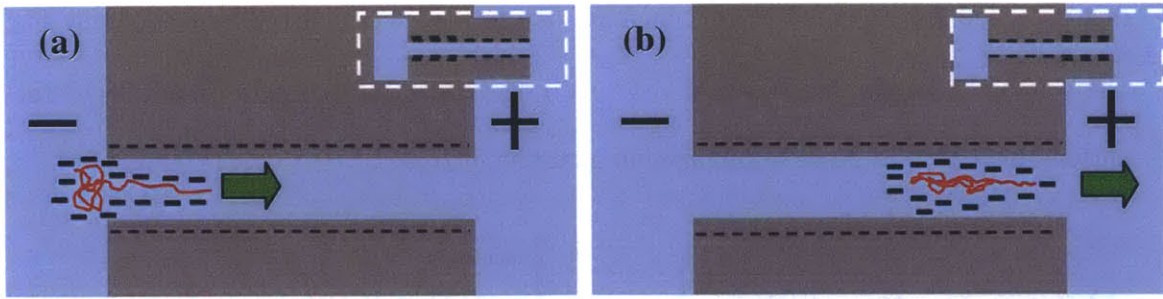
Figure 6.6 (a) In the first half of the DNA translocation, part of the negatively charged DNA molecule resides in the left half of the nanopore. (b) During the second half of the translocation event before exiting the nanopore, the DNA molecule presents an excess negative charge on the right side of the nanopore.

In the first half of the DNA translocation, part of the negatively charged DNA molecule resides in the left half of the nanopore. This charge configuration is similar to that in a nanofluidic diode under reverse bias (figure 6.6a inset), where concentration depletion occurs inside the nanopore, leading to a low conductance[80]. During the second half of the translocation event before exiting the nanopore, the DNA molecule presents an excess negative charge on the right side of the nanopore (figure 6.6b). This configuration is similar to that of a nanofluidic diode under forward bias (figure 6.6b inset), which results in concentration enhancement in the nanopore and high ionic conductance[80]. Thus, the DNA molecule may be expected to initially decrease the ionic current (reverse bias), followed by an increase (forward bias), as it translocates through the nanopore, provided the timescale of DNA translocation is sufficiently large to allow concentration enhancement and depletion to develop.

Translocation events at different buffer strengths and applied voltages were recorded for one minute and analyzed using a MATLAB program that identified the amplitudes of

current decrease and increase for each translocation. The MATLAB code for identifying and characterizing DNA translocation is similar to the one used in Chapter 4.

Figure 6.7 shows the histograms of conductance enhancement and decrease due to DNA translocation at different buffer strengths, with insets showing the normalized DNA translocation current signature. The current increase and decrease events fit well to Gaussian curves, suggesting the absence of clearly distinguishable DNA conformations during translocation as expected for nanopores with cross-sectional dimensions much larger than the DNA persistence length. At lower buffer strengths, the relative magnitudes of both current enhancement and decrease were larger than those at higher buffer strengths (figure 6.8). However, the relative magnitudes of current increase and decrease remained nearly independent of the buffer strength (figure 6.9). This result is consistent with that expected due to concentration polarization[84]. It also rules out the possibility that the current decrease results from geometric blockage at the nanopore entrance by the DNA, in which case the current decrease is expected to scale linearly with the magnitude of the open channel current through the nanopore, which in turn scales nearly linearly with ionic concentration. Similarly, the relative magnitude of conductance change for both current increase and decrease did not vary significantly with applied voltage, which is again consistent with that expected from concentration polarization. This result agrees with the hypothesis where the DNA charge causes ionic concentration distribution asymmetry and corresponding conductance bidirectional modulation during translocation.
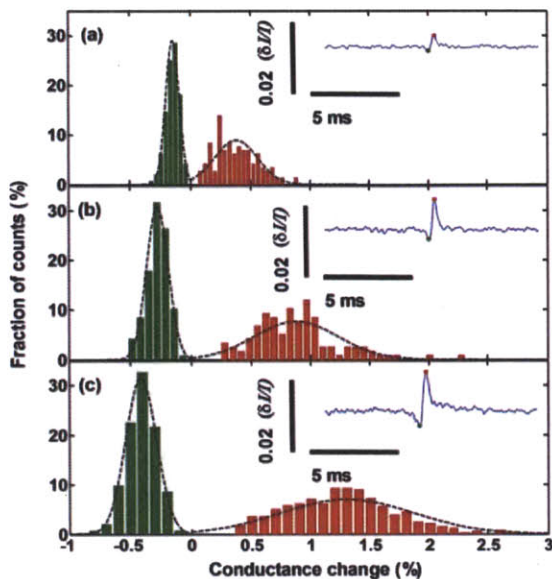
Figure 6.7 Histograms for relative current change at (a) 1/15X PBS (b) 1/30X PBS, and
(c) 1/60X PBS. Each inset shows a conductance rectification signature (ionic current
trace normalized by baseline current) induced by DNA translocation at each buffer
concentration.
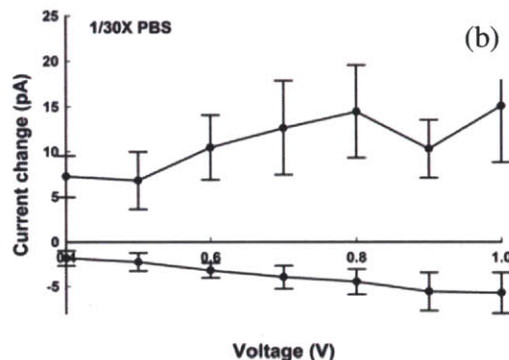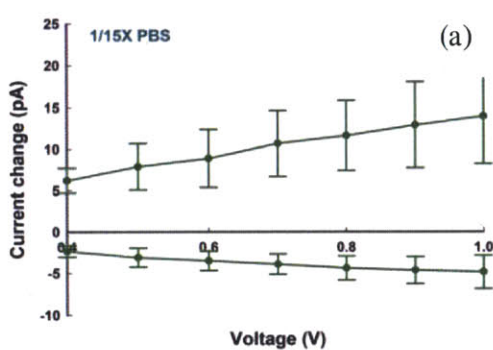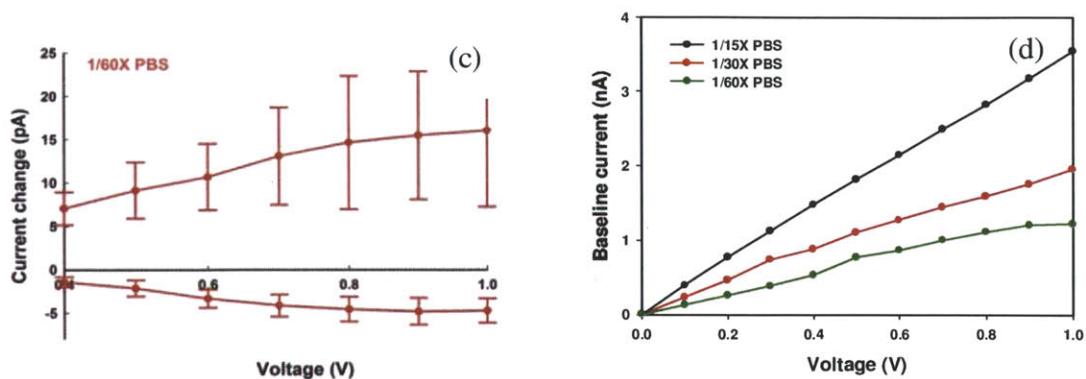
Figure 6.8 Current increase and decrease v.s. magnitude of voltage bias during single λ-DNA translocation in (a) 1/15X PBS (b) 1/30X PBS, and (c) 1/60X PBS. The absolute magnitudes of current increase and decrease remained nearly independent of the buffer strength and applied voltage. (d) Baseline current v.s. voltage relationship of PDMS nanopore device at each buffer concentration.

6.2.4 Numerical simulation

To further study the effect of bidirectional current modulation effect, we performed numerical simulations to calculate the magnitude of ionic current flowing through the nanopore assuming that the DNA molecule contributes a static charge in the nanopore (figure 6.6 insets, and figure 6.9). The calculation methodology and derivation presented in this section is similar to that used in reference [80]. In this situation, a system of equations comprising Poisson-Nerst-Planck and Navier-Stokes equation are the complete equations set for solving ion transport and therefore ionic current flowing through nanopore[80]. To simplify the calculation, here we made several assumptions:

(1) The electro-osmotic term is negligible and therefore it is not necessary to solve the Navier-Stokes equations in order to explain ionic transport through the nanopore.

(2) We consider only one-dimensional model with ionic transport only along the nanopore using quantities averaged over the nanopore cross-section.

(3) The nonlinear Poisson equation is replaced by an electro-neutrality condition.

(4) The DNA molecule is modeled as an additional mobile uniform negative surface charge being imposed on the inherent negative nanopore surface charges. The total charge resulting from the DNA molecule is constant, while the spatial extent of the extra layer of surface charge was found by numerical simulations and confirmed by deGennes theory.
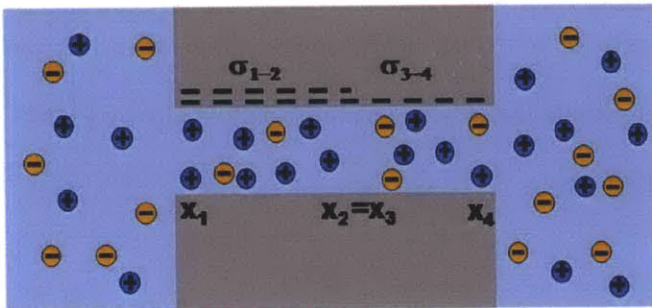
Figure 6.9 The numerical model for ionic transport within nanopore. $\sigma_{1\text{-}2}$ denotes the negative surface charge between X_1 and X_2, and its magnitude equals the addition of inherent nanopore surface charge and negative charges from DNA molecule. $\sigma_{3\text{-}4}$ denotes the negative surface charge between X_3 and X_4, and its magnitude equals the inherent nanopore surface charge.

With these assumptions, the nanopore model is simplified to a system of non-linear algebraic equations for our nanopore 1-D model. Below we will describe the origins and derivations of the equations.

Consider a nanopore connecting two reservoirs and at left end X_1 and right end X_4 of the 4 μm long nanopore, having a negative surface charge discontinuity between points X_2 and X_3. The height of the nanopore h and inherent surface charge σ_{3-4} were determined experimentally in previous section using both high and low buffer concentration. The extra negative surface charge between points X1 and X2 was used to model the negative charges from translocating DNA molecules. The magnitude of the density of this extra surface charge is equal to the total amount of DNA charges divided by its length (X_2 - X_1). Since our buffer solution consists mainly of NaCl, we can consider a 1:1 electrolyte, and denote the cations and anions by n_+ and n_-, respectively. The (constant) fluxes of cations and anions along the nanopore are denoted as J_+ and J_-, respectively. For unit channel width, J_+ and J_- with electrophoretic and diffusion mechanisms are:

$$J_+ = -Dh\frac{dn_+}{dx} - \frac{Dhe}{kT}n_+\frac{d\phi}{dx} \quad\text{...(6.1)}$$

$$J_- = -Dh\frac{dn_-}{dx} + \frac{Dhe}{kT}n_-\frac{d\phi}{dx} \quad\text{...(6.2)}$$

Adding and subtracting Equations 6.1 and 6.2 and using the electro-neutrality condition:

$\frac{2\sigma}{eh} = n_- - n_+$, we obtain:

$$I = J_+ - J_- = -Dh\frac{d(n_+ - n_-)}{dx} - \frac{Dhe}{kT}(n_+ + n_-)\frac{d\phi}{dx} \quad\text{...(6.3)}$$

$$M = J_+ + J_- = -Dh\frac{d(n_+ + n_-)}{dx} - \frac{Dhe}{kT}(n_+ - n_-)\frac{d\phi}{dx} \quad\text{Appendix ....(6.4)}$$

Equations 6.3 and 6.4 can be simplified to yield an analytical solution

$$x_2 = x_1 + (\frac{Dhn_1}{M} + \frac{2\sigma_{1-2}DI}{M^2e})\left[1 - \exp\left(\frac{Me(\phi_2 - \phi_1)}{IkT}\right)\right] + \frac{2\sigma_{1-2}D}{MkT}(\phi_2 - \phi_1) \dots\dots\dots (6.5)$$

$$M(x_2 - x_1) = -Dh(n_2 - n_1) + \frac{2\sigma_{1-2}D}{kT}(\phi_2 - \phi_1) \dots\dots\dots\dots\dots (6.6)$$

$$x_4 = x_3 + (\frac{Dhn_3}{M} + \frac{2\sigma_{3-4}DI}{M^2e})\left[1 - \exp\left(\frac{Me(\phi_4 - \phi_3)}{IkT}\right)\right] + \frac{2\sigma_{3-4}D}{MkT}(\phi_4 - \phi_3) \dots\dots\dots (6.7)$$

$$M(x_4 - x_3) = -Dh(n_4 - n_3) + \frac{2\sigma_{3-4}D}{kT}(\phi_4 - \phi_3) \dots\dots\dots\dots\dots (6.8)$$

Here M and I are constants, and the subscripts 6.1, 6.2, 6.3, 6.4 denote locations in the nanopore. In order to model a charge discontinuity in the nanopore, appropriate boundary conditions must be used at the junction. We use the well-known Donnan condition that relates the ionic concentrations and electric potentials on either side of a junction such as reservoir-nanopore (points 1 and 4) or across a surface charge discontinuity (between points 2 and 3). It assumes that the Boltzmann distribution is locally valid, and the concentrations at the two points (X_1 and left reservoir, or X_4 and right reservoir) are related by:

$$\frac{n_1}{n_{left}} = \sqrt{1 + \left(\frac{2\sigma_{1-2}}{ehn_{left}}\right)^2} \dots\dots\dots\dots\dots\dots\dots\dots (6.9)$$

$$\phi_1 - \phi_{left} = \frac{kT}{e}\cosh^{-1}\left(\sqrt{1 + \left(\frac{2\sigma_{1-2}}{ehn_{left}}\right)^2}\right) \dots\dots\dots\dots\dots (6.10)$$

$$\frac{n_4}{n_{right}} = \sqrt{1 + \left(\frac{2\sigma_{3-4}}{ehn_{right}}\right)^2} \dots\dots\dots\dots\dots\dots\dots\dots (6.11)$$

$$n_3 = \sqrt{n_2^2 + \left(\frac{2\sigma_{3-4}}{eh}\right)^2 - \left(\frac{2\sigma_{1-2}}{eh}\right)^2} \dots\dots\dots\dots\dots\dots (6.12)$$

$$\phi_3 - \phi_2 = \frac{kT}{q}\ln\left(\frac{n_3 + \dfrac{2\sigma_{3-4}}{eh}}{n_2 + \dfrac{2\sigma_{1-2}}{eh}}\right) \quad\text{.. (6.13)}$$

$$\phi_4 - \phi_{right} = \frac{kT}{e}\cosh^{-1}\left(\sqrt{1 + \left(\frac{2\sigma_{3-4}}{ehn_{right}}\right)^2}\right) \quad\text{... (6.14)}$$

Here Equations 6.5-6.14 with ten unknowns ($n_1, n_2, n_3, n_4, \phi_1, \phi_2, \phi_3, \phi_4, M, I$) form a system

of nonlinear algebraic equations that can be solved by MATLAB to yield the electric

potential, ionic concentrations, and ionic flux through the nanopore. The theoretical

results are compared with experimental results in the following section.

6.3 Results and discussion

The value of X_2 - X_1, which determines the length of the nanopore occupied by the DNA

molecule in the model ion both depletion and enhancement cases, was found to fall in the

range of 1.95 to 2.05 μm. As stated in Chapter 4, the equilibrium length L_{eq} of a DNA

molecule inside a nanopore can be calculated using the deGennes theory, and the

equilibrium lengths of T7 and λ-DNA molecules inside the 4 μm nanopore were

calculated to be 1.7 and 2.1 μm, respectively, and therefore are consistent with the above

calculations of X_2 - X_1 for current rectification.

Figure 6.10c and d show the numerical simulation results for the relationship between the

percentage of conductance change in current enhancement and decrease with applied

voltage and PBS concentration. It is seen that the conductance change decreases with the

increase of buffer concentration, and shows no dependence on the magnitude of applied voltage. This result agrees qualitatively with the experimental result (Figure 6.10a, b), which showed no dependence on voltage and an inverse relationship between buffer concentration and conductance change. The difference between predicted and experimental value may be attributed to the transient nature of the DNA translocation where the ion enhancement and depletion time of ~1.5 ms may not be sufficient to reach the magnitude of modulation predicted by our steady state model (Please refer to Appendix II).
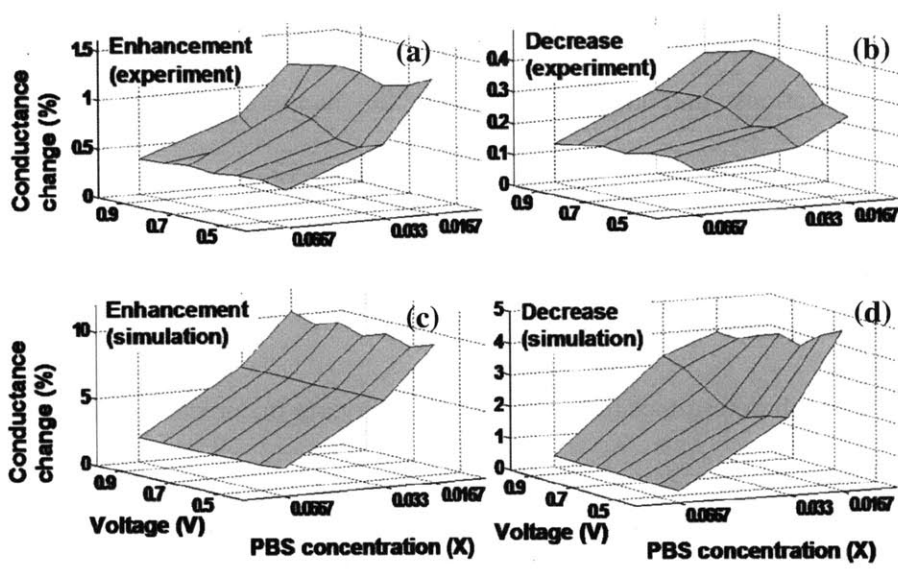
Figure 6.10 (a) Experimental result for the dependence of conductance enhancement on voltage and buffer concentration (b) Experimental result for the dependence of conductance depletion on voltage and buffer concentration (c) Simulation result for the dependence of conductance enhancement on voltage and buffer concentration (d) Simulation result for the dependence of conductance depletion on voltage and buffer concentration.

6.4 Conclusion

In conclusion, we have observed bidirectional ionic conductance modulation in a nanopore during DNA translocation. The origin of the phenomenon is similar to the ionic current rectification, in that charge asymmetry results in ionic current depletion and enhancement. This phenomenon was further studied with the DNA molecule being modeled as an extra layer of negative surface charge that moves in the nanopore using a 1-D electrokinetic model. This extra surface charge is superimposed onto uniformly charged PDMS nanopore surface, and therefore results in both depletion and accumulation during each DNA translocation event, depending on the position of the DNA in the nanopore. The electrokinetic model indicates a more prominent rectification effect at lower buffer concentration, which was also demonstrated in our system by showing larger percentage change in nanopore conductance at lower buffer concentration.

Chapter 7 Conclusion and outlook

In this thesis we focused on the development of nanofluidic nanopore devices for enhanced discrimination between DNA molecules of different lengths through statistical averaging over multiple detection events on the same molecule. Nanopore devices of dimensions 200 nm × 500 nm × 4 μm and 200 nm × 500 nm × 7 μm were fabricated using soft lithography in PDMS, and translocation events of single molecules of λ-DNA (48.5 kbp), T7 DNA (39.93 kbp), and a HindIII enzyme digest fragment of λ-DNA (23.13 kbp) were detected as transient increases in the baseline current due to the dominance in electro-neutrality effect. Multiple measurements on the same DNA molecule with feedback control were performed using LabVIEW, and DNA molecules were recaptured into the pore with an estimated probability exceeding 99%, enabling the measurement of multiple translocation events on the same molecule. Numerical simulations using a drift-diffusion model were performed to examine the DNA recapture physics and understand the origins of the high recapture rates in the nanopore devices. The measured DNA recapture time distribution was correctly predicted by the numerical simulations. Statistical averaging on multiple measurements resulted in enhancement of the ability of the nanopore to discriminate between DNA molecules of different lengths from a resolution of ~8.5 kbp for single measurements to ~4.5 kbp for multiple measurements, which enabled length-based discrimination of molecules in a mixture of λ-DNA and HindIII-digest λ-DNA, and in a mixture of λ-DNA and T7 DNA.

To isolate the DNA molecule being measured from the DNA sample being analyzed and to improve device stability, next generation nanopore devices were designed with the aims of better device surface control, capability of trapping and detecting DNA

molecules, and performing multiple measurements with neither side of the nanopore exposed to the DNA bulk solution. The SU-8 mold for microchannels and trapping chamber was fabricated with UV photolithography, and nanopores in silica substrate were fabricated with electron-beam lithography, followed by wet etch and RIE technique. Finally, a bidirectional modulation of ionic current was observed during the translocation of DNA molecules through the nanopore wherein the ionic current showed a slight decrease followed by a larger increase. Through experiment and simulation, this bidirectional current modulation was shown to be similar in origin to ionic current rectification in a nanofluidic diode, attributed to the spatially asymmetric charge distribution introduced by the DNA molecule as it moves through the nanopore.

This work has shown that multiple measurements on the same molecule in a nanopore device can enhance the ability of the nanopore to discriminate between long DNA molecules of different lengths. Further development of this approach may enable rapid, label-free, high-resolution electrical sizing of DNA molecules by nanofluidic devices, which could open many applications in medicine, forensics, and bioengineering areas.

Appendix (I)

Determination of Series Failure

The algorithm presented here is developed by Tarun Jain. The goal of this section is to describe the method by which series failure was determined. A series of measurements is strictly defined by the following criteria:

1. One and only one translocation occur between voltage reversals

2. No greater than 500 ms between translocation events

Consider a current trace in which a series of translocations, $\{\delta I_k\}$ is detected, where each translocation occurs at time t_k. The current trace also contains large discontinuities in the current corresponding to a change in the polarity of the voltage. These voltage reversals occur only when the real time feedback algorithm has triggered a voltage reversal. The last translocation in a series is denoted as: I_N, occurring at time t_N. The closest voltage reversal after the last translocation is denoted as: V^N, occurring at time T^N.

The series failures are:

1) Second Molecule Translocating before voltage reversal occurs

    a. Criterion: δI_{N+1} occurs before V^N, and $t_{N+1} - t_N < 50$ ms

    b. Explanation: This indicates a second molecule translocating through the nanopore, causing a break in the series

2) Failure of Real Time algorithm to detect DNA molecules

    a. Criterion: δI_{N+1} occurs before V^N, and $t_{N+1} - t_N > 50$ ms

b. Explanation: The mean pre-reversal time is 30 ms, with nearly no pre-reversal times greater than 50 ms. Had the program detected the molecule and reversed the voltage, then the second translocation would occur after V^N.

3) DNA molecule escape

    a. Criterion: δI_{N+1} occurs after V^N, and $t_{N+1} - t_N > 500$ ms, and

4) Real Time algorithm incorrectly detects a DNA molecule

    a. Criterion: δI_{N+1} occurs on the voltage reversal after V^N (corresponding to no translocations between two voltage reversals)

The only criterion that seems to be missing is when:

δI_{N+1} occurs after V^N, and $t_{N+1} - t_N < 500$ ms. If this is the case, and (4) is not satisfied, then it is easy to see that the translocation δI_{N+1} satisfies the criterion for being part of the series, and would have been included as such. Thus, these four criterion map out all possible causes of series failure.

(II)

Estimation of time scale for reaching steady state in bidirectional current modulation

Below we present a calculation to estimate the time scale for the development of ionic concentration enhancement in a nanochannel with charge asymmetry when a voltage bias is applied. The charge asymmetry is assumed to result from the presence of DNA in the

nanochannel. In the calculations presented below, Δn is the total number of excess ions in the nanochannel under steady state, n is the total number of ions inside the nanopore in the absence of ionic enhancement or depletion, ΔI is the change in ionic current under steady state (calculated from the model presented in Chapter 6), I is the baseline current without any DNA, $e = 1.6 \times 10^{-19}$ C, μ = ionic mobility = 7.9×10^{-8} m^2/V-s, L = the length of the nanopore = 4 μm, V = applied voltage = 1 V, and τ is the time scale for current enhancement in our nanopore device.

Since the current through the nanopore is related to the ionic concentration in the nanopore (except under strong current rectification, which does not occur in this case), we can assume $\dfrac{\Delta n}{n} \approx \dfrac{\Delta I}{I}$, and given that $I = \dfrac{ne\mu V}{L^2}$, it allows us to estimate the excess number of ions introduced into the pore due to concentration enhancement as

$$\Delta n \approx n\frac{\Delta I}{I} = \frac{\Delta I L^2}{e\mu V}.$$

Now, this change in the number of ions occurs due to the difference in the concentrations of ions resulting from the spatial variation of (relatively) fixed charges due to the DNA molecule being present in only part of the nanopore. We can therefore approximate that the rate of build-up of ions is governed by the difference between the nominal ionic currents in the two sides, i.e. approximated by the difference in the nominal ionic currents in the presence and absence of the DNA molecule in the nanopore, which we call ΔI_{DNA}. Its magnitude is the current change estimated for DNA translocation in the absence of any ionic concentration enhancement effects.

We can now estimate the timescale for development of the ionic concentration enhancement as:

$$\tau \sim \frac{\Delta ne}{\Delta I_{DNA}} = \frac{\Delta I}{\Delta I_{DNA}} \frac{L^2}{\mu V}$$

From Equation 2.1, $\Delta I_{DNA} = 37.5$ pA, which gives $\tau \sim 2$ ms.

References:

[1]   W. E. Moerner, "New directions in single-molecule imaging and analysis," Proceedings of the National Academy of Sciences of the United States of America **104** (31), 12596-12602 (2007).

[2]   H. Bayley and C. R. Martin, "Resistive-Pulse Sensing-From Microbes to Molecules," Chem Rev **100** (7), 2575-2594 (2000).

[3]   J. J. Kasianowicz, "Bio-inspired nanopore-based sensors: Comment on "Nanopores: A journey towards DNA sequencing" by M. Wanunu," Phys Life Rev.

[4]   J. J. Kasianowicz, E. Brandin, D. Branton et al., "Characterization of individual polynucleotide molecules using a membrane channel," Proceedings of the National Academy of Sciences of the United States of America **93** (24), 13770-13773 (1996); R. M. M. Smeets, U. F. Keyser, N. H. Dekker et al., "Noise in solid-state nanopores," Proceedings of the National Academy of Sciences of the United States of America **105** (2), 417-421 (2008).

[5]   A. Meller, L. Nivon, E. Brandin et al., "Rapid nanopore discrimination between single polynucleotide molecules," Proceedings of the National Academy of Sciences of the United States of America **97** (3), 1079-1084 (2000).

[6]   H Chang, F Kosari, G Andreadakis et al., "DNA-mediated fluctuations in ionic current through silicon oxide nanopore channels," Nano Lett **4** (8), 1551-1556 (2004).

[7]   A. Meller, L. Nivon, and D. Branton, "Voltage-driven DNA translocations through a nanopore," Physical Review Letters **86** (15), 3435-3438 (2001).

[8]   J. J. Kasianowicz, E. Brandin, D. Branton et al., "Characterization of individual polynucleotide molecules using a membrane channel," Proc Natl Acad Sci U S A **93** (24), 13770-13773 (1996).

[9]   J. J. Kasianowicz and S. M. Bezrukov, "Protonation Dynamics of the Alpha-Toxin Ion-Channel from Spectral-Analysis of Ph-Dependent Current Fluctuations," Biophysical Journal **69** (1), 94-105 (1995).

[10] S. Howorka and H. Bayley, "Probing distance and electrical potential within a protein pore with tethered DNA," Biophysical Journal **83** (6), 3202-3210 (2002).

[11] D. W. Deamer, Akeson, M. , "Nanopores and nucleic acids: prospects for ultrarapid sequencing.," Trends in Biotech. **18**, 147-151 (2000).

[12] M. Bates, M. Burns, and A. Meller, "Dynamics of DNA molecules in a membrane channel probed by active control techniques," Biophysical Journal **84** (4), 2366-2372 (2003).

[13] H. Wang, J. E. Dunning, A. P. H. Huang et al., "DNA heterogeneity and phosphorylation unveiled by single-molecule electrophoresis," Proceedings of the National Academy of Sciences of the United States of America **101** (37), 13472-13477 (2004).

[14] J. Clarke, H. C. Wu, L. Jayasinghe et al., "Continuous base identification for single-molecule nanopore DNA sequencing," Nat Nanotechnol **4** (4), 265-270 (2009).

[15] J. Li, D. Stein, C. McMullan et al., "Ion-beam sculpting at nanometre length scales," Nature **412** (6843), 166-169 (2001).

[16] A. J. Storm, J. H. Chen, X. S. Ling et al., "Fabrication of solid-state nanopores with single-nanometre precision," Nature Materials **2** (8), 537-540 (2003).

[17] R. M. M. Smeets, U. F. Keyser, D. Krapf et al., "Salt dependence of ion transport and DNA translocation through solid-state nanopores," Nano Letters **6** (1), 89-95 (2006).

[18] Z. Siwy, P. Apel, D. Baur et al., "Preparation of synthetic nanopores with transport properties analogous to biological channels," Surf Sci **532**, 1061-1066 (2003).

[19] C. C. Harrell, Z. S. Siwy, and C. R. Martin, "Conical nanopore membranes: controlling the nanopore shape," Small **2** (2), 194-198 (2006).

[20] A. J. Storm, J. H. Chen, H. W. Zandbergen et al., "Translocation of double-strand DNA through a silicon oxide nanopore," Physical Review E **71** (5) (2005).

[21] L.L. Sohn and O.A. Saleh, "Direct detection of antibody-antigen binding using an on-chip artificial pore," Proceedings of the National Academy of Sciences of the United States of America **100** (3), 820-824 (2003).

[22] O. A. Saleh and L. L. Sohn, "Binding assays and single molecule sensing using precision chip-based resistive sensing," Biophysical Journal **82** (1), 166A-166A (2002).

[23] O. A. Saleh and L. L. Sohn, "Quantitative sensing of nanoscale colloids using a microchip Coulter counter," Review of Scientific Instruments **72** (12), 4449-4451 (2001).

[24] M. Karhanek, J. T. Kemp, N. Pourmand et al., "Single DNA molecule detection using nanopipettes and nanoparticles," Nano Lett **5** (2), 403-407 (2005).

[25] R. W. Deblois and R. K. A. Wesley, "Sizes and Concentrations of Several Type-C Oncornaviruses and Bacteriophage-T2 by Resistive-Pulse Technique," J Virol **23** (2), 227-233 (1977).

[26] OA Saleh and LL Sohn, "An artificial nanopore for molecular sensing," Nano Letters **3** (1), 37-38 (2003).

[27] R. Karnik, R. Fan, M. Yue et al., "Electrostatic control of ions and molecules in nanofluidic transistors," Nano Letters **5** (5), 943-948 (2005).

[28] T. Ito, L. Sun, and R. M. Crooks, "Simultaneous determination of the size and surface charge of individual nanoparticles using a carbon nanotube-based coulter counter," Analytical Chemistry **75** (10), 2399-2406 (2003).

[29] J. D. Uram, K. Ke, A. J. Hunt et al., "Submicrometer pore-based characterization and quantification of antibody-virus interactions," Small **2** (8-9), 967-972 (2006).

[30] J. D. Uram, K. Ke, A. J. Hunt et al., "Label-free affinity assays by rapid detection of immune complexes in submicrometer pores," Angew Chem Int Edit **45** (14), 2281-2285 (2006).

[31] R. Karnik, K. Castelino, R. Fan et al., "Effects of biological reactions and modifications on conductance of nanofluidic channels," Nano Lett **5** (9), 1638-1642 (2005).

[32] T. Vuletic, S. D. Babic, D. Grgicin et al., "Manning free counterion fraction for a rodlike polyion: Aqueous solutions of short DNA fragments in presence of very low added salt," Physical Review E **83** (4) (2011).

[33] Y. H. Sen, T. Jain, C. A. Aguilar et al., "Enhanced discrimination of DNA molecules in nanofluidic channels through multiple measurements," Lab on a Chip **12** (6), 1094-1101 (2012).

[34] P. Chen, J. J. Gu, E. Brandin et al., "Probing single DNA molecule transport using fabricated nanopores," Nano Letters **4** (11), 2293-2298 (2004).

[35] Y. H. Sen and R. Karnik, "Investigating the translocation of lambda-DNA molecules through PDMS nanopores," Analytical and Bioanalytical Chemistry **394** (2), 437-446 (2009).

[36] S. E. Henrickson, M. Misakian, B. Robertson et al., "Driven DNA transport into an asymmetric nanometer-scale pore," Phys Rev Lett **85** (14), 3057-3060 (2000).

[37] M. Wanunu, W. Morrison, Y. Rabin et al., "Electrostatic focusing of unlabelled DNA into nanoscale pores using a salt gradient," Nat Nanotechnol **5** (2), 160-165.

[38] C. R. Reedy, K. A. Hagan, D. J. Marchiarullo et al., "A modular microfluidic system for deoxyribonucleic acid identification by short tandem repeat analysis (vol 687, pg 150, 2011)," Analytica Chimica Acta **699** (1), 126-126 (2011).

[39] H. C. Fan, Y. J. Blumenfeld, U. Chitkara et al., "Analysis of the Size Distributions of Fetal and Maternal Cell-Free DNA by Paired-End Sequencing," Clinical Chemistry **56** (8), 1279-1286 (2010).

[40] J.B.H Tok, *Nano and Microsensors for Chemical and Biological Terrorism Surveillance*. (Royal Soceity of Chemistry, Cambridge, 2008).

[41] J. Herschleb, G. Ananiev, and D. C. Schwartz, "Pulsed-field gel electrophoresis," Nature Protocols **2** (3), 677-684 (2007).

[42] E. M. Southern, R. Anand, W. R. A. Brown et al., "A Model for the Separation of Large DNA-Molecules by Crossed-Field Gel-Electrophoresis," Nucleic Acids Research **15** (15), 5925-5943 (1987).

[43] J. Voldman, M. L. Gray, and M. A. Schmidt, "Microfabrication in biology and medicine," Annu Rev Biomed Eng **1**, 401-425 (1999).

[44] J. Han and H. G. Craighead, "Separation of long DNA molecules in a microfabricated entropic trap array," Science **288** (5468), 1026-1029 (2000).

[45] J. Fu, R. B. Schoch, A. L. Stevens et al., "A patterned anisotropic nanofluidic sieving structure for continuous-flow separation of DNA and proteins," Nat Nanotechnol **2** (2), 121-128 (2007).

[46] E. Y. Chan, N. M. Goncalves, R. A. Haeusler et al., "DNA mapping using microfluidic stretching and single-molecule detection of fluorescent site-specific tags," Genome Res **14** (6), 1137-1146 (2004).

[47] M. Foquet, J. Korlach, W. Zipfel et al., "DNA fragment sizing by single molecule detection in submicrometer-sized closed fluidic channels," Anal Chem **74** (6), 1415-1422 (2002).

[48] L. C. Campbell, M. J. Wilkinson, A. Manz et al., "Electrophoretic manipulation of single DNA molecules in nanofabricated capillaries," Lab Chip **4** (3), 225-229 (2004).

[49] H. Bayley, "Are we there yet?: Comment on "Nanopores: A journey towards DNA sequencing" by Meni Wanunu," Phys Life Rev; A. Y. Grosberg and Y. Rabin, "What about a theory?: Comment on "Nanopores: A journey towards DNA sequencing" by Meni Wanunu," Phys Life Rev; U. F. Keyser, "Nanopores -

mission accomplished and what next?: Comment on "Nanopores: A journey towards DNA sequencing" by M. Wanunu," Phys Life Rev.

50 D. Branton, D. W. Deamer, A. Marziali et al., "The potential and challenges of nanopore sequencing," Nature Biotechnology **26** (10), 1146-1153 (2008).

51 J. J. Kasianowicz, "Nanopores: flossing with DNA," Nat Mater **3** (6), 355-356 (2004).

52 D. Fologea, E. Brandin, J. Uplinger et al., "DNA conformation and base number simultaneously determined in a nanopore," Electrophoresis **28** (18), 3186-3192 (2007).

53 D. W. Deamer and M. Akeson, "Nanopores and nucleic acids: prospects for ultrarapid sequencing," Trends in Biotechnology **18** (4), 147-151 (2000).

54 D. Fologea, M. Gershow, B. Ledden et al., "Detecting single stranded DNA with a solid state nanopore," Nano Letters **5** (10), 1905-1909 (2005).

55 M. Gershow and J. A. Golovchenko, "Recapturing and trapping single molecules with a solid-state nanopore," Nature Nanotechnology **2** (12), 775-779 (2007).

56 D. M. Stein, C. J. McMullan, J. L. Li et al., "Feedback-controlled ion beam sculpting apparatus," Review of Scientific Instruments **75** (4), 900-905 (2004); J. Gierak, A. Madouri, A. L. Biance et al., "Sub-5 nm FIB direct patterning of nanodevices," Microelectron Eng **84** (5-8), 779-783 (2007).

57 A. L. Biance, J. Gierak, E. Bourhis et al., "Focused ion beam sculpted membranes for nanoscience tooling," Microelectron Eng **83** (4-9), 1474-1477 (2006).

58 P. Chen, T. Mitsui, D. B. Farmer et al., "Atomic layer deposition to fine-tune the surface properties and diameters of fabricated nanopores," Nano Letters **4** (7), 1333-1337 (2004).

59 M. J. Kim, M. Wanunu, D. C. Bell et al., "Rapid fabrication of uniformly sized nanopores and nanopore arrays for parallel DNA analysis," Adv Mater **18** (23), 3149-+ (2006); J. M. Zhang, L. P. You, H. Q. Ye et al., "Fabrication of ultrafine nanostructures with single-nanometre precision in a high-resolution transmission electron microscope," Nanotechnology **18** (15), - (2007).

60 Z. Siwy, D. Dobrev, R. Neumann et al., "Electro-responsive asymmetric nanopores in polyimide with stable ion-current signal," Appl Phys a-Mater **76** (5), 781-785 (2003); P. Y. Apel, Y. E. Korchev, Z. Siwy et al., "Diode-like single-ion track membrane prepared by electro-stopping," Nucl Instrum Meth B **184** (3), 337-346 (2001); H. Bayley and C. R. Martin, "Resistive-pulse sensing - From microbes to molecules," Chemical Reviews **100** (7), 2575-2594 (2000).

61 G. M. Whitesides, E. Ostuni, S. Takayama et al., "Soft lithography in biology and biochemistry," Annu Rev Biomed Eng **3**, 335-373 (2001).

62 J. D. Uram, K. Ke, and M. Mayer, "Noise and bandwidth of current recordings from submicrometer pores and nanopores," ACS Nano **2** (5), 857-872 (2008).

63 U. F. Keyser, B. N. Koeleman, S. Van Dorp et al., "Direct force measurements on DNA in a solid-state nanopore," Nature Physics **2** (7), 473-477 (2006).

64 H. B. Peng and X. S. S. Ling, "Reverse DNA translocation through a solid-state nanopore by magnetic tweezers," Nanotechnology **20** (18) (2009).

65 R. Fan, R. Karnik, M. Yue et al., "DNA translocation in inorganic nanotubes," Nano Letters **5** (9), 1633-1637 (2005).

[66] D. Fologea, J. Uplinger, B. Thomas et al., "Slowing DNA translocation in a solid-state nanopore," Nano Letters **5** (9), 1734-1737 (2005).

[67] N. C. Seeman, "DNA in a material world," Nature **421** (6921), 427-431 (2003).

[68] G. S. Manning, "Limiting Laws and Counterion Condensation in Polyelectrolyte Solutions .I. Colligative Properties," Journal of Chemical Physics **51** (3), 924-& (1969).

[69] F. Zhou, W. Wang, W. Y. Wu et al., "Low electroosmotic flow measurement by tilting microchip," Journal of Chromatography A **1194** (2), 221-224 (2008).

[70] P. D. Ross and R. L. Scruggs, "Electrophoresis of DNA .3. The Effect of Several Univalent Electrolytes on the Mobility of DNA," Biopolymers **2** (3), 231-236 (1964).

[71] J. O. Tegenfeldt, C. Prinz, H. Cao et al., "The dynamics of genomic-length DNA molecules in 100-nm channels," Proceedings of the National Academy of Sciences of the United States of America **101** (30), 10979-10983 (2004).

[72] D. Huh, K. L. Mills, X. Y. Zhu et al., "Tuneable elastomeric nanochannels for nanofluidic manipulation," Nature Materials **6** (6), 424-428 (2007).

[73] D. Stein, Z. Deurvorst, F. H. J. van der Heyden et al., "Electrokinetic Concentration of DNA Polymers in Nanofluidic Channels," Nano Letters **10** (3), 765-772 (2010).

[74] J. C. McDonald, D. C. Duffy, J. R. Anderson et al., "Fabrication of microfluidic systems in poly(dimethylsiloxane)," Electrophoresis **21** (1), 27-40 (2000).

[75] S. K. Sia and G. M. Whitesides, "Microfluidic devices fabricated in poly(dimethylsiloxane) for biological studies," Electrophoresis **24** (21), 3563-3576 (2003).

[76] P. Mao and J. Y. Han, "Fabrication and characterization of 20 nm planar nanofluidic channels by glass-glass and glass-silicon bonding," Lab on a Chip **5** (8), 837-844 (2005).

[77] W. Sparreboom, A. van den Berg, and J. C. T. Eijkel, "Principles and applications of nanofluidic transport," Nature Nanotechnology **4** (11), 713-720 (2009).

[78] H. Daiguji, "Ion transport in nanofluidic channels," Chemical Society Reviews **39** (3), 901-911 (2010).

[79] D. Woermann, "Electrochemical transport properties of a cone-shaped nanopore: high and low electrical conductivity states depending on the sign of an applied electrical potential difference," Physical Chemistry Chemical Physics **5** (9), 1853-1858 (2003); Q. Liu, Y. Wang, W. Guo et al., "Asymmetric properties of ion transport in a charged conical nanopore," Physical Review E **75** (5) (2007).

[80] R. Karnik, C. H. Duan, K. Castelino et al., "Rectification of ionic current in a nanofluidic diode," Nano Letters **7** (3), 547-551 (2007).

[81] I. Vlassiouk and Z. S. Siwy, "Nanofluidic diode," Nano Lett **7** (3), 552-556 (2007).

[82] L. J. Cheng and L. J. Guo, "Rectified ion transport through concentration gradient in homogeneous silica nanochannels," Nano Letters **7** (10), 3165-3171 (2007).

[83] Z. Siwy and A. Fulinski, "Fabrication of a synthetic nanopore ion pump," Physical Review Letters **89** (19) (2002).

151

[84] S. Das, P. Dubsky, A. van den Berg et al., "Concentration Polarization in Translocation of DNA through Nanopores and Nanochannels," Physical Review Letters **108** (13) (2012).